Stony Brook University

Inhibition of Amyloid Beta-Protein Fibrillogenesis by Myelin Basic Protein

A Dissertation Presented

by

Michael David Hoos

to

The Graduate School

in Partial Fulfillment of the

Requirements

for the Degree of

Doctor of Philosophy

in

Molecular and Cellular Biology

Stony Brook University

May 2009

Stony Brook University

The Graduate School

Michael David Hoos

We, the dissertation committee for the above candidate for the

Doctor of Philosophy degree,

hereby recommend acceptance of this dissertation.

William E. Van Nostrand, Ph.D. (Advisor)
Professor, Department of Medicine

Steven O. Smith, Ph.D. (Chair)
Professor, Department of Biochemistry and Cell Biology

Styliani-Anna E. Tsirka, Ph.D.
Professor, Department of Pharmacological Sciences

Sanford R. Simon, Ph.D.
Professor, Department of Biochemistry and Cell Biology

Holly Colognato, Ph.D.
Assistant Professor, Department of Pharmacological Sciences

Michael P. Vitek, Ph.D.
Associate Professor, Department of Neurology and Neurobiology
Duke University Medical Center

This dissertation is accepted by the Graduate School

Lawrence Martin
Dean of the Graduate School

Abstract of the Dissertation

Inhibition of Amyloid Beta-Protein Fibrillogenesis by Myelin Basic Protein

by

Michael David Hoos

Doctor of Philosophy

in

Molecular and Cellular Biology

Stony Brook University

2009

Deposition of fibrillar amyloid β-protein (Aβ) in the brain is a prominent pathological feature of Alzheimer disease (AD) and related disorders, including familial forms of cerebral amyloid angiopathy (CAA). Aβ peptides are produced through the successive cleavage of the Aβ precursor protein by β and γ- secretase, producing peptides of between 39 and 43 amino acids in length. The most common of these wild-type peptides are Aβ40 and Aβ42, the first of which being the most abundant. Aβ42 is more fibrillogenic than Aβ40 and has been implicated in early Aβ plaque deposition in AD. Mutant forms of Aβ, including Dutch- and Iowa-type Aβ, which are responsible for familial CAA, deposit primarily as fibrillar amyloid along the cerebral vasculature and are either absent or present only as diffuse non-fibrillar plaques in the brain parenchyma. Despite the lack of parenchymal fibril formation *in vivo*, these CAA mutant Aβ peptides

exhibit a markedly increased rate and extent of fibril formation *in vitro* compared with wild-type Aβ. Based on these conflicting observations, we sought to determine whether brain parenchymal factors that selectively interact with and modulate CAA mutant Aβ fibril assembly exist. Using a combination of biochemical and ultrastructural techniques we identified myelin basic protein (MBP) as a prominent brain parenchymal factor that preferentially binds to the more fibrilllogenic CAA mutant Aβ compared with wild-type Aβ40. Further studies demonstrated a similar affinity for the fibrilllogenic Aβ42 wild-type peptide. We found that this interaction inhibited the fibril assembly of both CAA mutant Aβ as well as wild-type Aβ42. Structural studies of this interaction have identified a binding region for Aβ in the N-terminus of MBP that alone is sufficient to inhibit Aβ fibrillogenesis through an interaction with the unstructured N-terminus of Aβ peptides. These studies suggest a possible role for MBP in regulating parenchymal fibrillar Aβ deposition in familial CAA and the early formation of amyloid plaques in Alzheimer's disease. Further study will reveal if peptides derived from MBP show promise as effective inhibitors of amyloid plaques in AD patients.

TABLE OF CONTENTS

LIST OF TABLES

LIST OF FIGURES

ACKNOWLEDGEMENTS

This dissertation project could only have been possible with the patient mentoring of my advisor Dr. William E. Van Nostrand, to whom I owe a great deal of thanks. Bill has always been eager to provide guidance in all areas of my graduate work, while still managing to leave enough space to allow for my own professional growth. He always kept me on track but allowed my own abilities the room to grow. I would like to thank the chair of my dissertation committee Dr. Steven O. Smith for his valuable insights and fruitful collaboration on this project. Much of this work would have been impossible without the use of the equipment and experience within the Smith laboratory. I would also like to thank the other members of my dissertation committee, Dr. Styliana-Anna E. Tsirka, Dr. Sanford R. Simon, Dr. Holly Collagnato, and Dr. Michael P. Vitek from Duke University, for their challenging insights and contributions along the way.

A great deal of thanks is owed to the members of the Van Nostrand laboratory, past and present: Judianne Davis, M.S., Mary Lou Previti, soon to be Dr. Mei-Chen Liao, AnnMarie Armenti, M.S., Dr. Rong Fan, Dr. Feng Xu, Galina Romanov, Kelly Ziegler-DeFilippis, Shane McGowen, Kiran Kelkar, Jonathan Alfaro, Aaron Felfle, and Dianna Chiqui. The Van Nostrand lab has been a wonderful place to work. The support and knowledge of the members of the lab has been exceptional. I would also like to thank them for the many good times that were shared both in the lab and out. I would like to thank the members of the Smith lab, especially Dr. Mahiuddin Ahmed who has contributed a great deal of time and expertise to this project, Ian Brett, Daryl Aucoin,

Shivani Ahuja, Miki Itaya, Tony Tang, and Joe Goncalves for sharing their time, knowledge and experience with me.

I would like to thank my friends and fellow students in the Graduate School who have made my experience here more than just about the science. Thank you all for the softball and volleyball games, the trips to Fire Island, the parties and BBQs, and for all the support and friendship that have helped make my graduate career a memorable one. Thanks are owed to our program coordinator Carol Juliano as well, for helping me skillfully navigate the intricacies of the Graduate School's policies and procedures. Special thanks goes also to my good friends Chris and Stephanie Richardson, and John and Heather Methven, whose friendship and support have been immeasurable to me over the years. Special thanks and love also to Emily who has stood by patiently waiting to have me back from writing.

Finally, all of my love and thanks goes to my family who always stood behind me and gave me the support I needed to reach this point in my career and in my life. None of this would have been possible if it were not for you.

CHAPTER 1 – Introduction

1.1 – Amyloid β-Protein

Extracellular deposition of the amyloid β-protein (Aβ) in brain is a prominent feature of Alzheimer's disease (AD) and other related disorders (*1*). Aβ is a 39-43 amino acid peptide that exhibits a high propensity to self-assemble into β sheet-containing oligomeric forms and fibrils (*2*). Aβ peptides are proteolytically produced from the amyloid β-protein precursor (AβPP), a large type I integral membrane protein, through sequential proteolysis by β- and γ-secretase activities (*3-6*). Cerebral deposition of Aβ in the parenchyma can occur as diffuse plaques, with little surrounding pathology, or as fibrillar plaques associated with dystrophic neurons, neurofibrillary tangles, and inflammation (*1*). Fibrillar Aβ deposition also occurs within and along primarily small and medium-sized arteries and arterioles of the cerebral cortex and leptomeninges and in the cerebral microvasculature, a condition known as cerebral amyloid angiopathy (CAA) (*7-9*). This condition accounts for up to 20% of all spontaneous primary intracerebral hemorrhages and is a key pathological lesion in nearly all patients with AD and certain related disorders. Accumulation of fibrillar cerebral vascular Aβ has been shown to cause degeneration and cell death of smooth muscle cells and pericytes in affected larger cerebral vessels and in cerebral microvessels, respectively (*9-11*). Recent findings have implicated cerebral microvascular Aβ deposition in promoting neuroinflammation and dementia in AD (*12-15*).

1.2 - Familial Forms of CAA

There exist several familial monogenic forms of CAA resulting from specific point mutations within the Aβ sequence of the AβPP gene (*16-20*). The most recognized example of familial CAA is the Dutch-type resulting from an E22Q substitution in Aβ (*16, 17, 21*). A more recently identified form of familial CAA is the Iowa-type D23N substitution in Aβ (*20*). Both forms cause early and severe cerebral vascular amyloid deposition and are accompanied by only diffuse parenchymal Aβ deposits with the absence of fibrillar plaques (*20, 21*). Dutch-type CAA is characterized by vascular amyloid-associated neuroinflammation and recurrent, often fatal, intracerebral hemorrhages at mid-life (*22-24*) with little or no indication of neurofibrillary tangles and neuronal pathology (*24-26*). In contrast to the Dutch-type disease, Iowa-type CAA appears more localized to the cerebral microvasculature and although cerebral hemorrhage is not common, ischemic damage is observed (*20*). Also, neurofibrillary tangles and robust neuroinflammation can be found associated with the capillary amyloid in Iowa-type CAA (*27*). Both Dutch-type and Iowa-type CAA are accompanied by progressive cognitive impairment that appears to be driven by the extensive vascular amyloid deposition (*26-28*).

Previous *in vitro* studies by our laboratory and others have clearly shown that both the Dutch-type and Iowa-type mutations increase both the fibrillogenic and cerebrovascular cell pathogenic properties of Aβ compared with wild-type Aβ (*29-33*). It is noteworthy that the Dutch-type (E22Q) and Iowa-type (D23N) mutations are adjacent within the Aβ peptide and both result in loss of a negative charge at their respective sites

and we found that including each of these mutations together in the same Aβ peptide further enhances the fibrillogenic and pathogenic properties *in vitro* (*33*). However, the reason as to why the Dutch-type and Iowa-type mutations lead to preferential accumulation of fibrillar amyloid exclusively in the cerebral vasculature and not in the brain parenchyma is unclear.

1.3 - Transgenic Mouse Model of Familial CAA

We recently generated a novel transgenic mouse model, designated Tg-SwDI, that expresses very low levels of familial Dutch/Iowa CAA mutant human AβPP in brain (*34*). In creating these transgenic mice we took advantage of our earlier *in vitro* studies demonstrating that Dutch/Iowa double CAA mutant Aβ exhibits more robust fibrillogenic and pathogenic properties in the presence of cultured cerebrovascular cells compared with either single CAA mutant Aβ (*35*). As shown in our recent publications Tg-SwDI mice develop early-onset and progressive accumulation of fibrillar microvascular CAA (*34*). Although fibrillar vascular deposits are prominent the *Tg-SwDI mice do not develop parenchymal fibrillar Aβ plaque deposits* reminiscent of the Dutch-type and Iowa-type CAA disorders in humans. As recently published, we have shown that there is an early-onset and robust neuroinflamatory response in these mice (including highly increased numbers of reactive astrocytes and activated microglia and elevated levels of inflammatory cytokines) that is closely associated with cerebral microvascular fibrillar amyloid (*36*). The diffuse parenchymal Aβ deposits in this model do not induce a neuroinflamatory response again reminiscent of the Dutch-type and Iowa-type CAA

disorders in humans. Moreover, Tg-SwDI mice exhibit behavioral and performance deficits that coincide with the development of the cerebral microvascular amyloid. Our recent findings indicate that Tg-SwDI mice are a novel and unique model to investigate why these highly fibrillogenic forms of Aβ do not assemble into parenchymal fibrillar structures whose absence is characteristic of the Dutch-type and Iowa-type CAA disorders in humans.

1.4 - Chaperone Molecules that Alter Aβ Fibrillogenesis

A number of naturally occurring "Aβ chaperone" binding molecules have been identified that have been reported to modulate fibrillar assembly of the peptide. For example, apolipoprotein E (apoE) has been described to either promote or inhibit Aβ fibril formation *in vitro* (*37-41*)Subsequent studies have suggested that the dual effects of apoE were dependent on isoform (E3 vs. E4) and/or the extent of lipidation (*42, 43*). Similarly, apolipoprotein J, otherwise known as clusterin, is another chaperone that was identified to facilitate Aβ fibril formation *in vitro* and *in vivo* ((*35, 44, 45*). Some other reported Aβ chaperones include α_1-anti-chymotrypsin (*46, 47*), transthyretin (*36, 48*), proteoglycans (*48, 49*), and gangliosides (*50, 51*). In these reports the study of the interaction of chaperones was restricted to wild-type Aβ peptides. The involvement of these Aβ chaperones in promoting or inhibiting CAA mutant Aβ fibril formation remains largely unknown. With this in mind, one approach we have taken is to identify molecules that preferentially bind to CAA mutant forms of Aβ and may modulate their fibrillar assembly.

1.5 - Myelin Basic Protein

The gene encoding MBP belongs to a large family of developmentally regulated genes called the Golli complex (genes of the oligodendrocyte lineage) (*52-54*). Members of this family are involved in the formation and maintenance of myelin sheaths. However, Golli proteins are also found in fetal spinal chord, thymus, spleen and in cells derived from the immune system (*54*), as well as in neurons (*55, 56*). The Golli locus contains two distinct start sites under independent regulation and consists of 11 exons that can be alternatively spliced to form the various Golli/MBP proteins. Included are 7 exons that encode the MBP proteins (*53*). The major species of MBP are 21.5 kDa, 20.2 kDa, 18.5 kDa, and 17.2 kDa. (*57*). The 21.5 kDa, 20.2 kDa, and 17.2 kDa isoforms are found in fetal and developing brain. In adults the 18.5 kDa and 17.2 kDa isoforms are predominant (*58*).

It is suggested that all of the Golli/MBP proteins exhibit little intrinsic structure so that in their native state they are unfolded (*59, 60*). At least eight charge isomers have been shown to exist for the 18.5 kDa isoform. These result from deamidation, phosphorylation, C-terminal arginine loss, and the deimination of arginyl residues. These post-translational modifications in many cases are thought to regulate myelin assembly, MBP-ligand interactions and signaling functions (*61*). MBP interacts with many different ligands including lipids (*60, 62*), calmodulin (*63*), divalent cations (*64*), GTP (*65*), and cytoskeletal proteins such as tubulin (*66*) and actin (*67*).

Based on the localization of MBP in brain it seems plausible that it may interact with Aβ *in vivo*. For example, Aβ is largely produced by neurons in brain and is released

from axonal terminals (*68, 69*) Myelin sheaths, which are abundant in MBP, insulate neuronal axons placing MBP in proximity to Aβ. Also, several Golli-MBP proteins are themselves expressed in neurons (*55, 56*) and may be secreted by activated microglia (*70*). It is noteworthy that white matter in brain, which is rich in MBP, is largely devoid of fibrillar amyloid deposition. Demyelination, white matter damage, and inflammation are pathological processes from which MBP could be further exposed to interact with Aβ.

CHAPTER 2 - Inhibition of Familial Cerebral Amyloid Angiopathy Mutant Amyloid β-Protein Fibril Assembly by Myelin Basic Protein

2.1 – Summary

Deposition of fibrillar amyloid β-protein (Aβ) in the brain is a prominent pathological feature of Alzheimer disease and related disorders, including familial forms of cerebral amyloid angiopathy (CAA). Mutant forms of Aβ, including Dutch- and Iowa-type Aβ, which are responsible for familial CAA, deposit primarily as fibrillar amyloid along the cerebral vasculature and are either absent or present only as diffuse non-fibrillar plaques in the brain parenchyma. Despite the lack of parenchymal fibril formation *in vivo*, these CAA mutant Aβ peptides exhibit a markedly increased rate and extent of fibril formation *in vitro* compared with wild-type Aβ. Based on these conflicting observations, we sought to determine whether brain parenchymal factors that selectively interact with and modulate CAA mutant Aβ fibril assembly exist. Using a combination of immunoaffinity chromatography and mass spectrometry, we identified myelin basic protein (MBP) as a prominent brain parenchymal factor that preferentially binds to CAA mutant Aβ compared with wild-type Aβ. Surface plasmon resonance measurements confirmed that MBP bound more tightly to Dutch/Iowa CAA double mutant Aβ than to wild-type Aβ. Using a combination of biochemical and ultrastructural techniques, we found that MBP inhibited the fibril assembly of CAA mutant Aβ. Together, these

findings suggest a possible role for MBP in regulating parenchymal fibrillar Aβ deposition in familial CAA.

2.2 – Introduction

Extracellular deposition of amyloid β-protein (Aβ) in the brain is a prominent feature of Alzheimer disease and other related disorders (*1*). Aβ is a 39–43-amino acid peptide that exhibits a high propensity to self-assemble into β-sheet-containing oligomeric forms and fibrils (*2*). Aβ peptides are proteolytically produced from the amyloid β-protein precursor (AβPP), a large type I integral membrane protein, through sequential proteolysis by β- and β-secretase activities (*10, 12-14*). Cerebral deposition of Aβ in the parenchyma can occur as diffuse plaques, with little surrounding pathology, or as fibrillar plaques associated with dystrophic neurons, neurofibrillary tangles, and inflammation (*1*). Fibrillar Aβ deposition also occurs within and along primarily small and medium arteries and arterioles of the cerebral cortex and leptomeninges and in the cerebral microvasculature, a condition known as cerebral amyloid angiopathy (CAA) (*16-18*). This condition accounts for up to 20% of all spontaneous primary intracerebral hemorrhages and is a key pathological lesion in nearly all patients with Alzheimer disease and certain related disorders. Accumulation of fibrillar cerebral vascular Aβ has been shown to cause degeneration and cell death of smooth muscle cells and pericytes in affected larger cerebral vessels and cerebral microvessels, respectively (*18, 20*). Recent findings have implicated cerebral microvascular Aβ deposition in promoting neuroinflammation and dementia in Alzheimer disease (*21-24*).

There exist several familial monogenic forms of CAA resulting from specific point mutations within the Aβ sequence of the AβPP gene (*25-30*). The most recognized example of familial CAA is the Dutch-type E22Q substitution in Aβ (*25, 26, 31*). A more recently identified form of familial CAA is the Iowa-type D23N substitution in Aβ (*30*). Both forms cause early and severe cerebral vascular amyloid deposition and are accompanied by only diffuse parenchymal Aβ deposits with the absence of fibrillar plaques (*30, 31*). Dutch-type CAA is characterized by vascular amyloid-associated neuroinflammation and recurrent, often fatal intracerebral hemorrhages at midlife (*32, 33, 37*), with little or no indication of neurofibrillary tangles and neuronal pathology (*37, 38, 71*). In contrast to the Dutch-type disease, Iowa type CAA appears to be more localized to the cerebral microvasculature, and although cerebral hemorrhage is not common, ischemic damage is observed (*30*). Also, neurofibrillary tangles and robust neuroinflammation can be found associated with the capillary amyloid in Iowa-type CAA (*41*). Both Dutch- and Iowa-type CAAs are accompanied by progressive cognitive impairment that appears to be driven by the extensive vascular amyloid deposition (*40, 41, 71*).

Previous *in vitro* studies from our laboratory (*35, 42, 43, 45*) and others (*44*) have clearly shown that both the Dutch- and Iowa-type mutations increase the fibrillogenic and cerebrovascular cell pathogenic properties of Aβ compared with wild-type Aβ. It is noteworthy that the Dutch-type (E22Q) and Iowa-type (D23N) mutations are adjacent within the Aβ peptide and that both result in loss of a negative charge at their respective sites. We found that including each of these mutations together in the same Aβ peptide

(Dutch/Iowa CAA double mutant Aβ40 peptide (Aβ40DI)) further enhances the fibrillogenic and pathogenic properties *in vitro* (*35*). Furthermore, in transgenic mice, Aβ40DI retains the characteristic pattern of *in vivo* deposition of the Dutch and Iowa mutant peptides, including extensive fibrillar amyloid deposition along the cerebral vasculature accompanied by predominantly diffuse Aβ accumulation in the brain parenchyma (*34*). However, the reason as to why the Dutch- and Iowa-type mutations lead to preferential accumulation of fibrillar amyloid exclusively in the cerebral vasculature and not in the brain parenchyma is unclear.

A number of naturally occurring "Aβ chaperone"-binding molecules that have been reported to modulate fibrillar assembly of the peptide have been identified. For example, apoE has been described to either promote or inhibit Aβ fibril formation *in vitro* (*48-51, 72*). Subsequent studies have suggested that the dual effects of apoE are dependent on the isoform (apoE3 *versus* apoE4) and/or the extent of lipidation (*73-75*). Similarly, apoJ, otherwise known as clusterin, is another chaperone that was identified to facilitate Aβ fibril formation *in vitro* and *in vivo* (*76-78*). Other reported Aβ chaperones that may influence Aβ fibril assembly include α_1-antichymotrypsin (*79, 80*), transthyretin (*81, 82*), proteoglycans (*83, 84*), and gangliosides (*85, 86*). In these reports, the study of the interaction of chaperones was restricted to wild-type Aβ peptides. The involvement of these Aβ chaperones in promoting or inhibiting CAA mutant Aβ fibril formation remains largely unknown. With this in mind, one approach we have taken is to identify molecules that preferentially bind to CAA mutant forms of Aβ and that may modulate their fibrillar assembly.

In this study, we identified myelin basic protein (MBP) as an endogenous brain protein that preferentially binds to familial CAA mutant forms of Aβ. This was demonstrated by a combination of affinity chromatography of normal human brain homogenate and mass spectrometry analysis and confirmed by surface plasmon resonance (SPR) kinetic binding experiments. Furthermore, we show that MBP effectively inhibits the fibrillar assembly of CAA mutant Aβ by biochemical methods as well as by transmission electron microscopy (TEM) and atomic force microscopy (AFM). Therefore, we postulate that MBP may be involved, at least in part, in regulating the compartment-specific fibrillar deposition of CAA mutant Aβ within the brain.

2.3 -- Materials and Methods

Reagents and Chemicals—Aβ peptides were synthesized by solid-phase Fmoc (*N*-(9-fluorenyl)methoxycarbonyl) amino acid chemistry, purified by reverse-phase high performance liquid chromatography, and structurally characterized as described previously (*87*). N-terminally biotinylated Aβ peptides were purchased from American Peptide Company Inc. (Sunnyvale, CA). Aβ peptides were initially prepared in hexafluoroisopropyl alcohol, dried, and resuspended in Me2SO as described previously (*88*). Purified human MBP (purchased from Chemicon International Inc., Temecula, CA) was resuspended in acidic buffer, dialyzed into phosphate-buffered saline (PBS), and stored at -70°C at 1 mg/ml. Purified bovine α-lactalbumin and thioflavin T were purchased from Sigma. Mouse anti-Aβ monoclonal antibody (mAb) 6E10 was purchased from Senetek (Napa, CA). Anti-Aβ mAb 3D6 was generously provided by Lilly. Anti-

Aβ mAb 66.1 was prepared as described (*89*). Mouse anti-MBP mAbs 384 and 382 were purchased from Chemicon International Inc. Biotinylation of mAbs was carried out using EZ-Link sulfosuccinimidyl 6'-(biotinamido)-6-hexanamidohexanoate (Pierce) according to manufacturer's instructions.

Thioflavin T Fluorescence Assay—Lyophilized Aβ peptides were first resuspended with Me2SO to 2.5 mM, diluted to 12.5 μM in PBS, and then incubated at 37°C with rocking either alone or with 1.56 μM MBP or bovine α-lactalbumin. Control samples containing 0.5% Me2SO and 1.56 μM MBP or lactalbumin in PBS were also included. At each time point, 100 μl samples of each reaction were placed in a 96-well microplate in triplicate, and 5 μl of 100 μM thioflavin T was added. The plate was mixed and incubated at 22°C in the dark for 10 min. Fluorescence was measured at 490 nm with an excitation wavelength of 446 nm in a SpectraMax spectrofluorometer (Molecular Devices, Sunnyvale, CA) using SoftMax Pro control software.

Immunohistochemistry—Tg2576 and Tg-SwDI transgenic mice were killed at 24 months, and the brains were removed and bisected through the mid-sagittal plane. Cerebral hemispheres were immersion-fixed with 70% ethanol overnight and subjected to increasing sequential dehydration in ethanol, followed by xylene treatment and embedding in paraffin. Sagittal sections were cut at 10 μm thickness using a microtome, placed in a flotation water bath at 45 °C, and then mounted on ColorFrost Plus slides (Fisher). Paraffin was removed from the sections by washing with xylene, and the tissue

sections were rehydrated in decreasing concentrations of ethanol. Antigen retrieval was performed by treatment with proteinase K (0.001 mg/ml) for 5 min at 22°C. Immunostaining was performed using anti-Aβ mAb 66.1 (1:300 dilution). Primary antibody was detected with horseradish peroxidase-conjugated anti-mouse IgG and visualized with a stable diaminobenzidine solution (Invitrogen). Detection of fibrillar amyloid was performed by incubating the sections with 1% thioflavin S in PBS in the dark for 5 min at 22 °C, followed by washing three times (3 min each) with 50% ethanol. Images were captured using an Olympus BX60 optical microscope and an Olympus DP10 charge-coupled device camera.

Affinity Chromatography of Human Brain Homogenate—To prepare affinity resins, biotinylated wild-type Aβ40 peptide (Aβ40WT) and Aβ40DI were each redissolved in 20 mM NaHCO3 buffer (pH 8.5) and applied to ImmunoPure immobilized streptavidin beads (Pierce) following the manufacturer's instructions. Immobilized ligands were cross-linked with 2mM bis(sulfosuccinimidyl) suberate (Pierce) for 30 min with rocking at room temperature in 20 mM NaHCO3 (pH 8.5). Crosslinking reactions were stopped by the addition of 1 M Tris-HCl (pH 7.4) to a final concentration of 20 mM. Homogenates of normal human brain frontal cortex were prepared in Tris-buffered saline (50 mM Tris-HCl and 200 mM NaCl (pH 7.4)) containing Complete protease inhibitor cocktail (Roche). Homogenates were centrifuged at 12,000 x *g* for 30 min, and supernatants were loaded onto Tris-buffered saline-equilibrated affinity columns (0.8 x 4 cm) under gravity flow. After extensive washing, the columns were eluted with 0.2 M

glycine and 0.15 M NaCl (pH 2.7) and collected into tubes containing 200 mM Tris-HCl, 50 μM iodoacetate, 50 μM 4-(2-aminoethyl) benzenesulfonyl fluoride, 50 μM EDTA, and 50 μg/ml leupeptin. Fractions were analyzed by SDS-PAGE on 10–20% Tris/glycine gradient gels. All runs were carried out at 4°C. Three separate affinity chromatography runs were carried out for each column ligand.

Mass Spectrometry Analysis—Protein bands separated by SDS-PAGE were excised from the polyacrylamide gels and digested overnight with sequencing-grade trypsin *in situ* at 37°C. Samples were run on a Voyager-DE STR MALDI-TOF mass spectrometer (Applied Biosystems) operating in the reflector mode. Samples were dissolved in a 50% solution of acetonitrile and 0.1% trifluoroacetic acid containing α-cyano-4-hydroxycinnamic acid (5 mg/ml) and dried on the sample plate. A nitrogen laser operating at 337 nm was employed to ionize the sample. The accelerating voltage was set to 20 kV employing a 275-ns delay before introduction of ions into the flight tube of the mass spectrometer. The mass scale (*m*/*z* 500–5000) was calibrated with a mixture of peptides (400 fmol/μl), and ~100 laser shots were used to produce each spectrum. Peak lists were submitted to the Mascot search engine with no taxonomy limitation and a peptide tolerance set to 100 ppm.

Immunoblot Analysis—Briefly, samples were heated at 90 °C for 5 min in reducing SDS-PAGE loading buffer, loaded onto gels, and electrophoresed. Gels were transferred to Hybond ECL nitrocellulose membranes (Amersham Biosciences) at 50 V overnight at

4°C. Membranes were blocked in PBS containing 5% milk or bovine serum albumin (BSA; used with biotinylated primary antibodies) at room temperature for 1 h and washed 3 x 10 min with PBS and 0.05% Tween 20. Membranes were incubated with primary antibodies for 1 h and washed as described above. Next, the membranes were incubated with either horseradish peroxidase-conjugated sheep anti-mouse IgG or horseradish peroxidase-conjugated streptavidin (both from Amersham Biosciences) for 1 h and washed. Detection was accomplished using ECL Western blotting substrate (Pierce), and images were captured either on film or using a VersaDoc 3000 imaging system (Bio-Rad) and quantitated with the manufacturer's Quantity One software.

Co-immunoprecipitation—Aβ peptides were resuspended in Me2SO to 2.5 mM and used at 10.8 μM. MBP was used at 1.56 μM. Proteins were combined in 250 μl of incubation buffer (PBS, 0.05% Tween 20, and 1% BSA). Anti-MBP mAb 382 was added to each sample mixture and incubated for 1 h at 4°C with rocking. After incubation, 20 μl of washed GammaBind protein G-Sepharose beads (Amersham Biosciences) were added to each mixture, followed by incubation for an additional 1 h at 4°C with rocking. Beads were separated by centrifugation at 8000 x *g* for 2 min. Supernatants were removed, and beads were washed with 1 ml of incubation buffer. Separation and washing were repeated three times. A final wash was performed in PBS and 0.05% Tween 20 to remove excess BSA. Centrifuged beads were combined with 25 μl of reducing SDS-PAGE loading buffer and heated as described above. 10 μl of each sample/loading buffer mixture was loaded onto 10–20% Tricine gels (Invitrogen) and electrophoresed at 125 V

for 35 min. Immunoblotting was carried out as described above using either biotinylated anti-MBP mAb 384 or biotinylated anti-Aβ mAb 3D6 as primary antibody. Experiments were performed in triplicate.

Dot Blot Analysis—Aβ peptides and the AβPP-(744–763) and AβPP-(100–119) peptides (Multiple Peptide Systems, San Diego, CA) were diluted to 2 μg/ml in Tris-buffered saline from 10 mg/ml Me2SO stock solutions. Insulin (Sigma) was resuspended to 2 mg/ml in water at pH 2.0 and diluted to 2 μg/ml in Tris-buffered saline. 1 μg of each was immobilized onto Hybond ECL nitrocellulose membranes using a Bio-Dot microfiltration apparatus (Bio-Rad) according to the manufacturer's instructions. Each membrane was removed from the apparatus following immobilization and blocked overnight in 5% BSA and PBS at 4°C. The membrane was then incubated in 1 μg/ml MBP in 5% BSA, PBS, and 0.05% Tween 20 for 2 h at room temperature. The membrane was washed 3 x 10 min with 5% BSA, PBS, and 0.05% Tween 20 and incubated with mAb 384 (1:2000 dilution) for 1 h at room temperature. The membrane was next washed 3 x 10 min with PBS and 0.05% Tween 20 and incubated with horseradish peroxidase-conjugated sheep antimouse IgG (1:2000 dilution) for 1 h at room temperature. Detection and quantitation were performed as described above.

Surface Plasmon Resonance—All runs were performed on a Biacore 2000 instrument using 10mM HEPES (pH 7.4), 150mM NaCl, 3 mM EDTA, and 0.005% (v/v) Tween 20 as running buffer and diluent. Streptavidin was conjugated to the surface of three flow

cells of a CM5 chip at 10 μl/min using amine coupling chemistry to a final average response level of 1890.2 response units. N-terminally biotinylated Aβ peptides were resuspended in Me2SO to 2.5 mM and serially diluted to 13 nM immediately before application. Biotinylated Aβ40WT and Aβ40DI were bound to individual flow cells at 10 μl/min to achieve an average relative response level of 157.1 response units, leaving flow cell 1 as reference. This chip preparation procedure was found to result in a surface that minimized mass transfer effects for kinetic interaction experiments. The resultant *R*max of these surfaces was ~700 response units with MBP as analyte. Purified MBP was passed over all four flow cells at 5, 10, 25, 50, and 100 nM at a flow rate of 30 μl/min for kinetic measurements. Faster flow rates did not significantly improve the quality of data. Surfaces were regenerated with 0.2 M glycine (pH 2.0) and 150mM NaCl between runs. The resulting sensorgrams were analyzed by BIAanalysis software. Triplicate concentration series were used for each surface.

Immunoblot Analysis of Aβ40DI Fibril Assembly—Aβ40DI peptides were first resuspended in Me2SO to 2.5 mM, diluted to 12.5 μM in PBS, and then incubated at 37°C with rocking in the presence or absence of 1.56 μM MBP or lactalbumin. At each time point, 20 μl was removed and combined with 20 μl of SDS-PAGE loading buffer. The samples were heated as described above and frozen at -70 °C until assayed. 5 μl of each sample was analyzed for Aβ by quantitative immunoblotting using mAb 6E10 (1:2000 dilution) as described above. Each experiment was performed in triplicate.

Transmission Electron Microscopy—A 20 μl aliquot of the sample mixture was deposited onto a Formvar-coated copper mesh grid. The sample was allowed to stand for 60 s, and excess solution was wicked away. The samples were negatively stained with 2% (w/v) uranyl acetate. The excess stain was wicked away, and the sample was allowed to dry. The samples were viewed with an FEI Tecnai 12 BioTwin transmission electron microscope, and digital images were taken with an Advanced Microscopy Techniques camera.

Atomic Force Microscopy—AFM was carried out using a lifeScan controller (LifeAFM Inc., Port Jefferson, NY) interfaced with a MultiMode microscope (Digital Instruments, Santa Barbara, CA) fitted with an E scanner. With this instrument configuration, only a single contact of the AFM probe is made with the sample per pixel. Computer control of the cantilever position and angle during approach allows for detection of the sample height with minimum cantilever deflection, allowing for a minimum compressive force (30–100 piconewtons/nm) applied to the sample. A complete description of the instrument and application to imaging of soluble Aβ oligomers has been reported (*90*). AFM samples were prepared by adsorbing 20 μl of sample mixture to freshly cleaved ruby mica (S & J Trading, Inc., Glen Oaks, NY) for 45 min to 1 h. The samples were rehydrated with ultrapure Milli-Q water (Millipore Corp., Billerica, MA) and immediately imaged. Samples were imaged using SuperSharpSilicon probes (SSS-CONT, NANOSENSORS, Neuchatel, Switzerland) that were modified for magnetic retraction by attaching samarium cobalt particles. We estimated the effective diameter of

the SuperSharpSilicon probes to be 4 $\pm$ 1 nm at a height of 2 nm. Data analysis and graphics were performed using Interactive Display Language Version 5.0 (Research Systems, Inc., Boulder, CO). In the *Z*-scale bars, numbers in each color square indicate the *Z*-value at the middle of the range for that color.

2.4 -- Results

Aβ40DI Displays Rapid Fibrillar Assembly in Vitro, but Little Brain Parenchymal Assembly in-Vivo—Dutch- and Iowa-type CAA mutant peptides display rapid fibril assembly *in-vitro* (*35, 42-45*). Here, we found that Aβ40DI, containing both the Dutch and Iowa-type mutations, also exhibited markedly enhanced *in-vitro* fibril assembly. Aβ40DI showed rapid assembly compared with Aβ40WT using the thioflavin T fluorescence assay as a measure of fibril formation (Fig. 2.1*A*). The presence of abundant Aβ40DI fibrils (Fig. 2.1*B*) and the lack of Aβ40WT fibrils (Fig. 2.1*C*) was confirmed by TEM analysis.

Although Aβ40DI displays very rapid fibril formation *in-vitro*, fibrillar amyloid is restricted to the cerebral vasculature and is surprisingly absent in the brain parenchyma *in-vivo*. This point is demonstrated by histological analysis of brain tissue from different transgenic mouse lines. The commonly used Tg2576 mouse model produces neuronally derived wild-type Aβ peptides (*91*). Immunostaining Tg2576 mouse brain sections revealed abundant parenchymal Aβ deposits throughout the cortex and mostly in the brain gray matter (Fig. 2.2*A*). Thioflavin S staining of Tg2576 brain sections showed abundant fibrillar parenchymal plaque deposits (Fig. 2.2*C*). On the other hand, the Tg-

SwDI mouse model produces neuronally derived Dutch/Iowa CAA mutant Aβ peptides (*34*). Immunostaining Tg-SwDI mouse brain sections similarly showed abundant parenchymal Aβ accumulation throughout the cortex and again mostly in the brain gray matter (Fig. 2.2*B*). However, in contrast to Tg2576, thioflavin S staining of Tg-SwDI brain sections showed no fibrillar parenchymal plaque deposits (Fig. 2.2*D*). Fibrillar amyloid was restricted only to the cerebral microvasculature as focal deposits, as described previously (*34*). The stark contrast between the rapid fibrillar assembly of Aβ40DI *in-vitro* and the lack of parenchymal fibrillar amyloid in Tg-SwDI mice suggests that unknown brain parenchymal factors may selectively influence CAA mutant fibril assembly and deposition *in-vivo*.

MBP Preferentially Binds to CAA Mutant Aβ40DI—We initially sought to identify brain proteins that may differentially interact with CAA mutant Aβ40DI compared with Aβ40WT. To do this, we prepared affinity columns with Aβ40WT and Aβ40DI by binding and cross-linking each N-terminally biotinylated Aβ peptide to streptavidin beads. Homogenate was prepared from normal human brain tissue and passed through each Aβ40 peptide affinity column. After extensive washing, the bound proteins were eluted and analyzed by SDS-PAGE. As shown in Fig. 3*B*, a major band at ~20 kDa was eluted from the Aβ40DI column. This protein was not present in the Aβ40WT column elution. An additional protein band of ~65 kDa was also preferentially eluted from the Aβ40DI column and not the Aβ40WT column (Fig. 2.3).

Mass spectrometry analysis was performed on a tryptic digest of the ~20-kDa band, yielding multiple peptides (Fig. 2.4). The predicted sequences of nine of these peptides are shown in Table 2.1. These peptides were determined to be homologous to MBP and had sequence homology of >50% to the 18.5-kDa splice variant. To confirm that the ~20-kDa protein eluted from the Aβ40DI affinity column was indeed MBP, we performed immunoblot analysis on the eluates obtained from each of the columns. The ~20-kDa protein that eluted from the Aβ40DI column was strongly recognized by mAb to MBP, as shown in Figure 2.5 (*lane 2*). No MBP was detected by immunoblot analysis of the eluate from the Aβ40WT affinity column (Fig. 2.5, *lane 1*).

Mass spectrometry analysis of a tryptic digest of the ~65 kDa band identified eight peptides, six of which were found to have homology to ORP7 (oxysterol-binding protein-related protein 7). However, the sequence homology for these six peptides was only 8%, and the remaining two peptides could not be matched to any protein (data not shown). ORP7 has a reported mass of ~95 kDa, which is distinct from the ~65-kDa band. In this study, we focused on MBP interactions with Aβ40 peptides because this was the major species identified in the brain homogenate eluates.

Interaction of Aβ Peptides and MBP—To further investigate the interaction of MBP with Dutch/Iowa-type CAA mutant and wild-type Aβ40 peptides, we performed co-immunoprecipitation experiments. Samples of MBP, MBP and Aβ40WT, and MBP and Aβ40DI were incubated with anti-MBP mAb 382 and precipitated with protein G-coated beads (Fig. 2.6*A*). Duplicate immunoblot analysis was performed on each sample with

either biotinylated anti-MBP mAb 384 or biotinylated anti-Aβ mAb 3D6. As shown in Figure 2.6*A*, both Aβ40WT and Aβ40DI were precipitated with MBP in the assay. Neither Aβ peptide was pulled down in the absence of MBP. In addition, we also performed a quantitative dot blot analysis for MBP binding to Aβ and other peptides. Similar to the co-immunoprecipitation experiments, MBP exhibited binding to immobilized Dutch/Iowa mutant and wild-type Aβ peptides (Fig. 2.6, *C* and *D*). In contrast, no MBP binding to other AβPP peptides or insulin was observed.

The binding of Aβ40WT and MBP in these experiments appears to contrast with the results presented in Figures 2.3 and 2.5, which suggested that Aβ40WT does not bind MBP. However, the sample from which MBP was purified on the affinity columns was a total brain homogenate and most likely contained many competing factors that could have interfered with the binding between Aβ40WT and MBP. On the other hand, the co-immunoprecipitation and dot blot analyses were performed using purified proteins free of any potential competing factors.

To more quantitatively analyze the interactions between MBP and Aβ peptides, we next performed SPR measurements. Aβ40 peptide ligand surfaces and other assay parameters were designed to minimize the effects of mass transfer. By passing increasing concentrations of MBP over these surfaces and analyzing the resultant sensorgrams using BIAanalysis software, the kinetics of the interactions were determined. MBP bound more strongly to the Dutch/Iowa-type CAA double mutant Aβ40DI, with $KD = 1.69 \times 10^{-8}$ M. The strength of binding between MBP and Aβ40WT was ~10-fold less, with $KD = 1.15 \times 10^{-7}$ M.

MBP Inhibits CAA Mutant Aβ40DI Fibril Formation in Vitro—The results obtained above indicate that MBP preferentially binds to the more fibrillogenic Aβ40DI compared with the much less fibrillogenic Aβ40WT. We next determined whether this interaction could inhibit the fibrillar assembly of CAA mutant Aβ40DI.

Using the thioflavin T fluorescence assay, we found that Aβ40DI fibrillar assembly was dramatically prevented upon incubation in the presence of an 8-fold lower molar concentration of purified MBP (Fig. 2.7). No change in Aβ40DI thioflavin T fluorescence was seen in the presence of a similarly sized negative control protein (bovine lactalbumin) under these conditions.

The inhibition of fibril assembly of the highly fibrillogenic Aβ40DI by MBP was further examined by immunoblot analysis (Fig. 2.8). Aβ40DI (12.5μM) consisted of monomer and a range of intermediate oligomeric forms at the inception of the experiment and early in the incubation period, reflecting the strong propensity of this mutant form of Aβ to assemble (Fig. 2.8, *A* and *D*). Upon further incubation, assembly of very high molecular mass material was noted by 3 h, which continued to increase for up to 12 h. This increase in high molecular mass assembled peptide was accompanied by a strong concomitant loss of monomer and reduction in intermediate oligomers. The addition of 1.56 μM MBP essentially prevented the progressive assembly of Aβ40DI to high molecular mass assembled material (Fig. 2.8, *C* and *F*), leaving only monomer and intermediate oligomeric forms after 12 h. In the presence of the non-interacting control protein bovine lactalbumin (1.56 μM), there was a minimum effect on the rate of fibril

formation. These results suggest that, at substoichiometric concentrations, MBP effectively inhibits Aβ40DI fibrillar assembly.

Inhibition of fibril assembly was confirmed by TEM and single-touch AFM analyses (Fig. 2.9). At 6 h of incubation in the absence of MBP, Aβ40DI formed dense networks of fibrils as observed by TEM (Fig. 2.9*A*). In the presence of substoichiometric amounts of MBP, no evidence of fibril formation was found, and only amorphous aggregate staining was observed (Fig. 2.9*B*). At an earlier time point of 3 h, high resolution single-touch AFM showed that Aβ40DI formed long, well ordered fibrils with heights of ~4 nm and variable lengths (Fig. 2.9*D*). In the presence of MBP at 3 h, Aβ40DI peptides formed shorter, less-ordered oligomers and protofibrils with heights of ~2 nm and lengths of ~200 nm (Fig. 2.9*E*). TEM and AFM images of MBP alone showed that MBP did not aggregate significantly in these assays (Fig. 2.9, *C* and *F*, respectively).

2.5 -- Discussion

Dutch- and Iowa-type familial CAA mutant Aβ peptides are known to be highly fibrillogenic *in-vitro*. Moreover, Aβ containing both Dutch- and Iowa-type mutations together is markedly more fibrillogenic than that containing either single mutation alone (*35, 42*). Yet despite these enhanced fibrillogenic properties *in-vitro*, these CAA mutant forms of Aβ display little, if any, fibrillar deposition in the brain parenchyma in humans with these mutations or in transgenic mice expressing CAA mutant forms of these peptides in the central nervous system (*30, 31, 34*). The reasons for this disparity remain

unclear. We hypothesized that the brain parenchyma may contain factors that selectively bind to familial CAA mutant forms of Aβ and interfere with their fibrillar assembly and deposition within this specific compartment.

In this study, we have identified MBP as a prominent brain parenchymal factor that preferentially binds to CAA mutant Aβ containing both the Dutch and Iowa mutations and potently inhibits its assembly into fibrils. Similar to the affinity chromatography profiles (Fig. 2.3), SPR kinetic binding experiments showed that MBP had stronger affinity for Aβ40DI. It is somewhat surprising that an interaction between MBP and Aβ40WT was observed in co-immunoprecipitation and dot blot experiments. However, SPR binding measurements showed that the interaction of MBP with Aβ40WT was ~10- fold weaker than that with Aβ40DI. Although this binding interaction was detected, we did not observe MBP in the eluate from the Aβ40WT affinity column. It is possible that MBP was eluted from the Aβ40WT column during the extensive washing steps prior to the elution of the column because of its weaker interaction. Alternatively, perhaps other factors in the total brain homogenate that influenced the interaction between MBP and Aβ40WT were not present in the SPR or co-immunoprecipitation experiments using purified MBP.

Subsequently, we found that the interaction of MBP with the familial CAA mutant Aβ40DI resulted in the inhibition of fibril formation as detected in thioflavin T fluorescence assays (Fig. 2.7). Further analysis of the interaction between MBP and Aβ40DI using quantitative immunoblotting, TEM, and AFM also demonstrated effective inhibition of high molecular mass assembly, yet intermediate oligomeric structures

appeared unaffected (Figs. 2.8 and 2.9). The height of the fibrils and oligomers in the absence of MBP was measured to be ~4 nm (Fig. 2.9*D*), whereas the height of the oligomers in the presence of MBP was reduced to slightly ~2 nm (Fig. 2.9*E*). Although the precise nature of the interaction between Aβ40DI and MBP remains unclear, we speculate that MBP may inhibit fibril formation by capping oligomers and preventing the stacking of protofibrils.

These findings are consistent with the lack of thioflavin-positive parenchymal deposits in the brains of Dutch or Iowa-type familial CAA patients or in transgenic mice expressing cerebral Dutch/Iowa CAA double mutant Aβ peptides (*30, 34, 92*). Although fibrillar parenchymal Aβ deposits are absent in these brains, they do exhibit non-fibrillar diffuse accumulation in the parenchyma. Perhaps these diffuse parenchymal deposits are composed of intermediate oligomeric forms of Aβ similar to those we observed by AFM.

The gene encoding MBP belongs to a large family of developmentally regulated genes called the Golli complex (genes of the oligodendrocyte lineage) (*52-54*). Members of this family are involved in the formation and maintenance of myelin sheaths. However, Golli proteins are also found in fetal spinal chord, thymus, spleen, and cells derived from the immune system (*54*), as well as in neurons (*55, 56*). The Golli locus contains two distinct start sites under independent regulation and consists of 11 exons that can be alternatively spliced to form the various Golli-MBP proteins. Included are seven exons that encode the MBP proteins (*53*). The major species of MBP are 21.5, 20.2, 18.5, and 17.2 kDa (*57*). The 21.5-, 20.2-, and 17.2-kDa isoforms are found in fetal and developing brains. In adults, the 18.5- and 17.2-kDa isoforms are predominant (*58*).

It has been suggested that all of the Golli-MBP proteins exhibit little intrinsic structure, so they are unfolded in their native state (*59, 60*). At least eight charge isomers have been shown to exist for the 18.5-kDa isoform. These result from deamidation, phosphorylation, C-terminal arginine loss, and the deimination of arginyl residues (*93*). In many cases, these post-translational modifications are thought to regulate myelin assembly, MBP-ligand interactions, and signaling functions (*61*). MBP interacts with many different ligands, including lipids (*60, 62*), calmodulin (*63*), divalent cations (*64*), GTP (*65*), and cytoskeletal proteins such as tubulin (*66*) and actin (*67*). The binding of MBP to tubulin and actin is believed to stabilize their polymerization, which is essential to the formation of myelin sheaths (*94*).

Although Dutch and Iowa-type Aβ peptides do not form amyloid in the parenchyma, they strongly assemble and deposit as fibrils in the cerebral vasculature (*30-32, 38*). This suggests that specific factors in the parenchymal or cerebral vascular compartments of the central nervous system might differentially inhibit or enhance CAA mutant Aβ fibril formation. For example, we showed recently that specific gangliosides, that are found abundantly in cultured cerebrovascular cells and in isolated cerebral vessels, but not in the parenchyma, selectively promotes fibrillar assembly of these CAA mutant forms of Aβ (*46*). On the other hand, MBP may represent a parenchyma derived factor that inhibits CAA mutant Aβ from assembling into parenchymal fibrillar deposits, thus allowing it to travel to the cerebral vasculature, where it rapidly assembles and accumulates as fibrillar amyloid.

There are several possibilities as to how MBP may interact with Aβ *in-vivo*. For example, Aβ is produced largely by neurons in the brain and is released from axonal terminals (*68, 69*). Myelin sheaths, which contain a high abundance of MBP derived from oligodendrocytes, insulate neuronal axons, and MBP is thereby within proximity to Aβ. It is noteworthy that several Golli-MBP proteins are themselves expressed in neurons (*55, 56*). It is significant that white matter in the brain, which is rich in MBP, is largely devoid of fibrillar amyloid deposition. This is supported by the near absence of Aβ deposits in white matter of transgenic mouse brain (Fig. 2.2). Also, demyelination and white matter damage are pathological processes by which MBP could be further exposed to interaction with Aβ. Finally, although MBP is present largely in the brain as a cellular protein, soluble forms of MBP are readily detected in the cerebrospinal fluid of normal individuals and are elevated in several neurological disorders (*95, 96*). Thus, soluble forms of MBP are in position to interact with released Aβ peptides in the brain.

In conclusion, we have demonstrated that MBP preferentially interacts with CAA mutant forms of Aβ *in-vitro*. Such an interaction may influence Aβ fibrillogenesis and deposition in the central nervous system. The ultimate test of the physiological relevance of this interaction will involve ongoing future studies in which CAA mutant Aβ-depositing transgenic mice are placed on backgrounds of increased or decreased MBP expression to determine whether MBP influences the amount, form, or regional accumulation of Aβ. Further investigation of this interaction may yield a better understanding of factors that govern regional amyloid deposition in the brain. Nevertheless, our findings suggest that MBP could serve as a novel platform for

developing approaches to regulate pathological accumulation of CAA mutant (and perhaps wild-type) Aβ in disease.

2.6 -- Tables and Figures

Start - End	Observed	Mr(expt)	Mr(calc)	Delta	Miss	Sequence
1 - 19	2077.98	2076.97	2077.02	-0.05	1	AATSESLDVMASQKRPSQR Ox (M)
24 - 35	1336.63	1335.62	1335.62	-0.01	0	YLATASTMDHAR
36 - 41	726.40	725.40	725.40	-0.00	0	HGFLPR
42 - 53	1339.70	1338.69	1338.70	-0.01	1	HRDTGILDSIGR
44 - 53	1046.54	1045.54	1045.54	-0.00	0	DTGILDSIGR
54 - 59	698.32	697.32	697.32	-0.00	0	FFGGDR
90 - 101	1460.71	1459.70	1459.71	-0.01	0	TQDENPVVHFFK
90 - 107	2141.10	2140.09	2140.11	-0.02	1	TQDENPVVHFFKNIVTPR
124 - 140	1828.85	1827.84	1827.84	-0.00	0	FSWGAEGQRPGFGYGGR

AATSESLDVMASQKRPSQRHGSKYLATASTMDHARHG
FLPRHRDTGILDSIGRFFGGDRGAPKRGSGKDSHHPAR
TAHYGSLPQKSHGRTQDENPVVHFFKNIVTPRTPPPSQ
GKGRGLSLSRFSWGAEGQRPGFGYGGRASDYKSAHK
GFKGVDAQGTLSKIFKLGGRDSRSGSPMARR

Table 2.1 Major mass peaks obtained from the mass spectrometry analysis were submitted to the Mascot search engine. The predicted amino acid sequences are shown. The predicted sequences showed strong alignment with human MBP. Sequence homology (underlined) of the obtained peptide sequences was >50% for MBP.

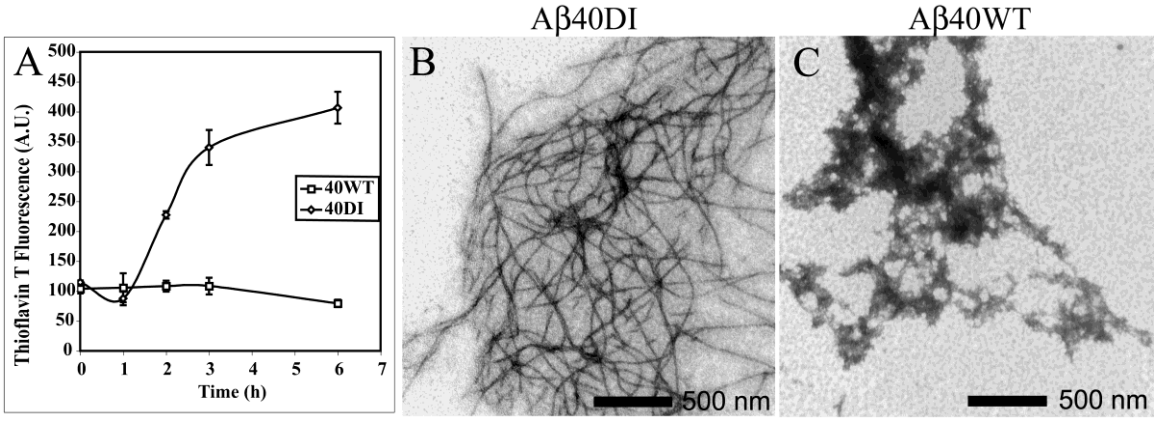

FIGURE 2.1 **Rapid fibril assembly of Dutch/Iowa CAA mutant Aβ.** Hexafluoroisopropyl alcohol-treated Aβ peptides were incubated at 12.5 μM in PBS at 37°C for 6 h. *A*, 6-h time course of Aβ40WT and Aβ40DI fibril formation measured by thioflavin T fluorescence as described under "Materials and Methods." Data represent the means ± S.D. of triplicate samples. *B* and *C*, representative TEM images of Aβ40DI and Aβ40WT, respectively, after 6 h of incubation. *A.U.*, arbitrary units.

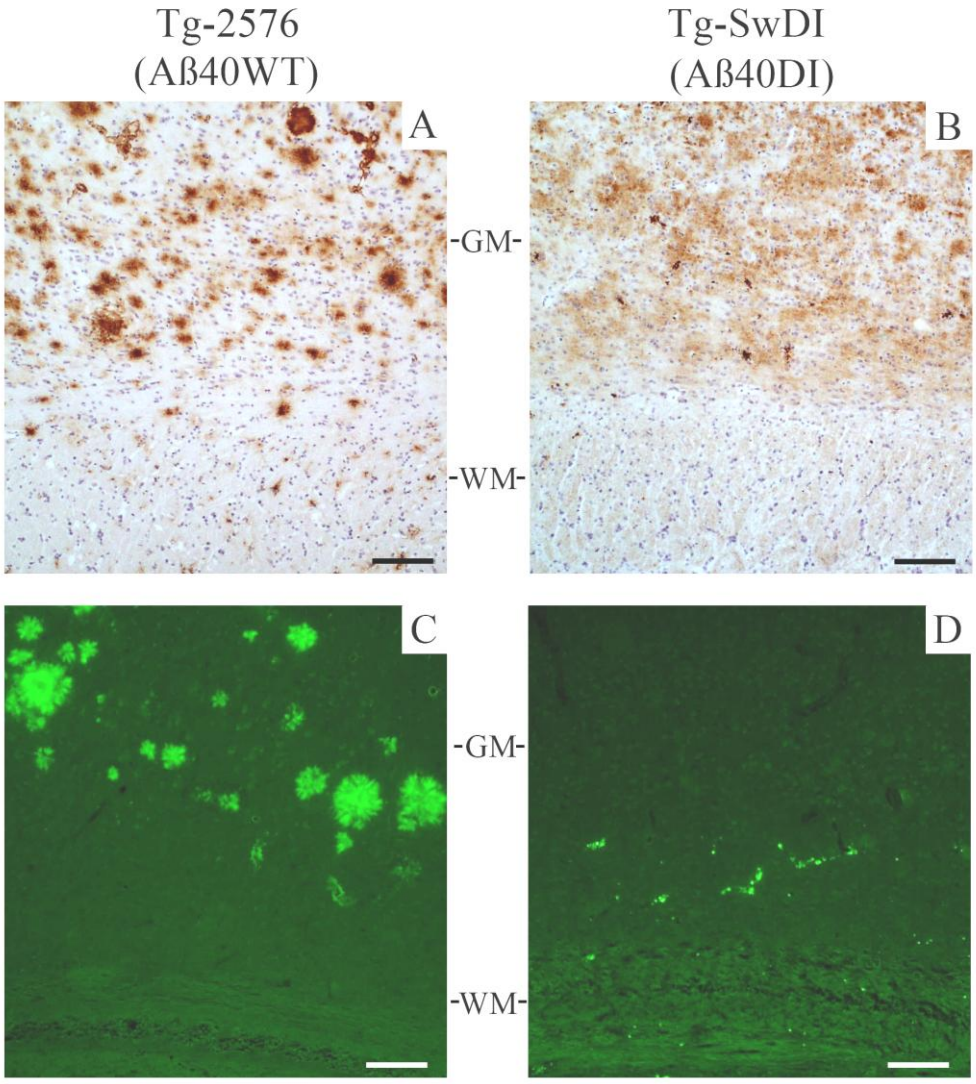

FIGURE 2.2 **Immunohistochemical analysis of Aβ deposition in transgenic mouse brain.** Presented are mid-sagittal cross-sections of the brain cortices of Tg2576 (*A* and *C*) and Tg-SwDI (*B* and *D*) mice at 24 months of age showing both gray matter (*GM*) and white matter (*WM*). In *A* and *B*, sections were immunostained with anti-Aβ mAb 66.1 as described under "Materials and Methods." In *C* and *D*, fibrillar amyloid was detected by staining with thioflavin S under "Materials and Methods." *Scale bars* = 50 μm.

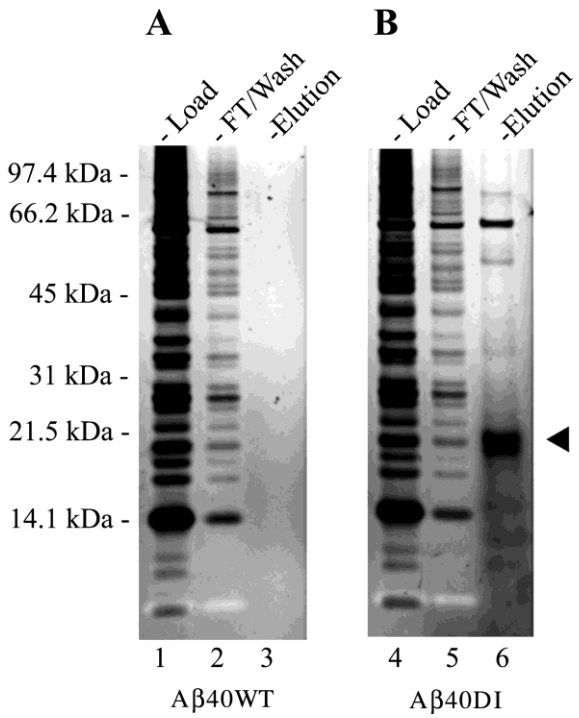

FIGURE 2.3 **Isolation of human brain proteins that selectively bind to CAA mutant forms of Aβ.** Homogenates were prepared from normal human brain frontal cortex and passed through affinity columns prepared from wild-type (*A*) or Dutch/Iowa CAA double mutant (*B*) Aβ40. The columns were extensively washed, eluted with a low pH buffer, and immediately neutralized. Aliquots of each fraction from each column were analyzed by SDS-PAGE and silver staining. The *arrowhead* designates a prominent band of ~20 kDa that was eluted from the Dutch/Iowa Aβ column (*lane 6*), but not from the wild-type Aβ column (*lane 3*). A band identified at ~65 kDa also specifically eluted from the CAA mutant Aβ40DI column. *Lanes 1* and *4*, brain homogenate load; *lanes 2* and *5*, column flow-through (*FT*) and wash; *lanes 3* and *6*, column eluates.

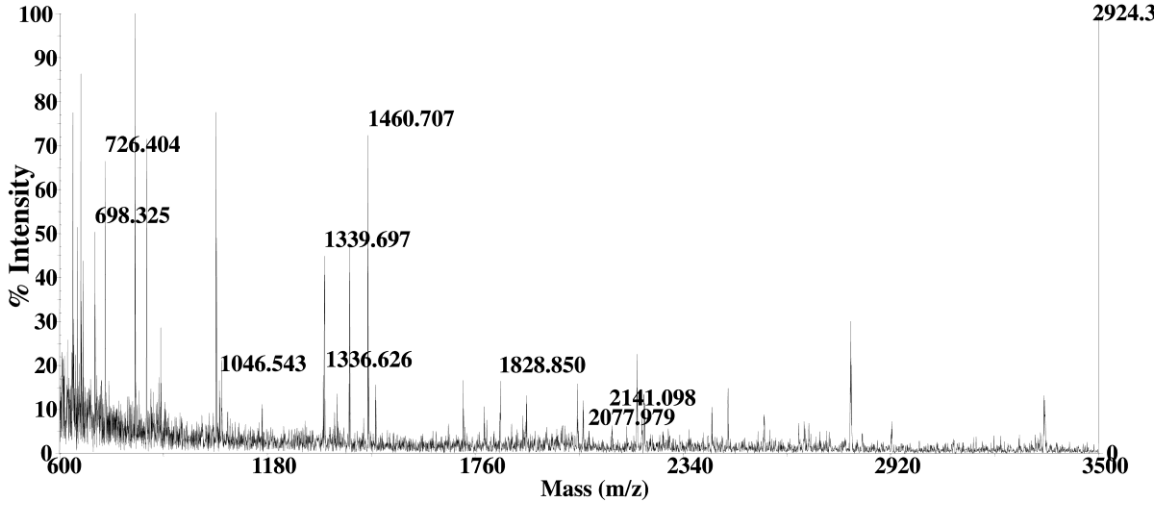

FIGURE 2.4 **Mass spectrometry analysis of trypsin-digested ~20-kDa CAA mutant Aβ-binding protein.** The ~20-kDa protein that bound to Aβ40DI was digested with trypsin and analyzed using a MALDI-TOF mass spectrometer. A number of prominent peptides between ~0.7 and 2.2 kDa were identified.

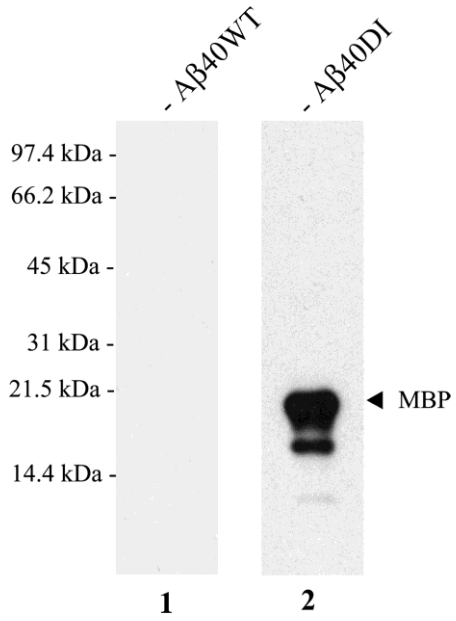

FIGURE 2.5 **Immunoblot for MBP in Aβ affinity column eluates.** Equivalent amounts of eluates from each of the Aβ affinity columns as shown in Fig. 3 were subjected to immunoblotting using mouse anti-MBP mAb 384. *Lane 1*, wild-type Aβ column eluate; *lane 2*, Dutch/Iowa-type Aβ column eluate.

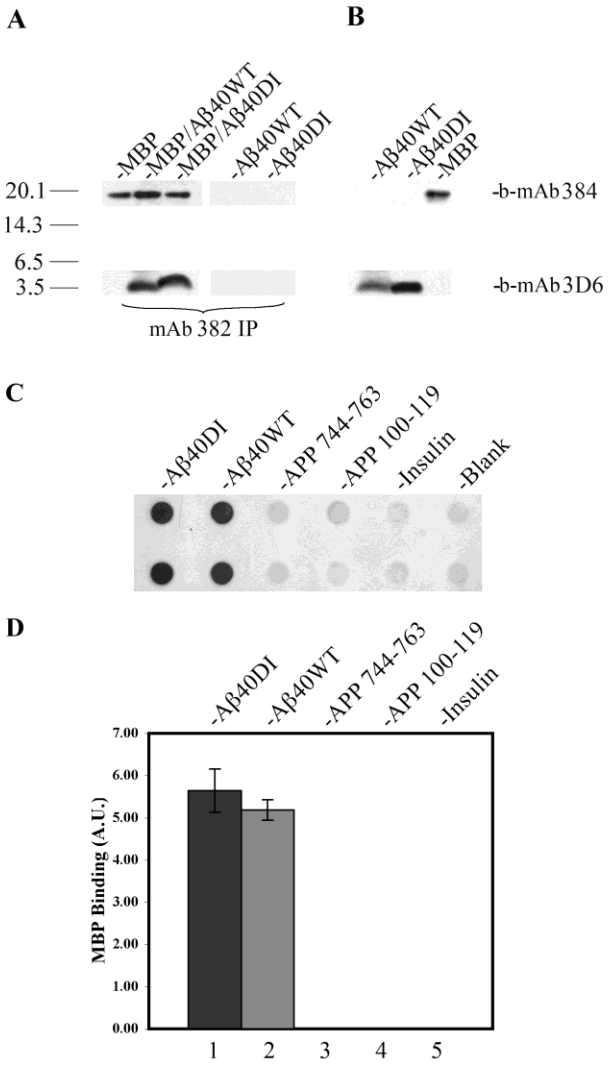

FIGURE 2.6 **Interaction of MBP and Aβ peptides.** Aβ peptides were immunoprecipitated (*IP*) with MBP using anti-MBP mAb 382. *A*, immunoprecipitated samples from *left* to *right*: MBP alone, MBP incubated with Aβ40WT, MBP incubated with Aβ40DI, Aβ40WT alone, and Aβ40DI alone. *B*, Western blot controls from *left* to *right*: Aβ40WT, Aβ40DI, and MBP. Duplicate immunoblots of all samples were prepared and probed with either biotinylated (*b*) anti-MBP mAb 384 or biotinylated anti-Aβ mAb 3D6 as described under "Materials and Methods." *C*, representative dot blot analysis of MBP binding to Aβ and control peptides. *APP*, AβPP. *D*, quantitation of MBP binding to peptides by dot blot analysis. Data represent the means ± S.D. (*n*=4 for each peptide). *Bar 1*, Aβ40DI; *bar 2*, Aβ40WT; *bar 3*, AβPP-(744 – 763); *bar 4*, AβPP- (100 –119); *bar 5*, insulin. *A.U.*, arbitrary units.

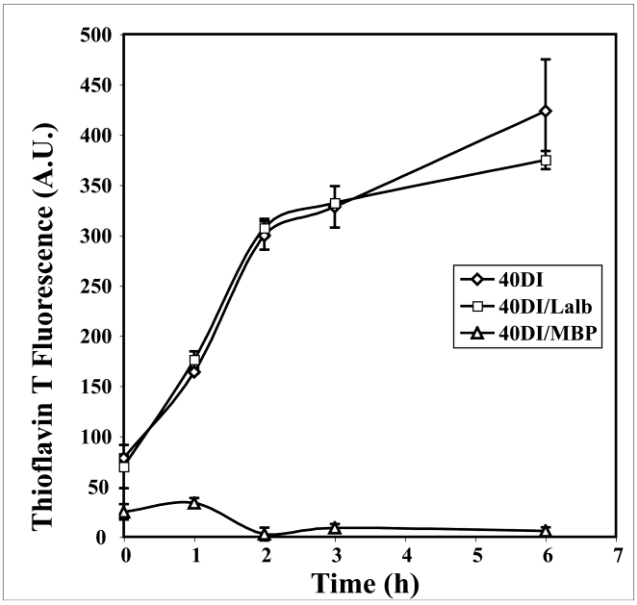

FIGURE 2.7 **Thioflavin T analysis of inhibition of CAA mutant Aβ fibril formation by MBP.** Aβ40DI was treated with hexafluoroisopropyl alcohol, resuspended to a concentration of 2.5 mM in Me2SO, and then diluted to a concentration of 12.5 μM in PBS in the absence (◊) or presence of 1.56 μM MBP(△) or bovine α-lactalbumin (*Lalb*;□) as a control. At specific time points, aliquots were collected from each sample and analyzed by thioflavin T binding and fluorescence to determine fibrillar assembly. Data represent the means ± S.D. of triplicate samples. *A.U.*, arbitrary units.

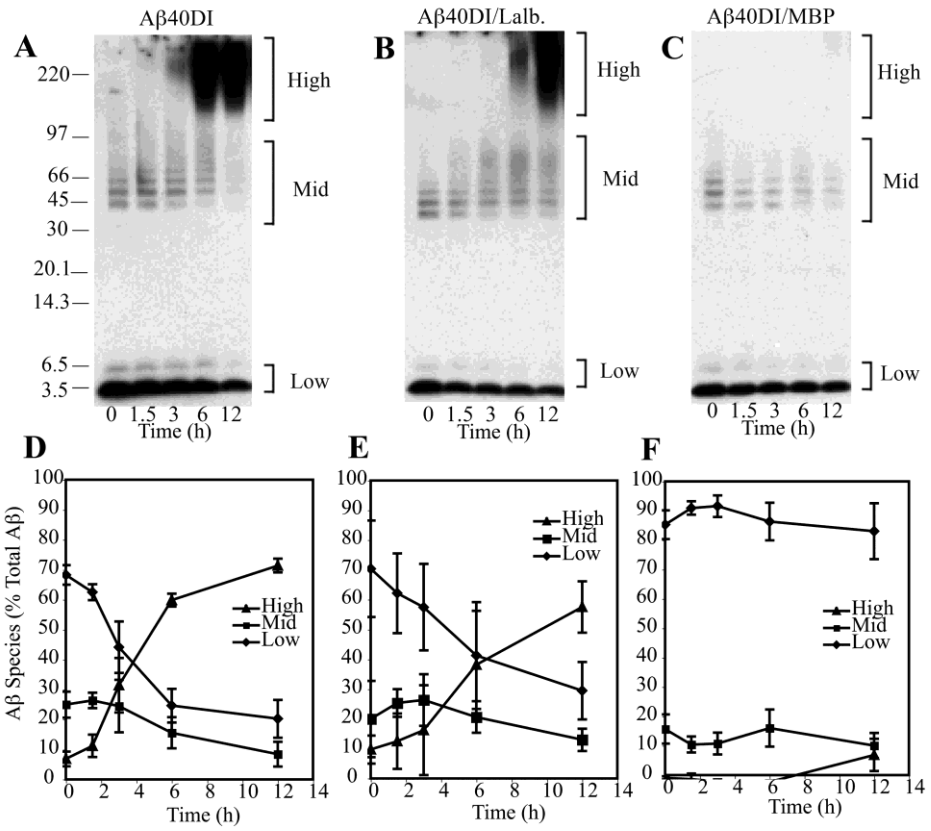

FIGURE 2.8 **Quantitative immunoblot analysis of MBP inhibition of Aβ40DI fibril assembly *in-vitro*.** Aβ40DI (12.5 μM) was incubated in the absence (*A* and *D*) or presence (*C* and *F*) of 1.56 μM purified MBP. Bovine α-lactalbumin (*Lalb.*; 1.56 μM) was included as a negative control (*B* and *E*). Aliquots were removed at specific time points and analyzed by quantitative immunoblot analysis using anti-Aβ mAb 6E10. *A*, representative immunoblot of Aβ40DI incubated alone for up to 12 h; *B*, representative immunoblot of Aβ40DI incubated with bovine α-lactalbumin for up to 12 h; *C*, representative immunoblot of Aβ40DI incubated with MBP for up to 12 h; *D–F*, relative abundance of low, mid, and high molecular mass species of Aβ40DI as determined by quantitative immunoblot analysis in the absence (*D*) or presence of bovine α-lactalbumin (*E*) or MBP (*F*). Data represent the means ± S.D. of three separate experiments.

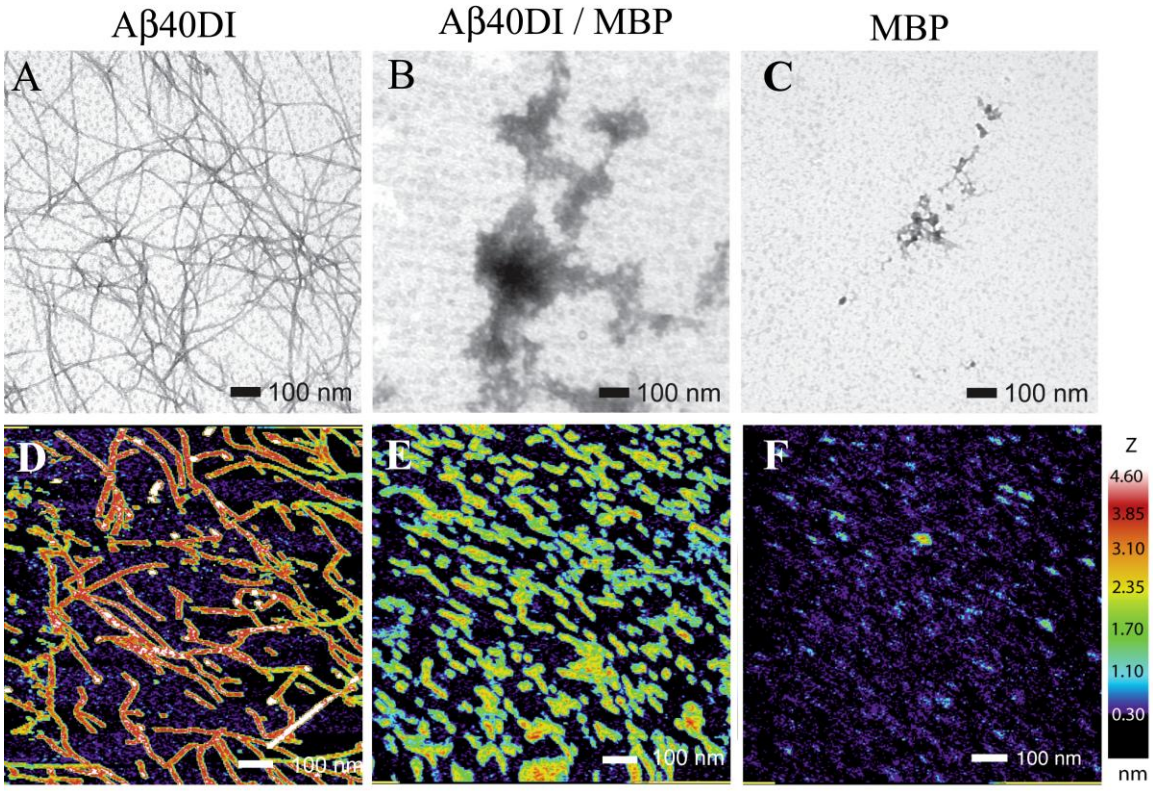

FIGURE 2.9 **Inhibition of Aβ40DI fibril formation by MBP as assessed by TEM and single-touch AFM analyses.** Aβ40DI peptides were treated with hexafluoroisopropyl alcohol, resuspended to a concentration of 2.5 mM in Me2SO, and then diluted to a concentration of 12.5 μM in PBS in the absence or presence of 1.56 μM MBP. Samples were imaged at 6 h by TEM (*A* and *B*) and at 3 h by single-touch AFM (*D* and *E*). Aliquots of 1.56 μM MBP alone were imaged by TEM (*C*) and by AFM (*F*).

CHAPTER 3 - Myelin Basic Protein Binds to and Inhibits the Fibrillar Assembly of Aβ42 in-vitro

3.1 -- Summary

The deposition of amyloid β-protein (Aβ) fibrils into plaques within the brain parenchyma and along cerebral blood vessels is a hallmark of Alzheimer's disease. Aβ peptides are produced through the successive cleavage of the Aβ precursor protein by β and γ- secretase, producing peptides of between 39 and 43 amino acids in length. The most common of these are Aβ40 and Aβ42, the first of which being the most abundant. Aβ42 is more fibrillogenic than Aβ40 and has been implicated in early Aβ plaque deposition. Our previous studies determined that myelin basic protein (MBP) was capable of inhibiting fibril formation of a highly fibrillogenic Aβ peptide containing both E22Q (Dutch) and D23N (Iowa) mutations associated with familial forms of cerebral amyloid angiopathy [Hoos et al. 2007 J. Biol. Chem. 282:9952-9961]. In the present study we show through a combination of biochemical and ultrastructural techniques that MBP is also capable of inhibiting the β-sheet fibrillar assembly of the normal Aβ42 peptide. These findings suggest that MBP may play a role in regulating the deposition of Aβ42 and thereby also may regulate the early formation of amyloid plaques in Alzheimer's disease.

3.2 -- Introduction

Deposits of amyloid β peptides (Aβ) into plaques in the brain parenchyma and cerebrovasculature are prominent features of Alzheimer's disease (AD) and other related disorders *(1)*. Aβ is derived through the sequential proteolysis of the amyloid β precursor protein (AβPP) by β and γ-secretase *(3-6)*. These cleavages produce Aβ peptides of between 39 and 43 amino acids with the most abundant being Aβ40 and Aβ42 (*97*). Aβ peptides exhibit a high propensity to self-assemble into β-sheet containing oligomeric forms and fibrils (*2*). It has been shown that the oligomerization and deposition of Aβ42 likely precedes and, possibly, seeds deposition of Aβ40 in amyloid plaques and cerebral vascular lesions leading to neurodegeneration and dementia (*98-100*). Elevated levels of soluble Aβ42 have also been shown to increase the risk of developing AD pathology (*100*). For these reasons it is important to understand the nature of Aβ42 in the CNS and how it interacts with other components of healthy and diseased brain.

Cerebral amyloid angiopathy (CAA), a condition prevalently found in AD, is characterized by fibrillar Aβ deposition within and along primarily small and medium-sized arteries and arterioles of the cerebral cortex and leptomeninges and in the cerebral microvasculature (*2, 16, 17*). Familial forms of CAA are caused by specific point mutations within the Aβ sequence of the AβPP gene (*24-29*). The most recognized example of familial CAA is the Dutch-type resulting from an E22Q substitution in Aβ, (*24, 25, 30*). Another more recently identified form of familial CAA is the Iowa-type D23N substitution in Aβ (*29*). *In vitro* these familial forms of Aβ exhibit an increased propensity to form amyloid fibrils when compared to wild-type Aβ40 (Aβ40WT) *(35, 42-*

45). Including each of these mutations together in the same Aβ peptide (Aβ40DI) further enhances the fibrillogenic and pathogenic properties *in vitro* (*35*). In a recent study using a combination of biochemical assays and high resolution microscopy techniques, we demonstrated that myelin basic protein (MBP) bound preferentially to the more fibrillogenic Aβ40DI over Aβ40WT (*101*). Furthermore, we showed that MBP effectively inhibits the fibrillar assembly of Aβ40DI. We postulated that MBP might play a role in the regulation of familial CAA mutant Aβ fibrillogenesis. However, with the growing understanding of the importance of Aβ42WT to disease processes such as AD and CAA, we examined if MBP can act in a similar fashion on this more fibrillogenic wild-type Aβ peptide as well.

In the present study we show that MBP binds to Aβ42WT *in-vitro*. Using a combination of biochemical assays and high resolution microscopy, we demonstrate that MBP impedes β-sheet formation and potently inhibits Aβ42WT fibril formation. These findings lead us to postulate that endogenous MBP may play a role in regulating the fibrillar assembly and deposition of Aβ42WT in Alzheimer's disease and other related conditions.

3.3 -- Materials and Methods

Reagents and Chemicals — Aβ42 peptide was synthesized by solid-phase Fmoc (9-fluorenylmethoxycarbonyl) amino acid chemistry, purified by reverse phase high performance liquid chromatography, and structurally characterized as previously described (*87*). N-terminally biotinylated Aβ42 peptide was purchased from American

Peptide Company (Sunnyvale, CA). Aβ42 peptides were initially prepared in hexafluoroisopropanol, lyophilized, and resuspended in either dimethylsulfoxide (Me_2SO) or 100 mM NaOH as previously described (*88*). Purified human MBP (purchased from Chemicon International, Temecula, CA) was resuspended in acidic buffer, dialyzed into phosphate-buffered saline (PBS) and stored at -70°C at 1 mg/ml. Purified bovine lactalbumin and thioflavin-T were purchased from Sigma-Aldrich (St. Louis, MO). Anti-Aβ mouse monoclonal antibody (mAb) 6E10 was purchased from Senetek (Napa, CA). The anti-Aβ mAb3D6 was generously provided by Lilly Research Laboratories (Indianapolis, IN). Anti-MBP mouse mAb384 and mouse mAb382 were purchased from Chemicon International. Biotinylation of mAbs was carried out using EZ-Link Sulfo-NHS-LC-LC-biotin (Pierce, Rockford, IL) according to manufacturer's instructions.

Co-Immunoprecipitation — Aβ42 peptides were resuspended in Me_2SO to 2.5 mM and used at 10.8 μM. MBP was used at 1.56 μM. Proteins were combined in 250 μl incubation buffer (PBS / 0.05% Tween 20 / 1% BSA). Anti-MBP mAb 382 was added to each sample mixture and incubated for 1 h at 4°C with rocking. After incubation 20 μl of washed GammaBind protein G Sepharose beads (Amersham) were added to each mixture, which then were incubated for an additional 1 h at 4°C with rocking. Beads were separated by centrifugation at 8,000 x *g* for 2 min. Supernatants were removed and beads were washed with 1 ml of incubation buffer. Separation and washing were repeated three times. A final wash was performed in PBS/0.05% Tween 20 to remove

excess BSA. Centrifuged beads were combined with 25 μl of reducing SDS-PAGE sample loading buffer and heated as described above. 10 μl of each sample/loading buffer mix were loaded onto 10-20% Tricine gels (Invitrogen) and electrophoresed at 125 V for 35 min. Immunoblotting was carried out as described above using either biotinylated anti-MBP mAb 384 or biotinylated anti-Aβ mAb 3D6 as primary antibodies. Experiments were performed in triplicate.

Surface Plasmon Resonance — All runs were performed on a BiaCore 2000 instrument (Uppsala, Sweden) with 10 mM HEPES pH 7.4, 150 mM NaCl, 3 mM EDTA, 0.005% (v/v) Tween 20 as running buffer and diluent. N-terminally biotinylated Aβ42 peptides were resuspended in Me_2SO to 2.5 mM and serially diluted to 13 nM immediately before application. Aβ42 was bound to flow cell 2 at 10 μl/min to achieve an average relative response level of 157.1 RU leaving flow cell 1 as a reference. This chip preparation procedure was found to result in a surface that minimized mass transfer effects for kinetic interaction studies. The resultant R_{max} of this surface was approximately 700 RU with MBP as the analyte. Purified MBP was passed over both flow cells at 5, 10, 25, 50, and 100 nM in triplicate at flow rates of 30 μl/min for kinetic measurements. Faster flow rates did not significantly improve the quality of data. Surfaces were regenerated with 0.2 M glycine pH 2.0, 150 mM NaCl between runs. The resulting sensorgrams were analyzed by BiaCore Analysis software.

Circular Dichroism Spectroscopy — Lyophilized Aβ42 peptides were first resuspended with 100 mM NaOH to 2.4 mM, diluted to 50 μM in 10 mM potassium phosphate, pH 8.0/11 mM NaCl, and then incubated at 37°C either alone or with 6.25 μM MBP. CD measurements from 190 nm to 260 nm were carried out using an Olis RSM 1000 CD Spectrophotometer (On-Line Instrument Systems, Bogart, GA). Six scans using adaptive acquisition timing were averaged for each sample using Olis software. The 1 mm quartz cuvettes used for sample data collection were cleaned between readings using 6N HCl followed by a methanol rinse.

Attenuated Total Reflection Infrared Spectroscopy — Lyophilized Aβ42 peptides were first resuspended with 100 mM NaOH to 2.4 mM, diluted to 50 μM in PBS and then incubated at 37°C either alone or with 6.25 μM MBP. At the required timepoints 100 ug of protein were dried onto an ATR plate and scanned using a Brucker IFS 66v/S infrared spectrometer. Spectra were recorded using 2000 scans over the range of 4000-400 cm^{-1}.

Thioflavin T Fluorescence Assay — Lyophilized Aβ42 peptides were first resuspended with Me_2SO to 2.5 mM, diluted to 12.5 μM in PBS, and then incubated at 37°C with rocking either alone, with 1.56 μM MBP, or with 1.56 μM bovine lactalbumin. Control samples containing 0.5% Me_2SO and 1.56 μM MBP, or 1.56 μM lactalbumin in PBS were also included. At each timepoint, 100 μl samples of each reaction were placed in a 96-well microplate in triplicate and 5 μl of 100 μM thioflavin T was added. The plate was mixed and incubated at 22°C in the dark for 10 min. Fluorescence was measured at

490 nm using an excitation wavelength of 446 nm in a SpectraMax spectrofluorometer (Molecular Devices, Sunnyvale, CA) using SoftMax Pro control software.

Transmission Electron Microscopy — Sample mixtures were deposited onto carbon-coated copper mesh grids (EM Sciences, Hatfield, PA) and negatively stained with 2% (w/v) uranyl acetate. The samples were viewed with a FEI Tecnai 12 BioTwin transmission electron microscope, and digital images were taken with an AMT camera.

Atomic Force Microscopy — AFM was carried out using a LifeScan controller developed by LifeAFM (Port Jefferson, NY) interfaced with a Digital Instruments (Santa Barbara, CA) MultiMode microscope fitted with an E scanner. AFM samples were first titrated to pH 4 using dilute HCl and then adsorbed onto freshly cleaved ruby mica (S & J Trading, Glen Oaks, NY). The lower pH allows for better adsorption of Aβ42 peptides to the negatively charged mica surface. Samples were imaged under hydrated conditions using super-sharp silicon probes (SSS-Cont, Nanosensors, Neuchatel, Switzerland) that were modified for magnetic retraction by attaching samarium cobalt particles (LifeAFM, Port Jefferson, NY). We estimate the effective diameter of the super-sharp silicon probes to be 4 ± 1 nm at a height of 2 nm. Data analysis and graphics was performed using Interactive Display Language 5.0 (Research Systems Inc., Boulder, CO). In the Z scale bars, numbers in each color square indicate the Z-value at the middle of the range for that color.

3.4 -- Results

MBP interacts with fibrillogenic Aβ42 peptide—Previously, we reported the interaction of MBP with a familial CAA mutant Aβ40 peptide containing E22Q (Dutch) and D23N (Iowa) mutations (Aβ40DI). It was also shown that MBP could bind the Aβ40WT peptide, but with significantly less affinity (*101*). Here, we demonstrate using co-immunoprecipitation that MBP also interacts with the longer, more fibrillogenic, Aβ42WT peptide. Samples containing MBP alone, MBP and Aβ42WT, or Aβ42WT alone were incubated with anti-MBP mAb 382 and precipitated with protein G-coated beads (Fig. 3.1). Duplicate immunoblot analyses were performed on each sample with either biotinylated anti-MBP mAb 384 or biotinylated anti-Aβ mAb 3D6. Aβ42WT was precipitated only in the presence of MBP and was not pulled down in the absence of MBP.

To more quantitatively analyze the affinity between MBP and Aβ42, we next performed SPR measurements. Aβ42WT peptide ligand surfaces and other assay parameters were designed as described in Methods. Increasing concentrations of MBP were passed over the ligand surface and the resultant sensorgrams were analyzed using BIAanalysis software. From this, the kinetics of the interactions were determined (Table 3.1). The calculated K_D between MBP and Aβ42WT is comparable to the affinity between MBP and Aβ40DI, and is stronger than that between MBP and Aβ40WT as reported previously (*101*).

MBP prevents the formation of β-sheet structures in Aβ42WT in-vitro—After demonstrating the affinity between Aβ42WT and MBP *in vitro* we next determined if this

interaction could inhibit Aβ42WT fibrillogenesis. The assembly of fibrils from Aβ monomers is accompanied by the formation of β-sheet secondary structure within and between individual monomers (*102*). Therefore, we sought to examine the effect of MBP on the secondary structure of Aβ42WT using circular dichroism spectroscopy during fibrillogenesis.

First, we measured the time dependent CD spectra between 190-260 nm for Aβ42WT, making scans at regular intervals from 0-36 h (Fig. 3.2A). At 0 h, the Aβ42WT CD spectra displayed a characteristic negative peak at 197 nm, which correlates with the presence of abundant random-coil conformation. Over the course of 36 h, Aβ42WT adopts a predominantly β-sheet conformation as shown by the emergence of a characteristic positive peak at 195 nm and a negative peak at 215 nm. Similar incubations were also performed on Aβ42WT with MBP, as well as with MBP alone. Throughout the time-course, MBP exhibited a characteristic random-coil conformation (data not shown) as has been previously reported (*103*).

It has been shown that plotting the absolute value of the CD signal at 215 nm versus time produces a curve indicative of the formation of β-sheet fibrils over time for Aβ peptides (*104*). In Fig. 3.2B the absolute values of the CD ellipticity for both MBP alone and Aβ42WT with MBP were compared to Aβ42WT alone. These data illustrate that Aβ42WT β-sheet formation proceeds linearly until 24 h where it begins to plateau. Conversely, for both MBP alone and Aβ42WT with MBP the signal remained low and decreased somewhat over the course of incubation, suggesting a lack of β-sheet formation. At 48 h, a sample of Aβ42WT, which demonstrated a high abundance of β-

sheet, was spiked with MBP and scanned immediately (Fig. 3.2C). This was compared to a scan at 48 h of Aβ42WT with MBP to illustrate the difference between a sample containing MBP in the presence of β-sheet structure, and a sample containing MBP and no β-sheet structure. These data suggest that MBP is able to inhibit the formation of β-sheet structures from unstructured Aβ42WT monomers.

Attenuated total reflection (ATR) infrared spectroscopy was used to further examine the secondary structure of Aβ42WT in the presence of MBP. The IR spectra of a protein, especially absorbance in the Amide I band (~1700-1600 cm^{-1}), is sensitive to changes in secondary structure (*105-107*). Spectra obtained for Aβ42WT incubated at 37°C for 24h had a main peak at 1635 cm^{-1} with a smaller shoulder peak at 1616 cm^{-1}, which were assigned to major β-sheet structure. The peak at 1673 cm^{-1} is due to β-turn structure. When Aβ42WT is incubated in the presence of MBP we measured two unresolved peaks at 1670 cm^{-1} and 1648 cm^{-1} assigned to β-turn and α-helical/unordered structures respectively (Fig 3.3A).

The contributing peaks in the Amide I band however are overlapping and convoluted making interpretation of secondary structure difficult in many cases as it is with these data. By plotting the second-derivative of the spectra the contributing components can be resolved and their relative contribution studied (*105*). When plotted in this way we see that both Aβ42WT alone and Aβ42WT with MBP contain identical peaks at 1681 cm^{-1} and 1675 cm^{-1} due to the presence of β-turn structure. Aβ42WT with MBP shows two peaks at 1658 cm^{-1} and 1650 cm^{-1} assigned to α-helical and unstructured elements. Both samples with and without MBP have peaks of 1697 cm^{-1} and 1616 cm^{-1}

in the β-sheet regions however the contribution is higher in the Aβ42WT sample without MBP. Aβ42WT alone also shows a strong β-sheet contribution at 1633 cm-1 that is much larger than the peak at 1635 cm^{-1} for Aβ42WT with MBP. The signal at 1635 cm^{-1} also is more shifted away from β-sheet and towards the α-helical and unstructured region of the band and contains unresolved α-helical and unstructured elements as well in its shoulder (Fig 3.3B). This confirms the CD measurements that show less β-sheet structure in Aβ42WT in the presence of MBP.

This inhibitory affect was also confirmed by using a thioflavin T fluorescence assay. We found that an 8-fold lower molar concentration of MBP was sufficient to dramatically inhibit Aβ42WT fibril formation (Fig. 3.4). No change in Aβ42WT thioflavin T fluorescence was seen when performed in the presence of a similarly sized negative control protein (bovine lactalbumin) under these conditions.

MBP inhibits the formation of Aβ42 fibrils—The inhibition of fibril assembly was further confirmed by TEM and single-touch AFM analysis. At 6 h of incubation in the absence of MBP, oligomeric structures become evident (Fig. 3.5). These oligomeric structures can reach lengths of up to 40 nm and heights of up to ~ 3.5 nm. By 24 h these oligomeric structures had assembled into fibrillar structures measuring several hundred nanometers in length with an average height of over 4 nm. In the presence of substoichiometric amounts of MBP, the formation of these structures was greatly reduced, indicating an inhibition of fibril formation by MBP.

3.5 – Discussion

Aβ42WT is much more fibrillogenic than Aβ40WT and has been shown to form different soluble and insoluble oligomeric forms than Aβ40WT (*108*). Many of these Aß42WT oligomeric assemblies have been shown to be more highly cytotoxic than Aβ40WT oligomeric assemblies (*109*) as well as acting as seeds for the formation of Aβ40WT fibrils (*99*). Aβ42WT levels in brain tissue have been shown to increase after head injury possibly predisposing patients to AD-like symptoms (*110*). Mutations that result in a high likelihood of developing AD often result in an increase in Aβ42WT production (*111*). For these reasons the role of Aβ42WT has increasingly come under scrutiny in the pathology of AD and related disorders.

Previously, we have demonstrated that MBP binds to and inhibits the fibrillogenesis of familial CAA mutant forms of Aβ as well as its weaker ability to bind to Aβ40WT (*101*). We hypothesized that this interaction may be a possible explanation for the regional differences seen in the deposition of fibrillar amyloid within the brains of patients and animal models with these familial CAA mutant forms of Aβ. Although we have begun to understand how MBP interacts with CAA mutant Aβ40, it was not known whether a similar interaction would take place with the more fibrillogenic Aβ42WT peptide.

In the present study we show that MBP can, in fact, bind to and inhibit the fibrillogenesis of Aβ42WT peptides *in vitro*. Co-immunoprecipitation experiments (Fig. 3.1) demonstrate that Aβ42WT interacts with MBP, a finding that is supported by SPR measurements that place the K_D value for this interaction between surface bound Aβ42WT and MBP, near the strength of the K_D value obtained for MBP and the familial

CAA mutant Aβ40DI peptide reported previously. Although Aβ42WT does not contain either the Dutch or the Iowa mutations, it is highly fibrillogenic, suggesting that the interaction does not require the mutant residues at positions 22 and 23, but rather that MBP may be interacting with a certain conformation common to both Aβ42WT and familial CAA mutant Aβ40DI. For example, both peptides rapidly form β-sheet-rich, oligomeric structures *in vitro* that Aβ40WT is slow to form. Further study will be necessary to elucidate the precise nature of these interactions.

By using CD spectroscopy we demonstrate that the interaction between MBP and Aβ42WT resulted in a reduction in the adoption of β-sheet structure when compared to Aβ42WT alone (Fig. 3.2). By plotting the absolute value at 215 nm for successive scans we were able to quantitate the emergence of β-sheet structure in our samples over time (Fig. 3.2B). We show that in the presence of MBP, which remains in a random coil conformation, Aβ42WT is unable to form appreciable β-sheet structures.

To determine whether this failure to detect a β-sheet signature was due to signal quenching by MBP present in the sample, we performed a scan on mature (48 h) Aβ42WT fibrils (as determined through CD analysis), which was spiked with MBP and immediately scanned. Comparisons of the signal obtained with this spiked control sample were compared to the signal obtained from a sample of Aβ42WT incubated for 48 h with MBP (Fig. 3.2C). The spiked sample clearly showed the presence of β-sheet structures as evidenced by a negative peak at 215 nm. This was an indication that had the Aβ42WT peptides formed β-sheet secondary structures in the presence of MBP, they would have been detected.

Further evidence for the inhibition of β-sheet structures was obtained through second-derivative ATR-IR analysis. In the presence of MBP the β-sheet contribution is much diminished though not completely extinguished suggesting an inhibition of larger β-sheet oligomers (Fig 3.3B). The typical β-hairpin loop structure of Aβ42WT monomers contains anti-parallel β-sheet structure, which if left intact would explain the small β-sheet structural component seen in the spectra of samples containing MBP. Further, the peaks at 1681 cm^{-1} and 1675 cm^{-1}, which are attributed to β-turn structure, remained unchanged even with the addition of MBP suggesting that the β-hairpin structure of Aβ42WT is intact in the presence of MBP. These data suggest that MBP is interacting with Aβ42WT monomers in a manner that leaves their β-hairpin structure intact but inhibits the formation of larger β-sheet oligomers.

The inhibition of the formation of β-sheet oligomers and fibrils in Aβ42WT by MBP is supported by thioflavin-T analysis, which demonstrates a lack of thioflavin-T fluorescence in samples containing Aβ42WT and MBP (Fig. 3.4). This observation further indicates an inhibition of fibril formation by MBP. The rate of fibril formation in the thioflavin-T assay, when compared to the rate observed in the CD measurements, was much more rapid. A plateau in thioflavin-T fluorescence was reached at approximately 2 h, while samples measured by CD reached a plateau only after 12 h. This difference can be explained by the difference in the NaCl concentrations used for these experiments. The NaCl concentration was 150 mM in samples used for thioflavin-T measurements, while for CD spectroscopy the NaCl concentration was 11 mM. A lower salt

concentration was used for CD experiments because high salt concentrations interfere with CD measurements between 190 nm – 210 nm.

These results are further supported by direct visualization of amyloid fibril assembly using both TEM and AFM at longer time points (Fig. 3.5). The formation of short oligomeric structures becomes evident at 6 h as detected by both AFM and TEM for Aβ42WT alone. However, when MBP is present there appears to be a marked reduction in the presence of these structures. Upon continuous incubation of Aβ42WT to 24 h larger fibrils are seen. By TEM these fibrils appear to range between 50 and 200 nm in length and are noticeably absent when MBP is present.

Our results indicate that MBP can interact with Aβ42WT *in-vitro* and inhibit its fibrillogenesis. Previous studies have shown that MBP can bind to and inhibit the fibrillogenesis of the CAA double mutant Aβ40DI peptide (*101*). Presently, it is unknown if MBP interacts with both peptides in a similar manner. Although both peptides are extremely fibrillogenic they may progress from monomer to fibril along different pathways. Consequently, it is possible that MBP may interact with distinct intermediate forms. Further study will be necessary to elucidate the molecular basis for the interaction between MBP and Aβ peptides.

However, this interaction raises intriguing questions as to what role MBP, or MBP related peptides, may exhibit in association with Aβ42WT, and what role this interaction may play in the pathogenesis of AD and other related disorders. For instance, MBP may serve to suppress the deposition and seeding of amyloid plaques at their earliest stages of formation. Alterations in levels of intact MBP or derived fragments

may affect how Aβ peptides are retained or cleared from brain. It may also be possible that although MBP is inhibiting the formation of fibrils that it may be stabilizing the formation of neurotoxic oligomers and thereby exacerbating disease pathology.

It is interesting to note that deposits of Aβ found in regions of white matter, which are rich in myelinated axons, are often diffuse and non-fibrillar (*112, 113*). Damage to white matter is known to result in an increase of myelin proteins and especially MBP related peptides in the cerebral spinal fluid (CSF) (*114*). This release of MBP into the extracellular environment in AD patients with white matter damage would provide ample opportunities for this interaction with Aβ to take place and inhibit the formation of fibrils, though further *in-vivo* study will be needed to confirm this. These findings point to the need to better understand the effect of changes in white matter and how it relates to AD progression.

3.6 – Tables and Figures

Table 3.1: Binding affinities of MBP for Aβ peptides.	
	KD (M)
40DI	**$1.69 \pm 0.14 \times 10^{-8}$**
42WT	**$4.29 \pm 0.28 \times 10^{-8}$**
40WT	**$1.16 \pm 0.12 \times 10^{-7}$**

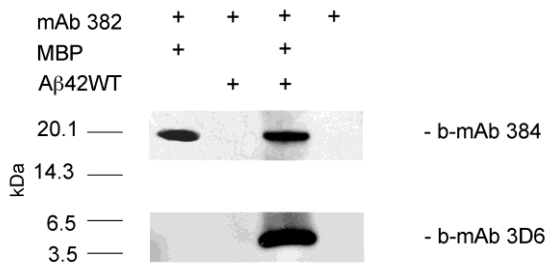

FIGURE 3.1 **Co-immunoprecipitation of MBP and Aβ42.** Aβ42 peptides were immunoprecipitated with MBP using anti-MBP mAb 382 as described in "Materials and Methods." Immunoprecipitated samples from left to right: MBP alone, Aβ42WT alone, MBP incubated with Aβ42, negative control (no MBP/no Aβ42). Duplicate immunoblots of all samples were prepared as described in "Materials and Methods" and probed with either biotinylated mAb 384 (anti-MBP) or biotinylated mAb 3D6 (anti-Aβ) as described.

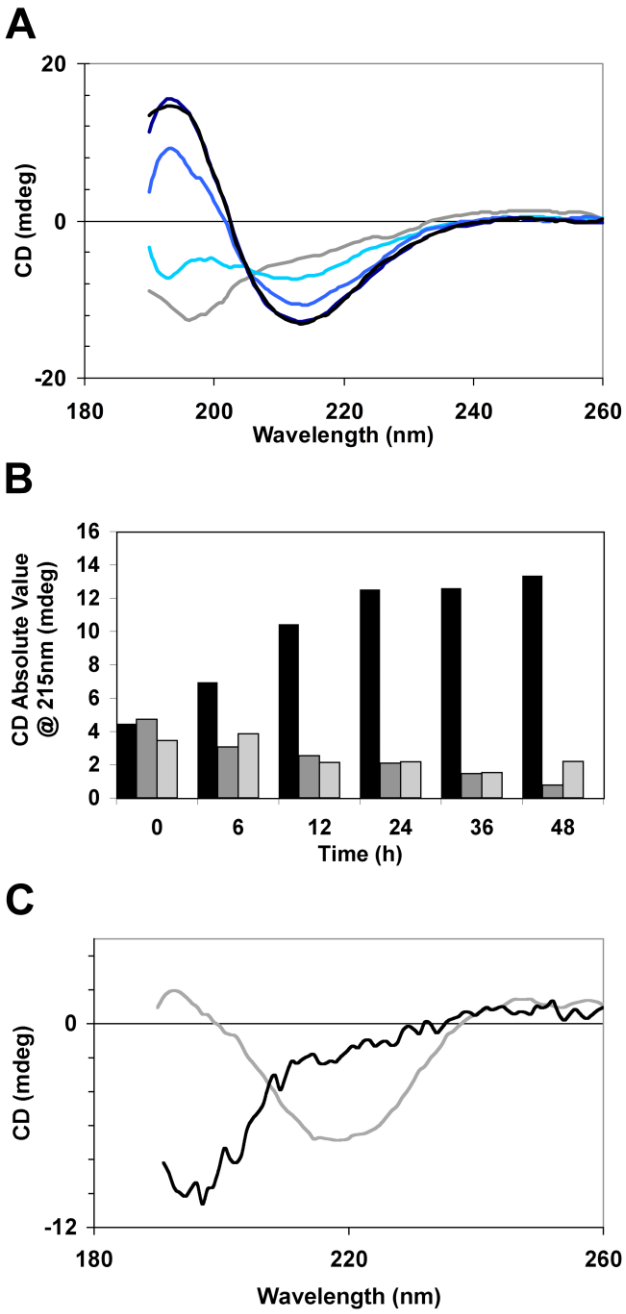

FIGURE 3.2 **Inhibition of Aβ42WT β-sheet formation by MBP, assessed by CD spectroscopy.** Peptides were prepared and scanned as described in "Materials and Methods." **A:** Successive scans of Aβ42WT incubated at 37°C taken at 0 (■), 6(■), 12(■), 24(■), 36h (■). **B:** Absolute values at 215nm charted from successive scans. Aβ42 (■), MBP (■), Aβ42 with MBP (■). **C:** Single scan of Aβ42WT with MBP at 48h (black) compared to a single scan of mature Aβ42WT fibrils spiked with MBP at 48h (gray).

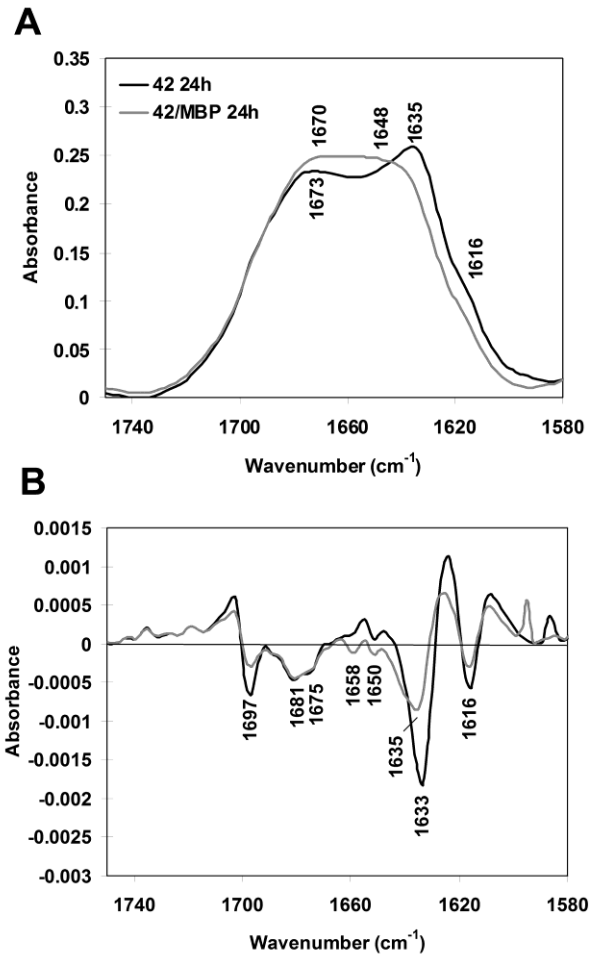

FIGURE 3.3 **Inhibition of Aβ42 β-sheet formation by MBP, assessed by ATR-IR.** Peptides prepared and scanned as described in "Materials and Methods." **A:** IR absorbance in the Amide I band for Aβ42WT alone (black line) or with MBP (gray line) incubated at 37°C at 24h. **B:** Second-derivative plot of IR spectra in **A**.

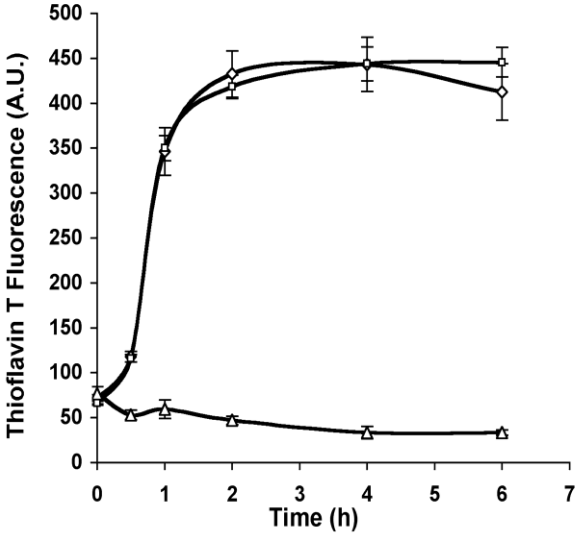

FIGURE 3.4 **Thioflavin T analysis for inhibition of Aβ42 fibril formation by MBP.** Aβ42 was treated with HFIP, resuspended to a concentration of 2.5 mM in DMSO, and then diluted to a concentration of 12.5 μM in PBS in the absence (diamond) or presence of 1.56 μM MBP (triangle) or 1.56 μM α-lactalbumin (square) as control. At specific timepoints aliquots were collected from each sample and subjected to thioflavin T binding and fluorescence to determine fibrillar assembly as described in "Materials and Methods". The data shown are the mean ± S.D. of triplicate samples.

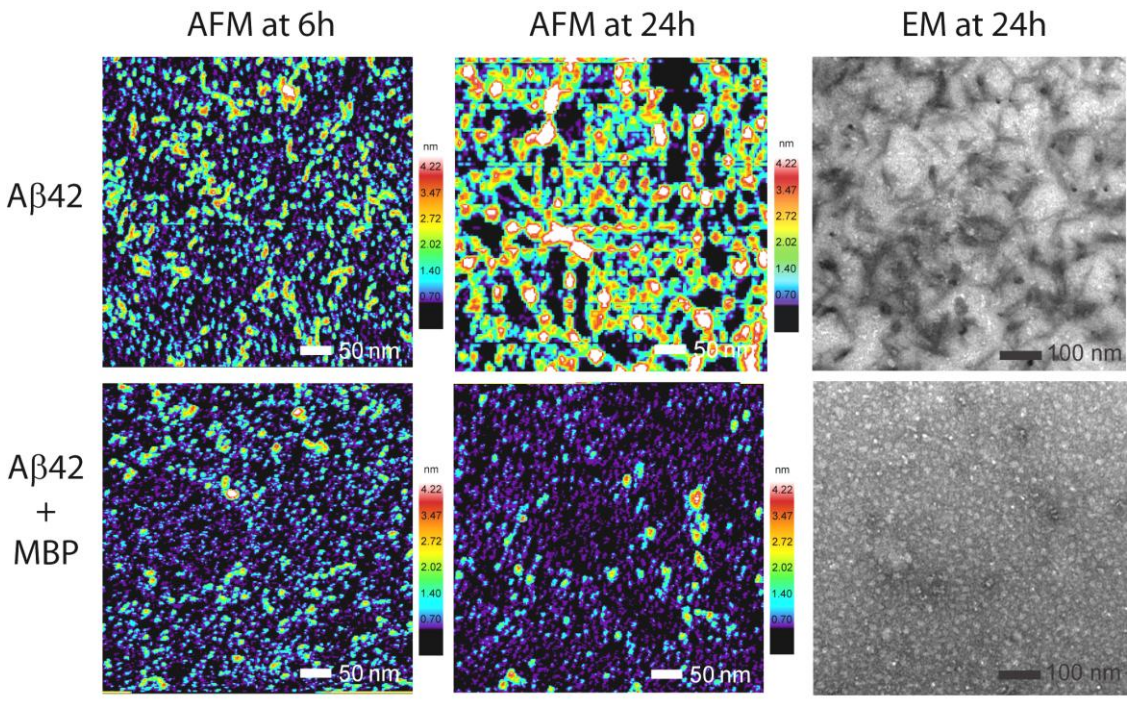

FIGURE 3.5 **AFM and TEM images of the inhibition Aβ42WT fibril formation by MBP.** Aβ42 samples were incubated at 37°C in the absence (top row) or presence (bottom row) of MBP at the same ratio of Aβ42:MBP used in the thioflavin T analysis. AFM images were scanned at 6 h and 24 h of incubation. EM images were taken at 24 h of incubation.

CHAPTER 4 – Mapping of an Aβ Binding Site to the N-Terminus of Myelin Basic Protein

4.1 -- Summary

Deposition of Amyloid β-protein (Aβ) into plaques in the brain parenchyma and cerebrovasculature are hallmarks of Alzheimer's disease (AD) and related disorders. Aβ is produced from the sequential proteolysis by β and γ-secretase of the amyloid β precursor protein (AβPP) yielding peptides of between 39 and 43 residue. Aβ peptides readily form β-sheet containing oligomers and fibrils. Previously, we had shown that the interaction of MBP with Aβ40DI was able to inhibit its fibril formation. We also demonstrated that MBP was capable of binding to Aβ42WT and blocking its fibril formation as well. In this study we demonstrate through a combination of biochemical and ultrastructural techniques that the binding site for Aβ40DI is located in the first 64 amino acids from the N-terminal of MBP and that a stable peptide (MBP1) comprised of these residues is sufficient to inhibit the fibrillogenesis of Aβ40DI. Here we present early solution NMR experiments to assign the backbone resonances of MBP1 and show the completed assignments of 52 of the 64 residues. We have identified, H11, G12, S13, S20, H27, H33, R34, R55, and G56 as residues in MBP1 that shift when incubated with Aβ40DI. Likewise we have identified residues G9, Y10, E11 in the N-terminus of Aβ40WT that interact with MBP1. This information will be key for understanding how MBP may play a role in the pathogenesis or possibly the treatment of AD and related

disorders.

4.2 – Introduction

The histopathology of Alzheimer's disease (AD) is characterized by the presence of plaques of amyloid β peptide (Aβ) in the brain parenchyma and cerebrovasculature *(1)*. Dystrophic neurons and neuronal loss are often associated with Aβ plaques leading to the clinical manifestation of cognitive decline and memory loss. Aβ is derived from the amyloid β precursor protein (AβPP) through sequential proteolysis by β and γ-secretase *yielding* peptides of between 39 and 43 residues *(3-6)*. These peptides exhibit a high propensity to self-assemble into β-sheet containing oligomers and fibrils of which the oligomeric forms are widely believed to be the toxic forms of the peptide, responsible for the majority of neuronal loss (*2*). The exact mechanism of this neurotoxicity has yet to be fully understood.

A condition found prevalently in AD, known as cerebral amyloid angiopathy (CAA) is characterized by fibrillar deposition of Aβ along arteries and arterioles of the cerebral cortex and leptomeninges and the cerebral microvasculature (*2, 16, 17*). Apart from the more typical CAA, which can occur in AD, familial forms of CAA exist that are the result of specific point mutations within the Aβ sequence of the AβPP gene (*24-29*). Two well studied examples of familial CAA are Dutch-type, resulting from an E22Q substitution in Aβ, (*24, 25, 30*) and Iowa type, resulting from a D23N substitution in Aβ. (*30*) In a recent study we demonstrated that myelin basic protein (MBP) bound preferentially to the more fibrillogenic Aβ40DI, which contains both Dutch and Iowa

mutations, over Aβ40WT (*101*). The presence of both of these mutations together in the same Aβ peptide (Aβ40DI) is known to enhance its fibrillogenic and pathogenic properties *in vitro* (*35*). It was shown that the interaction of MBP with Aβ40DI was able to inhibit its fibril formation.(*101*). We also demonstrated that MBP was capable of binding to Aβ42WT and blocking its fibril formation as well. Since this peptide contains no substitutions it was postulated that MBP may not be interacting with the mutant residues of Aβ40DI, but rather some oligomeric conformer that may be readily formed by both Aβ42WT and Aβ40DI.

The reason for MBP's high affinity for Aβ and its ability to inhibit the fibril formation of the more fibrillogenic Aβ peptides can only be understood through a systematic analysis of the structural interactions between MBP and Aβ. This has been made difficult thus far due to the extremely labile and intrinsically unstructured nature of MBP. In this study we sought to isolate the Aβ binding region on MBP and analyze its interaction with Aβ40DI. We demonstrate through a combination of biochemical and ultrastructural techniques that the binding site for Aβ40DI is located in the first 64 amino acids from the N-terminal of MBP and that a stable peptide (MBP1) comprised of these residues is sufficient to inhibit the fibrillogenesis of Aβ40DI. Observing a degree of homology between the Aβ binding site on Aβ precursor protein (APP) and this region of MBP we demonstrate that peptides lacking this homologous region or with directed mutations in this region have no affinity for Aβ40DI and lose their ability to inhibit its fibrillogenesis. Using NMR we identify several residues in the N-terminal of both MBP and Aβ40WT that shift when these peptides are incubated together. This understanding

will be key for deciphering what role, if any, MBP may play in the pathogenesis or possibly the treatment of AD and related disorders.

4.3 – Materials and Methods

Reagents and Chemicals — Aβ40DI peptide was synthesized by solid-phase Fmoc (9-fluorenylmethoxycarbonyl) amino acid chemistry, purified by reverse phase high performance liquid chromatography, and structurally characterized as previously described (*87*). Aβ40DI peptides were initially prepared in hexafluoroisopropanol, lyophilized, and resuspended in dimethylsulfoxide (Me_2SO) (*88*). Purified human MBP (purchased from Chemicon International, Temecula, CA) was resuspended in 20mM sodium acetate, 100mM sodium chloride, pH 4.0, dialyzed into phosphate-buffered saline (PBS) and stored at -70°C at 1 mg/ml. Synthetic peptides were prepared by GenScript Corporation (Scotch Plains, NJ). Thioflavin-T was purchased from Sigma-Aldrich (St. Louis, MO).

Recombinant MBP Peptide Expression — MBP derived peptides gene sequences were cloned into a pTYB11 plasmid vector (New England Biolabs, Ipswich, MA) and transformed into competent E. coli BL21 DE3 cells by heat shock. Cells were grown at 37°C in 1L cultures of LB broth containing 0.1mg/ml ampicillin until an optical density of 0.600 AU at 600nm was reached. Expression of the fusion protein was induced with either 0.3mM or 0.5mM isopropyl β-D-1-thiogalactopyranoside (IPTG) at 26°C for either 3h or 18h. Cells were harvested by centrifugation at 5000xg for 30min at 4°C and

cracked in a French press in 20mM Tris, pH 9.0 / 0.5M NaCl / 1mM EDTA containing Complete Protease Inhibitor (Roche, Mannheim, Germany). Cell lysate was clarified by centrifugation and passed over Chitin Beads (New England Biolabs, Ipswich, MA) equilibrated with 20mM Tris, pH 9.0 / 0.5M NaCl / 1mM EDTA (EQ buffer). The column was washed with EQ buffer containing 0.05% TX-100, and the peptide cleaved and eluted from the intein fusion protein by incubation of the column in 40mM dithiothreitol (DTT) as per manufacturers instruction. The eluate was diluted 10 fold into 50mM glycine, pH 9.0 and passed over a CM52 column equilibrated with glycine, pH 9.0 / 50mM NaCl (CM EQ). The column was washed in CM EQ and eluted with high salt. Fractions were analyzed by SDS-PAGE, pooled, dialyzed against water, lyophilized, and stored at -70°C.

Isotopic labeling of MBP1 peptides -- MBP derived peptides gene sequences were cloned into a pTYB11 plasmid vector (New England Biolabs, Ipswich, MA) and transformed into competent *E. coli* BL21 DE3 cells by heat shock. Cells were grown at 37°C in 1L cultures of LB broth containing 0.1mg/ml ampicillin until an optical density of 0.700 AU at 600nm was reached. Cultures were harvested by centrifugation at 5000xg for 30min at 4°C. Cells were resuspended in M9 minimal media lacking nitrogen and/or carbon sources and centrifuged again to remove residual LB media. Cells were next resuspended in M9 minimal media containing 5% ^{13}C D-glucose, 5% ^{15}N NH_4C and 0.1mg/ml ampicillin and the volume brought up to 250ml. Cultures were incubated for 1h at 37°C to eliminate unlabeled metabolites and allow growth recovery. Protein expression was

induced with the addition of 0.5 mM IPTG with incubation at 37°C for 5 hours. Cell harvesting and protein purification were performed as above in *Recombinant MBP Peptide Expression.*

Surface Plasmon Resonance — All runs were performed on a BiaCore 2000 instrument (Uppsala, Sweden) with 10 mM HEPES pH 7.4, 150 mM NaCl, 3 mM EDTA, 0.005% (v/v) Tween 20 as running buffer and diluent. N-terminally biotinylated Aβ40DI peptides were resuspended in Me_2SO to 2.5 mM and serially diluted to 13 nM immediately before application. Biotinylated Aβ40DI was immobilized to a Biacore SA sensor chip at 10 μl/min to achieve an average R_{max} of approximately 700 RU for each analyte leaving flow cell 1 as a reference. This chip preparation procedure was found to result in a surface that minimized mass transfer effects for kinetic interaction studies. Purified analyte was passed over flow cells at either 5, 10, 25, 50, and 100 nM, in triplicate at flow rates of 30 μl/min. Faster flow rates did not significantly improve the quality of data. Surfaces were regenerated with 0.2 M glycine pH 2.0, 150 mM NaCl between runs. The resulting sensorgrams were analyzed by BiaCore Analysis software.

Thioflavin T Fluorescence Assay — Lyophilized Aβ40DI peptides were first resuspended with Me_2SO to 2.5 mM, diluted to 12.5 μM in PBS, and then incubated at 37°C with rocking either alone, or with 1.56 μM peptide inhibitors. Control samples containing 0.5% Me_2SO and 1.56 μM inhibitors, in PBS were also included. At each timepoint, 100

μl samples of each reaction were placed in a 96-well microplate in triplicate and 5 μl of 100 μM thioflavin T was added. The plate was mixed and incubated at 22°C in the dark for 10 min. Fluorescence was measured at 490 nm using an excitation wavelength of 446 nm in a SpectraMax spectrofluorometer (Molecular Devices, Sunnyvale, CA) using SoftMax Pro control software.

Transmission Electron Microscopy — Sample mixtures were deposited onto carbon-coated copper mesh grids (EM Sciences, Hatfield, PA) and negatively stained with 2% (w/v) uranyl acetate. The samples were viewed with a FEI Tecnai 12 BioTwin transmission electron microscope, and digital images were taken with an AMT camera.

Nuclear Magnetic Resonance Spectroscopy — The spectra were collected on a Bruker 700mHz magnet equipped with a triple resonance inverse TXI probe at 277K. 10% D2O was added to the sample for deuterium lock. 0.05% NaN3 was added to prevent microbial growth. All experiments were carried out in PBS, pH 7.4. 2-D experiments were carried out with uniformly labeled ^{15}N-MBP1 with or without Aβ40DI, and fully labeled ^{15}N-Aβ40WT with or without MBP1. 3D experiments were carried out using uniformly labeled ^{15}N, ^{13}C-MBP1. Spectra were processed using TopSpin 2.0 (Bruker). All spectra were processed using linear prediction in the indirect dimensions. Spectra were loaded into Sparky, aligned and then peaks were picked manually. Peak lists were generated for the NHSQC, HNCACB and CBCACONH for automated assignment using PINE (http://pine.nmrfam.wisc.edu/).*Atomic Force Microscopy* — AFM was carried out using

a LifeScan controller developed by LifeAFM (Port Jefferson, NY) interfaced with a Digital Instruments (Santa Barbara, CA) MultiMode microscope fitted with an E scanner. AFM samples were first titrated to pH 4 using dilute HCl and then adsorbed onto freshly cleaved ruby mica (S & J Trading, Glen Oaks, NY). The lower pH allows for better adsorption of Aβ42 peptides to the negatively charged mica surface. Samples were imaged under hydrated conditions using super-sharp silicon probes (SSS-Cont, Nanosensors, Neuchatel, Switzerland) that were modified for magnetic retraction by attaching samarium cobalt particles (LifeAFM, Port Jefferson, NY). We estimate the effective diameter of the super-sharp silicon probes to be 4 ± 1 nm at a height of 2 nm. Data analysis and graphics was performed using Interactive Display Language 5.0 (Research Systems Inc., Boulder, CO). In the Z scale bars, numbers in each color square indicate the Z-value at the middle of the range for that color.

4.4 -- Results

Identification of Aβ binding motif near N-terminal of MBP — To assess the location of the binding motif for Aβ in MBP we first created shorter recombinant peptides from the larger MBP protein. Gene sequences of four different peptides representing different non-overlapping sequences (MBP1 aa 1-64, MBP2 aa 65-103, MBP3 aa 104-137, MBP4 138-171) were inserted into a pTYB11 vector and purified using the IMPACT-CN system (New England Biolabs, Ipswich, MA), followed by cation exchange chromatography. Purity was determined by SDS-PAGE (Fig. 4.1).

Using SPR analysis we were able to qualitative determine the relative binding affinity of MBP peptides to Aβ40DI. Ligand surfaces and other assay parameters were prepared as described in Methods. Figure 4.2 shows the sensorgrams after the injection of each MBP peptide over the Aβ40DI ligand surface. Only the peptide MBP1 displayed any affinity for Aβ40DI. Kinetic measurements of the affinity of MBP1 to Aβ40DI were comparable to those measured for whole MBP and Aβ40DI (data not shown). We concluded from these results that the binding motif for Aβ40DI is located in the first 64 N-terminal residues of MBP.

MBP1 inhibits the fibril formation of Aβ40DI — After demonstrating that MBP1 had affinity for Aβ40DI through SPR analysis we next determined if this interaction could inhibit Aβ40DI fibrillogenesis by directly visualizing fibrils with transmission electron microscopy. Similarly, Aβ40DI fibril inhibition was measured by using a thioflavin T fluorescence assay. Previously we have shown that MBP is able to dramatically inhibit fibril formation at an 8-fold lower molar concentration (*101*). In this assay we found that MBP1 was equally capable of inhibiting Aβ40DI fibrillogenesis at this stoichiometry (Fig. 4.3). Inhibition of fibrillogenesis was confirmed using transmission electron microscopy (TEM) (Fig 4.4). From this we concluded that MBP1 contained the necessary motif to not only bind to but to inhibit Aβ40DI fibril formation.

C-terminal truncation of MBP1eliminates Aβ40DI affinity and fibril inhibition — After narrowing the binding motif down to the N-terminal of MBP we wanted to more precisely identify this motif through the use of deletion mutants. The first peptide from

this series, missing residues 50-64 from the C-terminus, MBP1 ΔCT, lacked any affinity for Aβ40DI as determined through SPR analysis (Fig 4.5). MBP1 ΔCT's lack of affinity was confirmed by thioflavin T assay in which it had no inhibition of Aβ40DI fibrillogenesis (Fig 4.6). This indicates that the 15 residues corresponding to amino acids 50-64 are necessary for the binding and inhibition of Aβ40DI by MBP1.

Mutational analysis of the Aβ40DI binding motif in MBP1 — Focusing on residues 50-64, which we have shown to be necessary for binding to Aβ40DI, we compared the sequence to other known Aβ binding motifs. One that we have previously reported lies within the APP gene (*115*). A comparison of these two sequences demonstrates an intriguing homology (KRGxxxxxHP) between MBP residues 54-64, with APP residues 99-109 (Table 4.1). Alanine substitution mutants of the homologous residues were prepared (MBP1 ΔKRG, MBP1 ΔHP) and analyzed for binding using SPR analysis (Fig 4.7). Substitutions at these residues eliminated the affinity of MBP1 for Aβ40DI, while a substitution at Ser57 (MBP1 S57A) has no affect. These mutant peptides were confirmed to also lack fibril inhibition in a thioflavin T assay (Fig 4.8).

Determination of interacting residues by nuclear magnetic resonance .spectroscopy — We have shown that residues 54-56, and 63-64 are necessary to inhibit Aβ40DI fibrillogenesis. However this data alone does not indicate whether or not these residues interact directly with Aβ or are necessary for the stability of a conformation formed upon Aβ binding. It may be likely that there are other distal elements of the binding motif that

are also necessary for this activity. To more precisely identify the necessary residues of MBP1 that interact with Aβ40DI, we used solution NMR spectroscopy to probe for interacting amino acids.

Backbone resonance assignments were made using uniformly labeled ^{15}N, ^{13}C – MBP1 to obtain CBCACONH and HNCACB spectra as described in Materials and Methods. Assignments of 52 backbone peaks out of a possible 60 (64 residues minus 4 prolines) has been completed (Fig. 4.9). Most of the assignments have been made with a high degree of probability, although several peaks could not be resolved due possibly to the highly disordered nature of MBP1 in solution giving rise to heterogeneity in the sample.

Uniformly labeled ^{15}N – MBP1 was incubated with and without unlabeled Aβ40DI and its ^{1}H – ^{15}N HSQC spectra resolved as described in Materials and Methods. Comparisons of ^{1}H – ^{15}N HSQC spectra with and without Aβ40DI reveal significant cross-peak shifts in several residues (Fig 4.10). The identified residues demonstrate that the binding motif for Aβ40DI in MBP1 may be composed of several distal elements. These include Arg55 and Gly56, which as discussed above, were found to be homologous to a sequence in APP near an Aβ binding site and when subjected to alanine substitution, caused affinity for Aβ40DI to be lost.

In addition to this experiment we also incubated ^{15}N – labeled Aβ40WT with unlabeled MBP1 to examine which Aβ residues shift in response to binding by MBP1. Figure 13 shows that MBP1 primarily interacts with Aβ40WT in the N-terminal region, specifically residues Gly9, Tyr10, and Glu11.

4.5 -- Discussion

Deposition of Aβ into fibrillar deposits in the brain is a hallmark of AD, familial CAA and other related disorders (*1, 2*). These deposits are often associated with neuronal loss and cellular dysfunction leading to cognitive decline. Stopping or reversing this buildup has been a central theme in the treatment of AD. Previous *in-vitro* studies have shown that MBP has a high affinity for fibrilllogenic Aβ peptides and that it is capable of inhibiting Aβ fibrillogenesis (*101*). The mechanism of this inhibition is largely unknown, but fundamental to the understanding of the role MBP may play in AD and related disorders. Previous studies investigating MBP interactions with Aβ peptides have been hampered by the size and instability of the MBP protein. By identifying and isolating the motif responsible for the interaction, more in-depth studies such as in-vivo investigations may be possible in the future.

In this study, through the use of SPR we have shown that the binding site for the fibrilllogenic CAA mutant Aβ40DI in MBP is located on the N-terminus between residues 1 and 64 (Fig 4.2). We have shown through the use of TEM and thioflavin T assay that a peptide consisting of this sequence, MBP1, is capable of inhibiting the fibrillogenesis of Aβ40DI (Fig, 4.3, 4.4). The identification of a shorter peptide within the MBP protein that has the same affinity for Aβ and is also able to inhibit fibrillogenesis is significant in that we now have a more stable, smaller molecule with which to use in future studies.

We next sought to refine the search for the Aβ binding motif by examining the binding of truncated forms of MBP1. When we removed the C-terminal residues 50

through 64 from MBP1 to create the peptide MBP1 ΔCT we found that this truncation completely eliminated the affinity for Aβ40DI (Fig. 4.5) as well as MBP1 ΔCT's inhibition of Aβ40DI fibrillogenesis (Fig 4.6). From this data we tentatively concluded that the binding motif may lie between Arg50 and Pro64. We next performed a comparison of the sequence of MBP1 to an Aβ binding site that we previously reported to be found near residues 105-119 of APP (*115*). Aligning the sequence of MBP1 with APP we found there to be some degree of homology between residues 99-109 in APP and residues 54-64 in MBP1, giving the homologous motif KRGxxxxxxHP (Table 4.1). This region on MBP1, when removed eliminates its binding to Aβ, as has been shown with the deletion mutant MBP1 ΔCT above (Fig. 4.5, 4.6). The overlap and proximity of this motif with an Aβ binding domain on APP therefore was compelling. MBP1 peptides with alanine substitutions at the homologous residues (MBP1 ΔKRG, MBP1 ΔHP) were determined to lack Aβ affinity and fibril inhibition (Fig. 4.7, 4.8) indicating the necessity of these residues and verifying the loss of affinity seen in MBP1 ΔCT.

The lack of affinity to Aβ by the truncated MBP1 ΔCT as well as the lack of affinity of the MBP1 peptides with targeted mutations appears to indicate that the binding motif is located between residues Arg50 and Pro64, however it is known that MBP is an intrinsically unstructured protein and as such can take on a diverse array of conformational states depending on its ligand and environment (*103*). It may be expected that a ligand binding site in such a protein may be composed of distal elements that come together to form a binding groove, or other such tertiary structure, when in contact with its ligand. It is possible that the truncated region of MBP1 ΔCT from Arg50 and Pro64

may not contain a binding motif, but may be necessary for the stability of an Aβ binding conformation or rather these residues may only form part of a binding groove. Acknowledging this possibility it seemed likely that progressive truncation of the MBP1 sequence would not be ideal for identifying the Aβ binding motif. Progressive truncation of the sequence may be disruptive, if the binding motif is in fact conformationaly dependent.

Solution NMR was used to more precisely identify residues in MBP1 that may be shifting in response to interactions with Aβ40DI. First, the assignments of the backbone resonances of MBP1 were carried out. These assignments are not complete however. We should expect to see 60 individual cross-peaks (64 residues minus four prolines), but we only resolve approximately 56 peaks, of which 52 could be assigned (Fig. 4.9). This may be due to heterogeneity in the sample caused by aggregation or may be more simply due to a high degree of random coil conformation in MBP1. Another factor making assignments difficult is the tightness of the proton dispersion in the spectra. These problems are also evident with solution NMR measurements of 18.5kDa rmMBP as well (*116, 117*) making assignments a challenge for this protein. However, in light of this we have been successful at identifying several cross-peaks that shift in the presence of Aβ40DI with a high degree of accuracy. H11, G12, S13, S20, H27, H33, R34, R55, and G56 all have been assigned and show significant peak shifts in the presence of Aβ40DI (Fig 4.10A). It is interesting to note that among the residues that have interactions R55 and G56 are included. These residues lie within the deleted portion of MBP1 ΔCT and

are part of the KRGxxxxxxHP motif identified above as possibly important to Aβ binding.

Although the solution NMR spectra are informative they cannot yet answer the question of whether these interacting residues are involved in direct binding to Aβ or to each other, thereby stabilizing a conformational change important to the interaction. Mutational analysis of these residues may be informative in order to confirm their involvement in Aβ binding. Alternatively, cross-linking experiments have been proposed to identify which regions of the peptide are coming into contact. Still, as NMR spectral data continue to be improved it may be possible to construct 3D models of MBP1 that will be more informative.

The location of interacting residues G9, Y10, E11 on the N-terminus of Aβ40WT is the first confirmation of a binding site for MBP on Aβ (Fig 4.10B). How this interaction may inhibit fibril formation remains a mystery that will have to be solved through further structural studies.

This study sought to provide insight into the structural relationship between MBP and Aβ peptides that leads to their affinity and the inhibition of Aβ fibrillogenesis. MBP is an intrinsically unstructured protein capable of taking on different conformations depending on its ligand. This property has complicated many structural studies of MBP in the past. However, here we have provided the first evidence of interacting residues on both MBP and Aβ40WT that furthers the understanding of this interaction. The results show that MBP's interaction with Aβ is mediated through an N-terminal domain that

operates independently of the larger protein and that this domain is capable of inhibiting the fibrillogenesis of Aβ peptides.

4.6 – Tables and Figures

APP - 83-ITNVVEANQPVTIQNWCKRGRKQCKTHPHFV-112

MBP - 37-GILDSIGRFFGGDRGAPKRGSGKDSHHP-64

TABLE 4.1 **Alignment of APP and MBP.** Alignment of the sequences of APP and MBP identified homology at APP 99-109 and MBP 54-64. This region of APP is near a reported Aβ binding site *(114).*

FIGURE 4.1 **Purification of MBP peptides.** MBP was arbitrarily divided into four peptides and recombinantly expressed in E. coli using pTYB11 and the IMPACT-CN system (New England BioLabs (Ipswich, MA). Cultures were grown, harvested and purified as described in Materials and Methods. **A.** Peptide sequences of the four MBP peptides. **B.** SDS-PAGE of column fractions from the final purification of MBP1. Purity is representative of all batches and peptides.

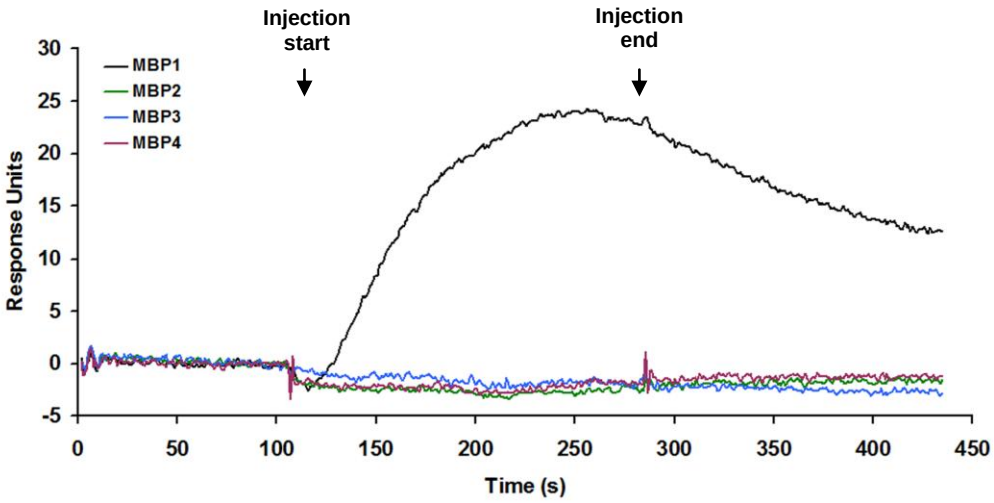

FIGURE 4.2 **Binding of MBP peptides measured by SPR analysis.** MBP peptides were passed over immobilized Aβ40DI ligands at 50nM each. Resulting sensorgrams were baseline corrected and plotted as overlays. Binding is identified by an increase in response during injection (association) followed by a gradual decrease in response following injection (dissociation). Only MBP1 demonstrated any affinity for the Aβ40DI ligand, identifying an Aβ binding motif in this peptide.

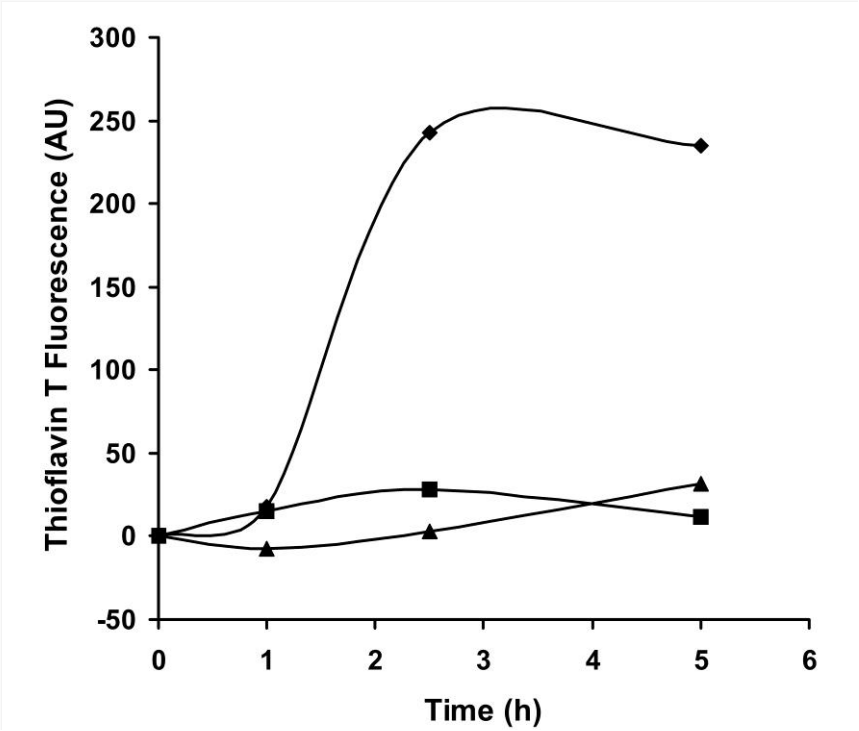

FIGURE 4.3 **Thioflavin T analysis for inhibition of Aβ40DI fibril formation by MBP1.** Aβ40DI was treated with HFIP, resuspended to a concentration of 2.5 mM in DMSO, and then diluted to a concentration of 12.5 μM in PBS in the absence (diamond) or presence of 1.56 μM MBP1 (triangle) or 1.56 μM MBP (square). At specific timepoints aliquots were collected from each sample and subjected to thioflavin T binding and fluorescence to determine fibrillar assembly as described in "Materials and Methods". The data shown are the mean ± S.D. of triplicate samples.

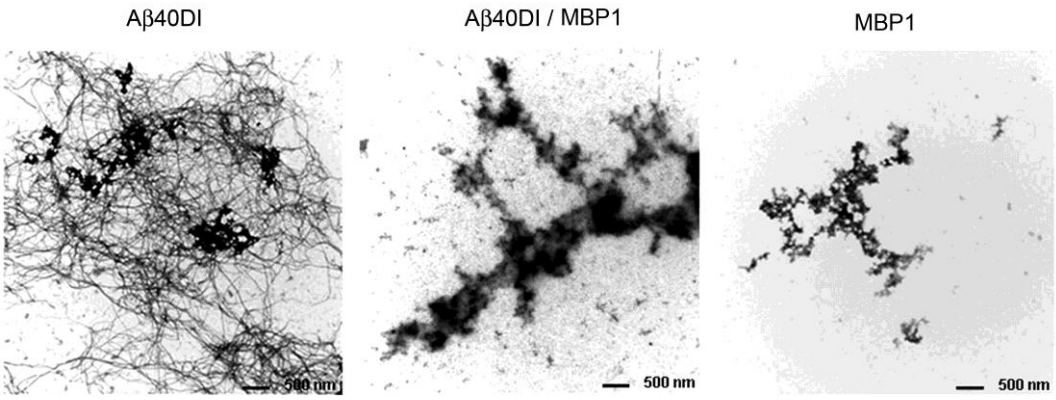

FIGURE 4.4 **Inhibition of Aβ40DI fibril formation by MBP1 as assessed by TEM.** Aβ40DI peptides were treated with HFIP, resuspended to a concentration of 2.5 mM in Me2SO, and then diluted to a concentration of 12.5 μM in PBS in the absence or presence of 1.56 μM MBP1. Samples were imaged at 6 h by TEM.

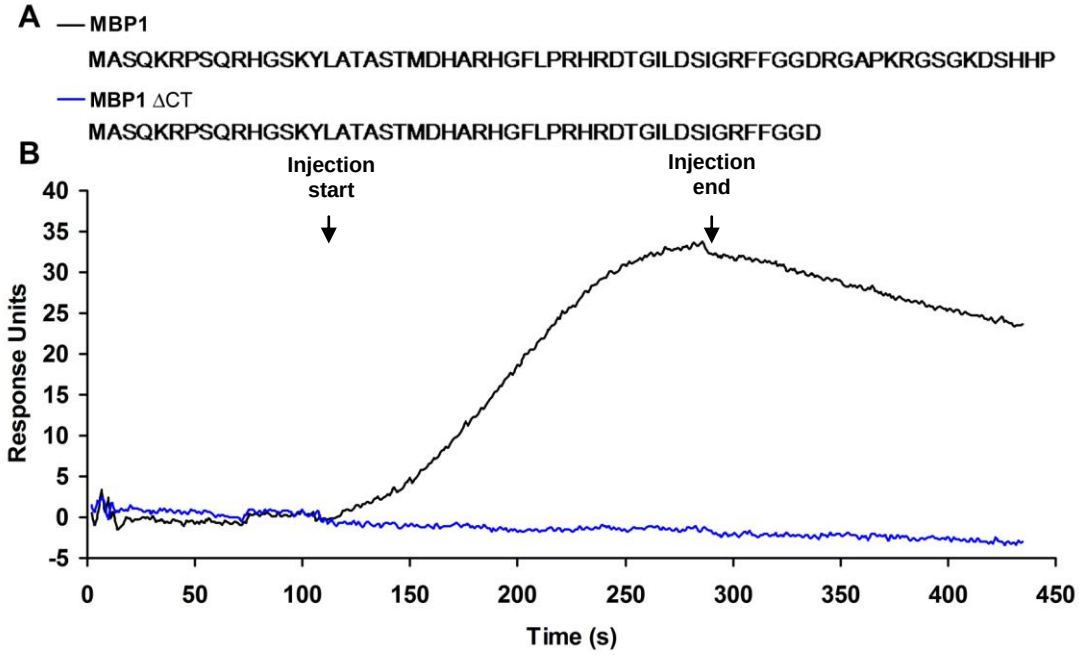

FIGURE 4.5 **Binding of MBP1 and MBP1 ΔCT peptides measured by SPR analysis.** MBP1 and MBP1 ΔCT peptides were passed over immobilized Aβ40DI ligands at 50nM each. Resulting sensorgrams were baseline corrected and plotted as overlays. Binding is identified by an increase in response during injection (association) followed by a gradual decrease in response following injection (dissociation). **A.** Comparison of the sequences of MBP1 and the truncated MBP1 ΔCT. **B.** MBP ΔCT lacked affinity for the Aβ40DI ligand,

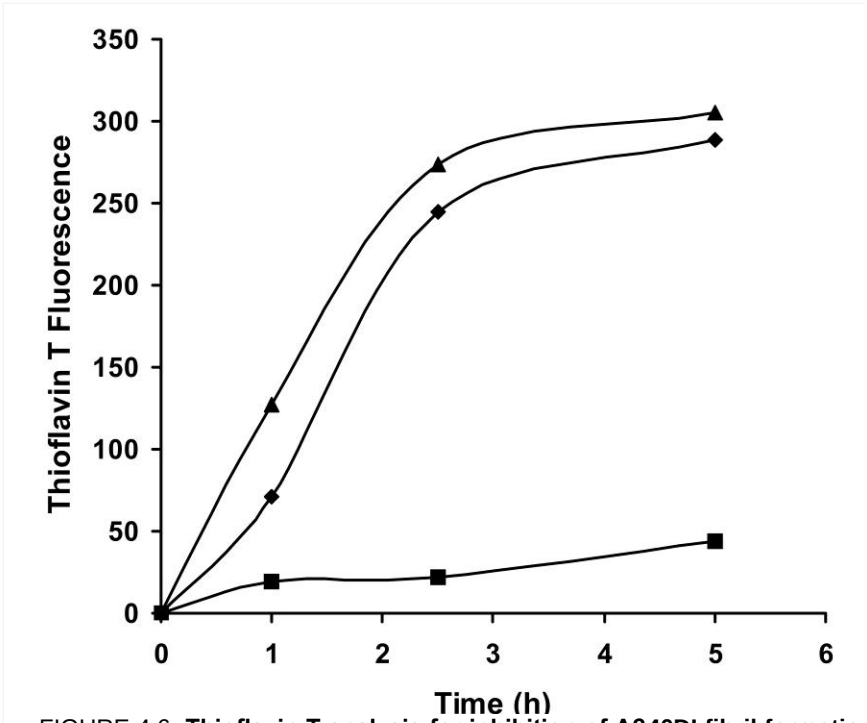

FIGURE 4.6 **Thioflavin T analysis for inhibition of Aβ40DI fibril formation by MBP1 ΔCT.** Aβ40DI was treated with HFIP, resuspended to a concentration of 2.5 mM in DMSO, and then diluted to a concentration of 12.5 μM in PBS in the absence (diamond) or presence of 1.56 μM MBP1 ΔCT (triangle) or 1.56 μM MBP1 (square). At specific timepoints aliquots were collected from each sample and subjected to thioflavin T binding and fluorescence to determine fibrillar assembly as described in "Materials and Methods". The data shown are the mean ± S.D. of triplicate samples.

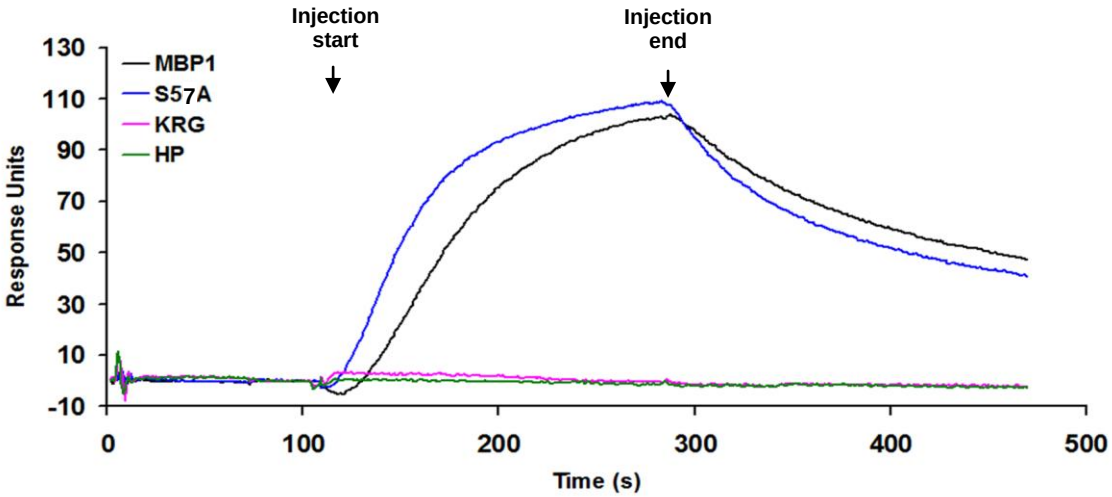

FIGURE 4.7 **Binding of MBP1 and MBP1 mutant peptides measured by SPR analysis.** MBP1, MBP1 S57A, MBP1 ΔKRG, and MBP1 ΔHP peptides were passed over immobilized Aβ40DI ligands at 100nM each. Resulting sensorgrams were baseline corrected and plotted as overlays. Binding is identified by an increase in response during injection (association) followed by a gradual decrease in response following injection (dissociation).

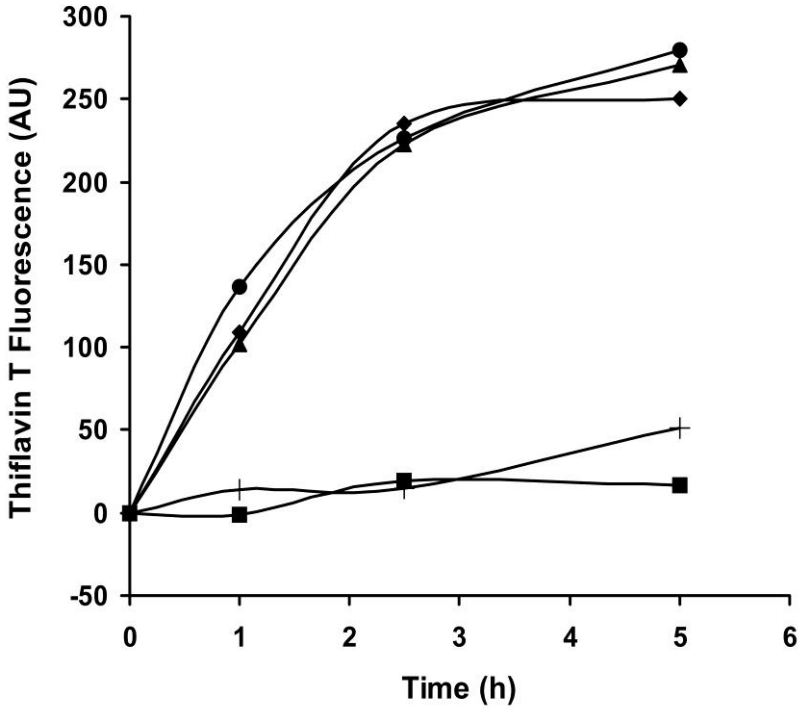

FIGURE 4.8 **Thioflavin T analysis for inhibition of Aβ40DI fibril formation by MBP1 mutants.** Aβ40DI was treated with HFIP, resuspended to a concentration of 2.5 mM in DMSO, and then diluted to a concentration of 12.5 μM in PBS in the absence (diamond) or presence of 1.56 μM MBP1 ΔHP (triangle), 1.56 μM MBP1 ΔKRG (circle), 1.56 μM MBP1 S57A (plus), or 1.56 μM MBP1 (square). At specific timepoints aliquots were collected from each sample and subjected to thioflavin T binding and fluorescence to determine fibrillar assembly as described in "Materials and Methods". The data shown are the mean ± S.D. of triplicate samples.

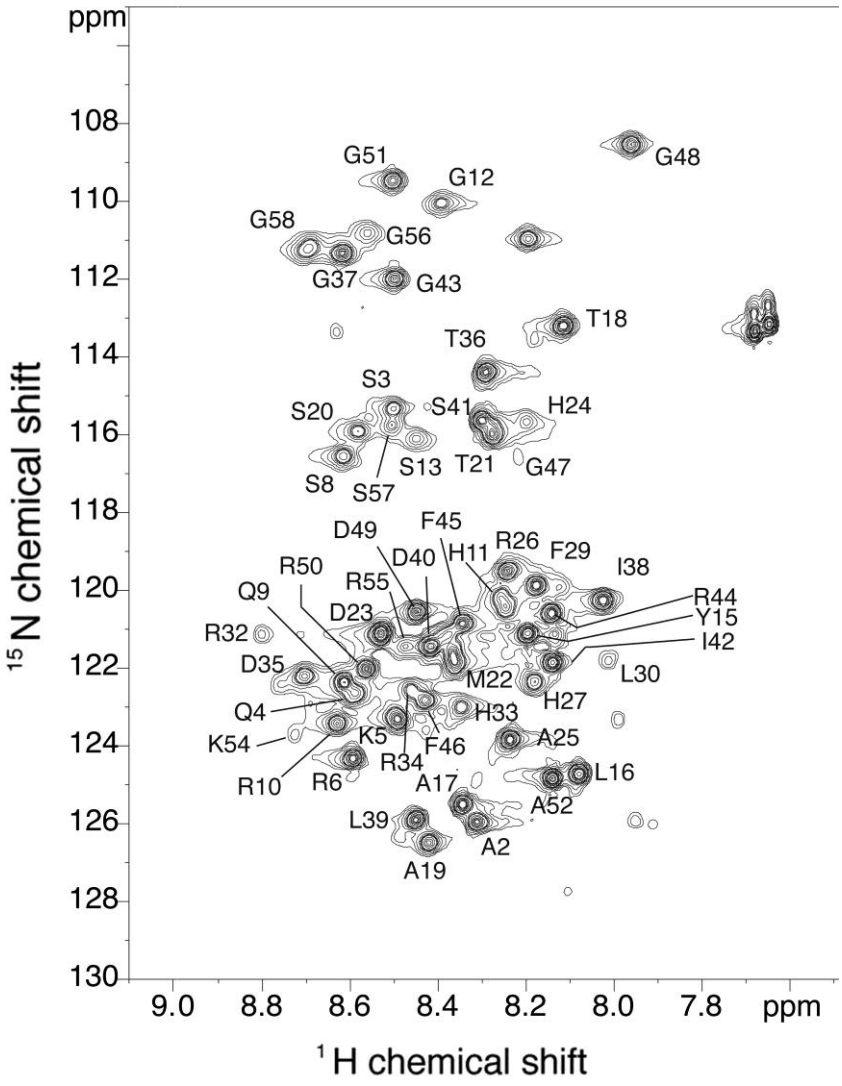

FIGURE 4.9 **^{1}H, ^{15}N HSQC spectrum of uniformly labeled ^{15}N, ^{13}C – MBP1.** 0.5 mM ^{15}N, ^{13}C – MBP1 was diluted to 0.5mM in PBS. 52 residues were assigned out of a possible 60 (64 minus 4 prolines).

A **B**

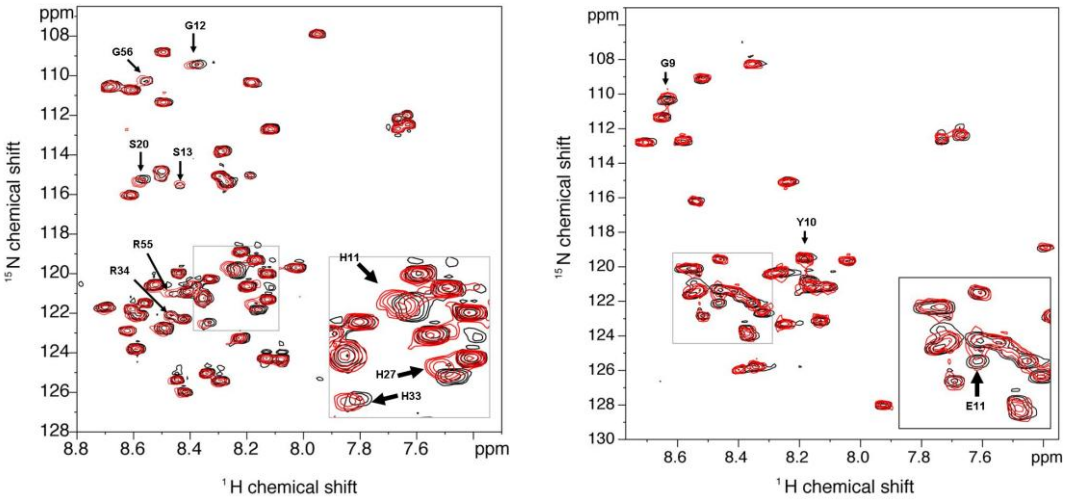

C 1 - **MASOKRPSORHGSKYLATASTMDHARHGFLPRHRDTGILDSIGRFFGGDRGAPKRGSGKDSHHP** - 64

D 1 - **DAEFRHDSGYEVHHQKLVFFAEDVGSNKGAIIGLMVGGVV** - 40

FIGURE 4.10 **^{1}H –^{15}N HSQC of MBP1 interaction with Aβ40WT.** **A.** Uniformly labeled ^{15}N – MBP1 measured with (red) and without (black) Aβ40DI. **B.** Uniformly labeled Aβ40WT measured with (red) and without (black) MBP1. **C.** MBP1 sequence with the locations of residues (red) found to shift in the presence of Aβ40DI. **D.** Sequence of Aβ40WT with the locations of residues (red) found to shift in the presence of MBP1.

CHAPTER 5 – Conclusions

5.1 – Summary of Results

In this study we endeavored to explain a peculiarity of familial CAA in which mutant Aβ peptides deposit in diffuse non-fibrillar plaques in the brain parenchyma (*30, 31*), yet exhibit a high propensity to form amyloid fibrils *in-vitro* (*35, 42, 43, 45*) This is in contrast to wild-type Aβ that deposits in fibrillar plaques in AD, yet exhibits a much slower rate of fibrillogenesis compared to CAA mutant Aβ *in-vitro*. We postulated that some unknown endogenous factors in the brain may be regulating the fibrillogenesis of CAA mutant Aβ peptides (Chapter 2). Employing Aβ peptides as ligands we used affinity chromatography to isolate MBP out of a soluble fraction of normal human brain homogenates. We found that MBP bound most strongly to the more fibrilllogenic CAA double mutant Aβ40DI peptide over the Aβ40WT. This was confirmed with SPR measurements showing MBP had a higher affinity for Aβ40DI than it did for Aβ40WT. Using a combination of thioflavin T fibrillogenesis assays, SDS-PAGE, TEM, and AFM we demonstrated MBP's ability to inhibit the fibrillogenesis of Aβ40DI *in-vitro*. We found that a stoichiometry of 1:8 (MBP:Aβ) to be effective for inhibition. These results support our original hypothesis with MBP as the endogenous factor capable of inhibiting CAA mutant Aβ fibrillogenesis.

Apart from fibrillogenic CAA mutant Aβ peptides, Aβ42WT, a longer variant of wild-type Aβ, also exhibits a high rate of fibrillogenesis *in-vitro*. It has been shown that Aβ42WT deposition may seed deposition of Aβ40WT in amyloid plaques and cerebral

vascular lesions (*98-100*). An increase in the risk of developing AD pathology can result from elevated levels of soluble Aβ42 (*100*). In view of the growing evidence of the importance of Aβ42WT to AD pathology we determined to examine what interaction MBP may have with Aβ42WT (Chapter 3).

We discovered that MBP was capable of binding to Aβ42WT through co-immunoprecipitation. These results were confirmed with the use of SPR in which Aβ42WT was used as a surface ligand for MBP. It was found that the affinity MBP has for Aβ42WT was similar to its affinity for Aβ40DI and that this affinity was higher than the less fibrilllogenic Aβ40WT.

We used several methods to demonstrate that MBP could inhibit the fibrillogenesis of Aβ42WT. Beta sheet structures give a characteristic positive signal at 195 nm and a negative signal at 215 nm when measured using CD spectroscopy. Plots of the absolute value of the CD signal at 215 nm of Aβ42WT over a 48 h time course showed an increase in beta sheet structure. When incubated with MBP this increase was not evident indicating inhibition of beta sheet formation. This finding was supported by total reflectance ATR in which comparisons of the Amide I band of Aβ42WT with and without MBP showed an inhibition in the formation of both β-turn and β-sheet structure over time. Thioflavin T assays added further support to the evidence that MBP could inhibit Aβ42WT fibril formation. Direct visual evidence of fibril inhibition was provided through TEM and AFM. Together, these data prove that MBP can interact with Aβ42WT and that this interaction is similarly as strong as it is with Aβ40DI. The data also demonstrates that MBP can inhibit the fibrillogenesis of Aβ42WT *in-vitro* at a

similar stoichiometry as with Aβ40DI.

The similarities in the binding affinity and inhibition of both Aβ40DI and Aβ42WT with MBP raised further questions. Originally it was assumed that MBP's high affinity was mediated by the E22Q and D23N mutations in Aβ40DI, but Aβ42WT has no substitutions. So we next determined to understand the mechanism behind MBP's high affinity for Aβ and its inhibition of fibril formation of the more fibrillogenic Aβ peptides. To do this we began a systematic analysis of the structural interactions between MBP and Aβ40DI (Chapter 4). Initially MBP was divided into four shorter peptides and recombinantly expressed. These peptides were analyzed for binding to aβ40DI by SPR in order to narrow down the region on MBP that mediates this interaction. We found that the peptide, MBP1, constituting the first 64 amino acids at the N-terminus of MBP exhibited an ability to bind to Aβ40DI while the rest of the peptides demonstrated no binding. It was confirmed through thioflavin T assay as well as TEM that MBP1 contained the motif necessary to inhibit Aβ40DI fibrillogenesis.

We next produced C-terminal truncations of MBP1, first removing residues 50-64, to narrow down the sequence further (MBP1ΔCT). SPR analysis showed that without this truncated region the binding to Aβ40DI was lost. This loss of binding was also associated with a loss in Aβ40DI fibril inhibition, demonstrated by thioflavin T assay. This suggested that this truncated region must contain a necessary element for the binding of Aβ, although the exact motif could still not be determined from this alone. It is known that MBP is an intrinsically unstructured protein (*103*). As such, it is capable of assuming many different conformations depending on the environment and ligand to

which it interacts. With this in mind it seemed possible that MBP1 may adopt a tertiary structure upon interaction with Aβ40DI that requires the interaction of several distal motifs. The truncated region of MBP1 ΔCT may be necessary for the formation of this conformation and may or may not be involved in the direct binding to Aβ.

A sequence comparison of MBP to an Aβ binding site in APP (*115*) revealed an interesting homology within the truncated region of MBP1 ΔCT (KRGxxxxxxHP). From this motif several alanine substitution mutants were recombinantly prepared. The mutant peptides MBP1 ΔKRG and MBP1 ΔHP both showed a lack of binding to Aβ40DI by SPR and a loss of fibril inhibition by thioflavin T assay. The mutant MBP1 S57A however retained its binding and inhibition.

Solution NMR studies were performed to more accurately identify residues involved in the interaction with Aβ. 3D scans of uniformly labeled ^{13}C, ^{15}N – MBP1 were carried out in order to place assignments for the backbone resonances. 52 of the residues were identified out of a possible 60 (64 residues minus 4 prolines). Some of the cross peaks could not be resolved, possibly due to heterogeneity in the sample associated with the unstructured conformation of MBP1. Analysis of the ^{1}H – ^{15}N HSQC spectra of ^{15}N – MBP1 both with and without Aβ40DI revealed several shifting cross peaks. These could be identified as residues H11, G12, S13, S20, H27, H33, R34, R55, and G56. The reverse experiment was performed on ^{15}N – Aβ40WT with and without MBP1 resulting in peak shifts at residues G9, Y10, E11 on Aβ40WT. These results indicate that MBP1 mediates its binding of Aβ through several distal residues, and that Aβ interacts with MBP1 through its N-terminus.

5.2 – Open Questions

These studies began with the conflicting observations of non fibrillar plaques in brain parenchyma of familial CAA mutant Aβ peptides and their high rate of fibrillogenesis *in-vitro*. The opposite seemed to be true of wild type Aβ40. We have shown that MBP is an endogenous brain protein that selectively inhibits the fibrillogenesis of Aβ40DI, a double mutant CAA Aβ peptide. We have since seen that MBP does bind Aβ40WT and binds and inhibits Aβ42WT as well. Based on this line of reasoning it would seem that in AD and related conditions that produce wild-type Aβ that MBP should prevent amyloid fibrillogenesis as well. However, although it seems likely, we do not yet know if MBP can in fact inhibit the fibril formation of Aβ40WT. Our studies were hampered by the long incubation times necessary for Aβ40WT fibrillogenesis and the instability of MBP in solution. Now that we have generated a stable peptide, MBP1, these studies can proceed.

One possible model for the interaction of MBP with Aβ peptides is that it does so not with monomers, but with Aβ oligomers. This is consistent with the 1:8 stoichiometry that was found in our studies. It is highly likely that different Aβ peptides follow different folding pathways towards fibril formation. Several different oligomeric structures have been proposed and MBP may not necessarily interact with all of these. It may be possible that Aβ40WT does not form oligomeric species that MBP would exhibit a high affinity. It is also possible that there are other molecules in the brain that interact with MBP, Aβ, or both which may modulate the interaction of MBP with Aβ40WT, but that the higher affinity of MBP for Aβ40DI and Aβ42WT can overcome these

inhibitions. Further study will need to be done to understand MBP's interactions with Aβ40WT and the implications of those interactions.

We have shown evidence for the *in-vitro* inhibition of Aβ peptide fibrillogenesis by MBP, but it remains to be seen however, if this *in-vitro* inhibition has *in-vivo* significance. It is known that many types of injury in the brain, such as traumatic head injury, and diseases like multiple sclerosis (MS) and Parkinson's disease all can elevate the levels of MBP related peptides in the cerebral spinal fluid (CSF) (*114, 118-121*). This elevation is due to direct damage to white matter and myelin. The pathology of AD includes the involvement of white matter lesions in the brain that contribute directly to cognitive decline (*122, 123*). Although there is little evidence in the literature on the elevation of MBP specifically in AD, it seems likely that MBP degradation products should increase during periods of white matter damage.

One hypothetical model for the interaction of MBP with Aβ during AD and related disorders would be upon the release of MBP from damaged myelin. One approach to test for this association would be to determine if Aβ and MBP co-localize in brain tissue sections. However, upon the release of MBP from myelin the protein is subjected to proteolytic degradation into several smaller peptides (*119, 120*). These peptides may be difficult to detect with antibodies in tissue, due primarily to the unavailability of commercial antibodies spanning the whole sequence of MBP. Further, a small peptide fragment bound to Aβ may be blocked from detection by an antibody. To address co-localization in tissue of Aβ and MBP peptides it will be necessary to design

other techniques for direct visualization.

Indirect evidence of Aβ interactions with MBP peptides obtained through the use of animal knockouts such as the Shiverer mouse is not useful. This animal has a natural deletion of exons 3-7 in the classical MBP genes (*124*). Crosses with AD or CAA model animals should be expected to change the deposition of Aβ in the offspring due to less MBP in the brain. However, the changes to the brain physiology of these animals may be too drastic to allow for meaningful interpretation of AD or CAA model animals crossed with these Shiverer animals. Also, these animals still produce certain Golli-MBP proteins containing the region that interacts with Aβ further complicating interpretation of results. Better approaches to look at Aβ and MBP *in-vivo* may include transfection of tagged-MBP through the use of viral vectors in AD and CAA model animals. Alternatively, shorter peptides of MBP, such as MBP1, containing the minimal required Aβ binding motif may be delivered into the brains of model animals through various means and the effects on Aβ measured.

Other possible models for the interaction of MBP with Aβ may not necessarily involve white matter lesions at all, but rather the release of MBP during inflammation. It has been shown that both peripheral macrophages and microglia express Golli-MBP and that this expression increases during inflammation (*70, 125*). Peripheral macrophages infiltrate the brain during episodes of inflammation and in response to brain injury. Further, Golli-MBP has been shown to be secreted from microglia in response to LPS induced inflammation in culture (*70*). This could place MBP-related peptides in direct contact with Aβ lesions in AD in which activated microglia are found surrounding Aβ

plaques. It will need to be determined experimentally, however, if microglia and infiltrating macrophages secrete Golli-MBP in response to inflammatory signals associated with Aβ deposits in AD. If this hypothesis is correct then it would indicate that MBP peptides may have a much earlier involvement with Aβ deposition than if they were released only after white matter lesions were formed. This would also suggest a potential non-pathological role for MBP peptides in the clearance of Aβ in healthy individuals.

Within the brain it is theorized that there are local specialized populations of microglia that may respond differently to different stimuli (*126-128*). These sub-populations may contain hematopoetically derived infiltrating macrophages as well as resident CNS microglia whose heterogeneity may arise through a variety of different mechanisms involving specific interactions with the local environment of different brain regions in both healthy and pathological states (*128, 129*). These macrophages along with the many theorized sub-populations of microglia may respond differently to stimuli such as Aβ deposition. If we are to understand the potential role that Golli-MBP secreting microglia and macrophages have in the response to Aβ deposition, then these differences must be more fully understood. For instance, it may be possible that not all sub-populations of microglia and infiltrating macrophages will secrete Golli-MBP at similar levels in response to inflammatory signals. Deposits of different familial CAA mutant Aβ peptides may not ultimately induce similar levels of activation in all microglial sub-populations as well. These possibilities could lead to the differences in microglial activation, possible Golli-MBP secretion, Aβ fibrillogenesis, and inflammation

induced cellular toxicity seen in AD and related disorders.

Another confounding question that is still a topic of debate relates to the causes of the regional differences in Aβ deposition seen in familial CAA. In Dutch and Iowa type CAA the parenchymal Aβ deposits are primarily non-fibrillar, while there is robust amyloid deposition along the cerebral vasculature (*26, 30*). If MBP peptides that interact with Aβ are primarily derived from white matter, then the distance of the cerebral vasculature from regions of white matter (and therefore MBP peptides) may partially explain why they are so affected by fibrillar amyloid while regions of the parenchyma closer to white matter are not. It could be expected that the closer an Aβ deposit is to regions of white matter, the higher the concentration of MBP and related peptides it would likely encounter leading to what is observed as a lesser degree of fibril formation. However, this model is almost certainly too simplistic. There are many other factors that drive and inhibit Aβ fibril formation and their interactions with MBP peptides and Aβ need to be considered.

It is known that the fibrillization of Aβ can be seeded by the interaction with certain cell surface receptors such as GM1 and GM3 gangliosides (*46, 126, 127*), which are not found evenly distributed throughout the brain. Cerebral vascular smooth muscle cells, which are primarily affected by fibrillar deposits of Aβ in familial CAA, express both GM1 and GM3. The expression of GM3 is exclusive to these cells, which may partially explain why they are affected so severely in familial CAA. It is known that MBP interacts with several gangliosides including GM1 and GM3 (*128*). It is not known

however, what the affect of MBP peptide binding to gangliosides would have on the seeding of Aβ fibrils by these gangliosides. Perhaps the interaction may increase the affinity of Aβ for gangliosides thereby increasing cell surface fibril formation. If true this could possibly explain why cerebrovascular smooth muscle cells suffer such a high degree of amyloid deposition in fCAA. However, it is just as likely that MBP peptide interactions with gangliosides may inhibit Aβ seeding leading to less fibrillar amyloid. If this is true then it suggests other factors must be involved in the high degree of Aβ fibrillization associated with gangliosides and cerebrovascular smooth muscle cells in fCAA. The third possibility, of course, is that MBP peptide interactions with gangliosides may have no affect on the seeding of Aβ fibrils. The potential secretion of Golli proteins by infiltrating macrophages at sites of vascular amyloidosis and possible interactions with gangliosides must be understood better if these questions are to be answered.

The effects of MBP peptides on different cell populations must also be taken into account. For instance, MBP peptides have been shown to have mitogenic affects on astrocytes (*129*) and to promote the proliferation of Schwann cells (*130*). Whole MBP has been shown to be cytotoxic to mature oligodendrocytes (*131*). Understanding the different effects MBP may have on different cell populations must be taken into account when performing studies designed to examine the effect endogenous MBP has on Aβ cytotoxicity and fibril formation in culture.

It is also worth noting that MBP proteins are extensively modified *in-vivo*

resulting in a highly heterogeneous population of proteins and peptides that can display very different properties (*61*). What effect MBP heterogeneity may have on interactions with Aβ peptides remains an area that is little understood, but one that may ultimately be important.

Recent findings in the study of Aβ and AD suggest that fibrils of Aβ may not necessarily be the toxic species. Some recent studies have shown that, in fact, soluble oligomers are the most toxic (*132, 133*). We have shown that MBP is able to inhibit fibril formation in both fibrilllogenic Aβ40DI and Aβ42WT. It appears from some of our AFM data that oligomeric species of Aβ may in fact be interacting with and stabilized by MBP. The fact that MBP interacts most strongly to the most fibrillogenic Aβ peptides may be viewed as a function of their rate and extent of oligomer formation in solution. Also, the stoichiometry of the interaction suggests that MBP is interacting with up to as many as 10 monomers of Aβ at once. It is difficult to imagine how this could be unless those monomers are actually organized into an oligomeric structure. It remains to be understood whether or not the interaction between Aβ and MBP (or MBP peptides) actually protects cells or whether, in fact, this interaction may be cytotoxic. Protective and cytotoxic effects of this interaction may also vary from cell type to cell type in the brain.

Structural studies of the mechanism of interaction between Aβ peptides and MBP have only just begun. Future studies using NMR are planned with the ultimate goal of

creating a 3-dimensional model of the backbone assignments of MBP1 with and without Aβ present. It remains to be seen whether clear information on the structure of Aβ oligomers in the presence of MBP can be obtained, however it remains a goal. Structural data may give us insight into the nature of Aβ peptides as well as the structure and function of MBP and what role if any it plays in AD and related disorders.

The study of the properties of Aβ and MBP in both pathology and health is an important and fundamental part of the understanding of neurobiology. Diseases such as AD, Parkinson's, CAA, MS and many others, are the result of imbalances in the metabolism and functioning of these proteins. There is much that is yet to be understood. This study provides insight into the functions of both Aβ peptides and MBP that may ultimately be useful in furthering greater understanding of human health.

REFERENCES

1. Selkoe, D. J. (2001) Alzheimer's disease: genes, proteins, and therapy, *Physiol Rev 81*, 741-766.
2. Masters, C. L., Simms, G., Weinman, N. A., Multhaup, G., McDonald, B. L., and Beyreuther, K. (1985) Amyloid plaque core protein in Alzheimer disease and Down syndrome, *Proc Natl Acad Sci U S A 82*, 4245-4249.
3. Kang, J., Lemaire, H. G., Unterbeck, A., Salbaum, J. M., Masters, C. L., Grzeschik, K. H., Multhaup, G., Beyreuther, K., and Muller-Hill, B. (1987) The precursor of Alzheimer's disease amyloid A4 protein resembles a cell-surface receptor, *Nature 325*, 733-736.
4. Goldgaber, D., Lerman, M. I., McBride, O. W., Saffiotti, U., and Gajdusek, D. C. (1987) Characterization and chromosomal localization of a cDNA encoding brain amyloid of Alzheimer's disease, *Science 235*, 877-880.
5. Tanzi, R. E., Gusella, J. F., Watkins, P. C., Bruns, G. A., St George-Hyslop, P., Van Keuren, M. L., Patterson, D., Pagan, S., Kurnit, D. M., and Neve, R. L. (1987) Amyloid beta protein gene: cDNA, mRNA distribution, and genetic linkage near the Alzheimer locus, *Science 235*, 880-884.
6. Robakis, N. K., Ramakrishna, N., Wolfe, G., and Wisniewski, H. M. (1987) Molecular cloning and characterization of a cDNA encoding the cerebrovascular and the neuritic plaque amyloid peptides, *Proc Natl Acad Sci U S A 84*, 4190-4194.
7. Ponte, P., Gonzalez-DeWhitt, P., Schilling, J., Miller, J., Hsu, D., Greenberg, B., Davis, K., Wallace, W., Lieberburg, I., and Fuller, F. (1988) A new A4 amyloid mRNA contains a domain homologous to serine proteinase inhibitors, *Nature 331*, 525-527.
8. Tanzi, R. E., McClatchey, A. I., Lamperti, E. D., Villa-Komaroff, L., Gusella, J. F., and Neve, R. L. (1988) Protease inhibitor domain encoded by an amyloid protein precursor mRNA associated with Alzheimer's disease, *Nature 331*, 528-530.
9. Kitaguchi, N., Takahashi, Y., Tokushima, Y., Shiojiri, S., and Ito, H. (1988) Novel precursor of Alzheimer's disease amyloid protein shows protease inhibitory activity, *Nature 331*, 530-532.
10. Vassar, R., Bennett, B. D., Babu-Khan, S., Kahn, S., Mendiaz, E. A., Denis, P., Teplow, D. B., Ross, S., Amarante, P., Loeloff, R., Luo, Y., Fisher, S., Fuller, J., Edenson, S., Lile, J., Jarosinski, M. A., Biere, A. L., Curran, E., Burgess, T., Louis, J. C., Collins, F., Treanor, J., Rogers, G., and Citron, M. (1999) Beta-secretase cleavage of Alzheimer's amyloid precursor protein by the transmembrane aspartic protease BACE, *Science 286*, 735-741.
11. Sinha, S., Anderson, J. P., Barbour, R., Basi, G. S., Caccavello, R., Davis, D., Doan, M., Dovey, H. F., Frigon, N., Hong, J., Jacobson-Croak, K., Jewett, N.,

Keim, P., Knops, J., Lieberburg, I., Power, M., Tan, H., Tatsuno, G., Tung, J., Schenk, D., Seubert, P., Suomensaari, S. M., Wang, S., Walker, D., Zhao, J., McConlogue, L., and John, V. (1999) Purification and cloning of amyloid precursor protein beta-secretase from human brain, *Nature 402*, 537-540.

12. John, V., Beck, J. P., Bienkowski, M. J., Sinha, S., and Heinrikson, R. L. (2003) Human beta-secretase (BACE) and BACE inhibitors, *J Med Chem 46*, 4625-4630.
13. De Strooper, B., Saftig, P., Craessaerts, K., Vanderstichele, H., Guhde, G., Annaert, W., Von Figura, K., and Van Leuven, F. (1998) Deficiency of presenilin-1 inhibits the normal cleavage of amyloid precursor protein, *Nature 391*, 387-390.
14. Wolfe, M. S., Xia, W., Ostaszewski, B. L., Diehl, T. S., Kimberly, W. T., and Selkoe, D. J. (1999) Two transmembrane aspartates in presenilin-1 required for presenilin endoproteolysis and gamma-secretase activity, *Nature 398*, 513-517.
15. Edbauer, D., Winkler, E., Regula, J. T., Pesold, B., Steiner, H., and Haass, C. (2003) Reconstitution of gamma-secretase activity, *Nat Cell Biol 5*, 486-488.
16. Vinters, H. V. (1987) Cerebral amyloid angiopathy. A critical review, *Stroke 18*, 311-324.
17. Jellinger, K. A. (2002) Alzheimer disease and cerebrovascular pathology: an update, *J Neural Transm 109*, 813-836.
18. Vinters, H. V., and Farag, E. S. (2003) Amyloidosis of cerebral arteries, *Adv Neurol 92*, 105-112.
19. Rensink, A. A., de Waal, R. M., Kremer, B., and Verbeek, M. M. (2003) Pathogenesis of cerebral amyloid angiopathy, *Brain Res Brain Res Rev 43*, 207-223.
20. Kawai, M., Kalaria, R. N., Cras, P., Siedlak, S. L., Velasco, M. E., Shelton, E. R., Chan, H. W., Greenberg, B. D., and Perry, G. (1993) Degeneration of vascular muscle cells in cerebral amyloid angiopathy of Alzheimer disease, *Brain Res 623*, 142-146.
21. Bailey, T. L., Rivara, C. B., Rocher, A. B., and Hof, P. R. (2004) The nature and effects of cortical microvascular pathology in aging and Alzheimer's disease, *Neurol Res 26*, 573-578.
22. Attems, J., and Jellinger, K. A. (2004) Only cerebral capillary amyloid angiopathy correlates with Alzheimer pathology--a pilot study, *Acta Neuropathol 107*, 83-90.
23. (2001) Pathological correlates of late-onset dementia in a multicentre, community-based population in England and Wales. Neuropathology Group of the Medical Research Council Cognitive Function and Ageing Study (MRC CFAS), *Lancet 357*, 169-175.
24. Thal, D. R., Ghebremedhin, E., Orantes, M., and Wiestler, O. D. (2003) Vascular pathology in Alzheimer disease: correlation of cerebral amyloid angiopathy and arteriosclerosis/lipohyalinosis with cognitive decline, *J Neuropathol Exp Neurol 62*, 1287-1301.
25. Levy, E., Carman, M. D., Fernandez-Madrid, I. J., Power, M. D., Lieberburg, I., van Duinen, S. G., Bots, G. T., Luyendijk, W., and Frangione, B. (1990) Mutation

of the Alzheimer's disease amyloid gene in hereditary cerebral hemorrhage, Dutch type, *Science 248*, 1124-1126.

26. Van Broeckhoven, C., Haan, J., Bakker, E., Hardy, J. A., Van Hul, W., Wehnert, A., Vegter-Van der Vlis, M., and Roos, R. A. (1990) Amyloid beta protein precursor gene and hereditary cerebral hemorrhage with amyloidosis (Dutch), *Science 248*, 1120-1122.
27. Hendriks, L., van Duijn, C. M., Cras, P., Cruts, M., Van Hul, W., van Harskamp, F., Warren, A., McInnis, M. G., Antonarakis, S. E., Martin, J. J., and et al. (1992) Presenile dementia and cerebral haemorrhage linked to a mutation at codon 692 of the beta-amyloid precursor protein gene, *Nat Genet 1*, 218-221.
28. Kamino, K., Orr, H. T., Payami, H., Wijsman, E. M., Alonso, M. E., Pulst, S. M., Anderson, L., O'Dahl, S., Nemens, E., White, J. A., and et al. (1992) Linkage and mutational analysis of familial Alzheimer disease kindreds for the APP gene region, *Am J Hum Genet 51*, 998-1014.
29. Tagliavini, F., Rossi, G., Padovani, A., Magoni, M., Andora, G., Sgarzi, M., Bizzi, A., Savioardo, M., Carella, F., Morbin, M., Giaccone, G., Bugiani, O. (1999) A new APP mutation related to hereditary cerebral hemorrhage. , *Alzheimer's Reports 2*, S28.
30. Grabowski, T. J., Cho, H. S., Vonsattel, J. P., Rebeck, G. W., and Greenberg, S. M. (2001) Novel amyloid precursor protein mutation in an Iowa family with dementia and severe cerebral amyloid angiopathy, *Ann Neurol 49*, 697-705.
31. van Duinen, S. G., Castano, E. M., Prelli, F., Bots, G. T., Luyendijk, W., and Frangione, B. (1987) Hereditary cerebral hemorrhage with amyloidosis in patients of Dutch origin is related to Alzheimer disease, *Proc Natl Acad Sci U S A 84*, 5991-5994.
32. Wattendorff, A. R., Frangione, B., Luyendijk, W., and Bots, G. T. (1995) Hereditary cerebral haemorrhage with amyloidosis, Dutch type (HCHWA-D): clinicopathological studies, *J Neurol Neurosurg Psychiatry 58*, 699-705.
33. Maat-Schieman, M. L., van Duinen, S. G., Rozemuller, A. J., Haan, J., and Roos, R. A. (1997) Association of vascular amyloid beta and cells of the mononuclear phagocyte system in hereditary cerebral hemorrhage with amyloidosis (Dutch) and Alzheimer disease, *J Neuropathol Exp Neurol 56*, 273-284.
34. Davis, J., Xu, F., Deane, R., Romanov, G., Previti, M. L., Zeigler, K., Zlokovic, B. V., and Van Nostrand, W. E. (2004) Early-onset and robust cerebral microvascular accumulation of amyloid beta-protein in transgenic mice expressing low levels of a vasculotropic Dutch/Iowa mutant form of amyloid beta-protein precursor, *J Biol Chem 279*, 20296-20306.
35. Van Nostrand, W. E., Melchor, J. P., Cho, H. S., Greenberg, S. M., and Rebeck, G. W. (2001) Pathogenic effects of D23N Iowa mutant amyloid beta -protein, *J Biol Chem 276*, 32860-32866.
36. Miao, J., Xu, F., Davis, J., Otte-Holler, I., Verbeek, M. M., and Van Nostrand, W. E. (2005) Cerebral microvascular amyloid beta protein deposition induces vascular degeneration and neuroinflammation in transgenic mice expressing

human vasculotropic mutant amyloid beta precursor protein, *Am J Pathol 167*, 505-515.
37. Maat-Schieman, M. L., Yamaguchi, H., Hegeman-Kleinn, I. M., Welling-Graafland, C., Natte, R., Roos, R. A., and van Duinen, S. G. (2004) Glial reactions and the clearance of amyloid beta protein in the brains of patients with hereditary cerebral hemorrhage with amyloidosis-Dutch type, *Acta Neuropathol 107*, 389-398.
38. Rozemuller, A. J., Roos, R. A., Bots, G. T., Kamphorst, W., Eikelenboom, P., and Van Nostrand, W. E. (1993) Distribution of beta/A4 protein and amyloid precursor protein in hereditary cerebral hemorrhage with amyloidosis-Dutch type and Alzheimer's disease, *Am J Pathol 142*, 1449-1457.
39. Bornebroek, M., De Jonghe, C., Haan, J., Kumar-Singh, S., Younkin, S., Roos, R., and Van Broeckhoven, C. (2003) Hereditary cerebral hemorrhage with amyloidosis Dutch type (AbetaPP 693): decreased plasma amyloid-beta 42 concentration, *Neurobiol Dis 14*, 619-623.
40. Natte, R., Maat-Schieman, M. L., Haan, J., Bornebroek, M., Roos, R. A., and van Duinen, S. G. (2001) Dementia in hereditary cerebral hemorrhage with amyloidosis-Dutch type is associated with cerebral amyloid angiopathy but is independent of plaques and neurofibrillary tangles, *Ann Neurol 50*, 765-772.
41. Shin, Y., Cho, H. S., Rebeck, G. W., and Greenberg, S. M. (2002) Vascular changes in Iowa-type hereditary cerebral amyloid angiopathy, *Ann N Y Acad Sci 977*, 245-251.
42. Davis, J., and Van Nostrand, W. E. (1996) Enhanced pathologic properties of Dutch-type mutant amyloid beta-protein, *Proc Natl Acad Sci U S A 93*, 2996-3000.
43. Verbeek, M. M., de Waal, R. M., Schipper, J. J., and Van Nostrand, W. E. (1997) Rapid degeneration of cultured human brain pericytes by amyloid beta protein, *J Neurochem 68*, 1135-1141.
44. Miravalle, L., Tokuda, T., Chiarle, R., Giaccone, G., Bugiani, O., Tagliavini, F., Frangione, B., and Ghiso, J. (2000) Substitutions at codon 22 of Alzheimer's abeta peptide induce diverse conformational changes and apoptotic effects in human cerebral endothelial cells, *J Biol Chem 275*, 27110-27116.
45. Melchor, J. P., McVoy, L., and Van Nostrand, W. E. (2000) Charge alterations of E22 enhance the pathogenic properties of the amyloid beta-protein, *J Neurochem 74*, 2209-2212.
46. Yamamoto, N., Hirabayashi, Y., Amari, M., Yamaguchi, H., Romanov, G., Van Nostrand, W. E., and Yanagisawa, K. (2005) Assembly of hereditary amyloid beta-protein variants in the presence of favorable gangliosides, *FEBS Lett 579*, 2185-2190.
47. Deane, R., Wu, Z., Sagare, A., Davis, J., Du Yan, S., Hamm, K., Xu, F., Parisi, M., LaRue, B., Hu, H. W., Spijkers, P., Guo, H., Song, X., Lenting, P. J., Van Nostrand, W. E., and Zlokovic, B. V. (2004) LRP/amyloid beta-peptide interaction mediates differential brain efflux of Abeta isoforms, *Neuron 43*, 333-344.

48. Strittmatter, W. J., Weisgraber, K. H., Huang, D. Y., Dong, L. M., Salvesen, G. S., Pericak-Vance, M., Schmechel, D., Saunders, A. M., Goldgaber, D., and Roses, A. D. (1993) Binding of human apolipoprotein E to synthetic amyloid beta peptide: isoform-specific effects and implications for late-onset Alzheimer disease, *Proc Natl Acad Sci U S A 90*, 8098-8102.
49. LaDu, M. J., Falduto, M. T., Manelli, A. M., Reardon, C. A., Getz, G. S., and Frail, D. E. (1994) Isoform-specific binding of apolipoprotein E to beta-amyloid, *J Biol Chem 269*, 23403-23406.
50. Pillot, T., Goethals, M., Najib, J., Labeur, C., Lins, L., Chambaz, J., Brasseur, R., Vandekerckhove, J., and Rosseneu, M. (1999) Beta-amyloid peptide interacts specifically with the carboxy-terminal domain of human apolipoprotein E: relevance to Alzheimer's disease, *J Neurochem 72*, 230-237.
51. Sanan, D. A., Weisgraber, K. H., Russell, S. J., Mahley, R. W., Huang, D., Saunders, A., Schmechel, D., Wisniewski, T., Frangione, B., Roses, A. D., and et al. (1994) Apolipoprotein E associates with beta amyloid peptide of Alzheimer's disease to form novel monofibrils. Isoform apoE4 associates more efficiently than apoE3, *J Clin Invest 94*, 860-869.
52. Campagnoni, A. T., Pribyl, T. M., Campagnoni, C. W., Kampf, K., Amur-Umarjee, S., Landry, C. F., Handley, V. W., Newman, S. L., Garbay, B., and Kitamura, K. (1993) Structure and developmental regulation of Golli-mbp, a 105-kilobase gene that encompasses the myelin basic protein gene and is expressed in cells in the oligodendrocyte lineage in the brain, *J Biol Chem 268*, 4930-4938.
53. Pribyl, T. M., Campagnoni, C. W., Kampf, K., Kashima, T., Handley, V. W., McMahon, J., and Campagnoni, A. T. (1993) The human myelin basic protein gene is included within a 179-kilobase transcription unit: expression in the immune and central nervous systems, *Proc Natl Acad Sci U S A 90*, 10695-10699.
54. Givogri, M. I., Bongarzone, E. R., and Campagnoni, A. T. (2000) New insights on the biology of myelin basic protein gene: the neural-immune connection, *J Neurosci Res 59*, 153-159.
55. Pribyl, T. M., Campagnoni, C. W., Kampf, K., Ellison, J. A., Landry, C. F., Kashima, T., McMahon, J., and Campagnoni, A. T. (1996) Expression of the myelin basic protein gene locus in neurons and oligodendrocytes in the human fetal central nervous system, *J Comp Neurol 374*, 342-353.
56. Tosic, M., Rakic, S., Matthieu, J. M., and Zecevic, N. (2002) Identification of Golli and myelin basic proteins in human brain during early development, *Glia 37*, 219-228.
57. Roth, H. J., Kronquist, K. E., Kerlero de Rosbo, N., Crandall, B. F., and Campagnoni, A. T. (1987) Evidence for the expression of four myelin basic protein variants in the developing human spinal cord through cDNA cloning, *J Neurosci Res 17*, 321-328.
58. Baumann, N., and Pham-Dinh, D. (2001) Biology of oligodendrocyte and myelin in the mammalian central nervous system, *Physiol Rev 81*, 871-927.
59. Moscarello, M. A. (1990) Myelin basic protein: a dynamically changing structure, *Prog Clin Biol Res 336*, 25-48.

60. Smith, R. (1992) The basic protein of CNS myelin: its structure and ligand binding, *J Neurochem 59*, 1589-1608.
61. Zand, R., Li, M. X., Jin, X., and Lubman, D. (1998) Determination of the sites of posttranslational modifications in the charge isomers of bovine myelin basic protein by capillary electrophoresis-mass spectroscopy, *Biochemistry 37*, 2441-2449.
62. Wood, D. D., and Moscarello, M. A. (1989) The isolation, characterization, and lipid-aggregating properties of a citrulline containing myelin basic protein, *J Biol Chem 264*, 5121-5127.
63. Polverini, E., Boggs, J. M., Bates, I. R., Harauz, G., and Cavatorta, P. (2004) Electron paramagnetic resonance spectroscopy and molecular modelling of the interaction of myelin basic protein (MBP) with calmodulin (CaM)-diversity and conformational adaptability of MBP CaM-targets, *J Struct Biol 148*, 353-369.
64. Berlet, H. H., Bischoff, H., and Weinhardt, F. (1994) Divalent metals of myelin and their differential binding by myelin basic protein of bovine central nervous system, *Neurosci Lett 179*, 75-78.
65. Chan, C. K., Ramwani, J., and Moscarello, M. A. (1988) Myelin basic protein binds GTP at a single site in the N-terminus, *Biochem Biophys Res Commun 152*, 1468-1473.
66. Pirollet, F., Derancourt, J., Haiech, J., Job, D., and Margolis, R. L. (1992) Ca(2+)-calmodulin regulated effectors of microtubule stability in bovine brain, *Biochemistry 31*, 8849-8855.
67. Hill, C. M., and Harauz, G. (2005) Charge effects modulate actin assembly by classic myelin basic protein isoforms, *Biochem Biophys Res Commun 329*, 362-369.
68. Kokubo, H., Kayed, R., Glabe, C. G., and Yamaguchi, H. (2005) Soluble Abeta oligomers ultrastructurally localize to cell processes and might be related to synaptic dysfunction in Alzheimer's disease brain, *Brain Res 1031*, 222-228.
69. Cirrito, J. R., Yamada, K. A., Finn, M. B., Sloviter, R. S., Bales, K. R., May, P. C., Schoepp, D. D., Paul, S. M., Mennerick, S., and Holtzman, D. M. (2005) Synaptic activity regulates interstitial fluid amyloid-beta levels in vivo, *Neuron 48*, 913-922.
70. Filipovic, R., and Zecevic, N. (2005) Lipopolysaccharide affects Golli expression and promotes proliferation of oligodendrocyte progenitors, *Glia 49*, 457-466.
71. Bornebroek, M., Van Buchem, M. A., Haan, J., Brand, R., Lanser, J. B., de Bruine, F. T., and Roos, R. A. (1996) Hereditary cerebral hemorrhage with amyloidosis-Dutch type: better correlation of cognitive deterioration with advancing age than with number of focal lesions or white matter hyperintensities, *Alzheimer Dis Assoc Disord 10*, 224-231.
72. Wisniewski, T., Castano, E. M., Golabek, A., Vogel, T., and Frangione, B. (1994) Acceleration of Alzheimer's fibril formation by apolipoprotein E in vitro, *Am J Pathol 145*, 1030-1035.
73. Aleshkov, S., Abraham, C. R., and Zannis, V. I. (1997) Interaction of nascent ApoE2, ApoE3, and ApoE4 isoforms expressed in mammalian cells with amyloid

peptide beta (1-40). Relevance to Alzheimer's disease, *Biochemistry 36*, 10571-10580.
74. Bentley, N. M., Ladu, M. J., Rajan, C., Getz, G. S., and Reardon, C. A. (2002) Apolipoprotein E structural requirements for the formation of SDS-stable complexes with beta-amyloid-(1-40): the role of salt bridges, *Biochem J 366*, 273-279.
75. Manelli, A. M., Stine, W. B., Van Eldik, L. J., and LaDu, M. J. (2004) ApoE and Abeta1-42 interactions: effects of isoform and conformation on structure and function, *J Mol Neurosci 23*, 235-246.
76. Ghiso, J., Matsubara, E., Koudinov, A., Choi-Miura, N. H., Tomita, M., Wisniewski, T., and Frangione, B. (1993) The cerebrospinal-fluid soluble form of Alzheimer's amyloid beta is complexed to SP-40,40 (apolipoprotein J), an inhibitor of the complement membrane-attack complex, *Biochem J 293 (Pt 1)*, 27-30.
77. Matsubara, E., Frangione, B., and Ghiso, J. (1995) Characterization of apolipoprotein J-Alzheimer's A beta interaction, *J Biol Chem 270*, 7563-7567.
78. DeMattos, R. B., O'Dell M, A., Parsadanian, M., Taylor, J. W., Harmony, J. A., Bales, K. R., Paul, S. M., Aronow, B. J., and Holtzman, D. M. (2002) Clusterin promotes amyloid plaque formation and is critical for neuritic toxicity in a mouse model of Alzheimer's disease, *Proc Natl Acad Sci U S A 99*, 10843-10848.
79. Mucke, L., Yu, G. Q., McConlogue, L., Rockenstein, E. M., Abraham, C. R., and Masliah, E. (2000) Astroglial expression of human alpha(1)-antichymotrypsin enhances alzheimer-like pathology in amyloid protein precursor transgenic mice, *Am J Pathol 157*, 2003-2010.
80. Potter, H., Wefes, I. M., and Nilsson, L. N. (2001) The inflammation-induced pathological chaperones ACT and apo-E are necessary catalysts of Alzheimer amyloid formation, *Neurobiol Aging 22*, 923-930.
81. Tsuzuki, K., Fukatsu, R., Yamaguchi, H., Tateno, M., Imai, K., Fujii, N., and Yamauchi, T. (2000) Transthyretin binds amyloid beta peptides, Abeta1-42 and Abeta1-40 to form complex in the autopsied human kidney - possible role of transthyretin for abeta sequestration, *Neurosci Lett 281*, 171-174.
82. Schwarzman, A. L., Tsiper, M., Wente, H., Wang, A., Vitek, M. P., Vasiliev, V., and Goldgaber, D. (2004) Amyloidogenic and anti-amyloidogenic properties of recombinant transthyretin variants, *Amyloid 11*, 1-9.
83. Yang, D. S., Serpell, L. C., Yip, C. M., McLaurin, J., Chrishti, M. A., Horne, P., Boudreau, L., Kisilevsky, R., Westaway, D., and Fraser, P. E. (2001) Assembly of Alzheimer's amyloid-beta fibrils and approaches for therapeutic intervention, *Amyloid 8 Suppl 1*, 10-19.
84. Cotman, S. L., Halfter, W., and Cole, G. J. (2000) Agrin binds to beta-amyloid (Abeta), accelerates abeta fibril formation, and is localized to Abeta deposits in Alzheimer's disease brain, *Mol Cell Neurosci 15*, 183-198.
85. Choo-Smith, L. P., Garzon-Rodriguez, W., Glabe, C. G., and Surewicz, W. K. (1997) Acceleration of amyloid fibril formation by specific binding of Abeta-(1-

40) peptide to ganglioside-containing membrane vesicles, *J Biol Chem 272*, 22987-22990.
86. Kakio, A., Nishimoto, S. I., Yanagisawa, K., Kozutsumi, Y., and Matsuzaki, K. (2001) Cholesterol-dependent formation of GM1 ganglioside-bound amyloid beta-protein, an endogenous seed for Alzheimer amyloid, *J Biol Chem 276*, 24985-24990.
87. Burdick, D., Soreghan, B., Kwon, M., Kosmoski, J., Knauer, M., Henschen, A., Yates, J., Cotman, C., and Glabe, C. (1992) Assembly and aggregation properties of synthetic Alzheimer's A4/beta amyloid peptide analogs, *J Biol Chem 267*, 546-554.
88. Stine, W. B., Jr., Dahlgren, K. N., Krafft, G. A., and LaDu, M. J. (2003) In vitro characterization of conditions for amyloid-beta peptide oligomerization and fibrillogenesis, *J Biol Chem 278*, 11612-11622.
89. Deane, R., Du Yan, S., Submamaryan, R. K., LaRue, B., Jovanovic, S., Hogg, E., Welch, D., Manness, L., Lin, C., Yu, J., Zhu, H., Ghiso, J., Frangione, B., Stern, A., Schmidt, A. M., Armstrong, D. L., Arnold, B., Liliensiek, B., Nawroth, P., Hofman, F., Kindy, M., Stern, D., and Zlokovic, B. (2003) RAGE mediates amyloid-beta peptide transport across the blood-brain barrier and accumulation in brain, *Nat Med 9*, 907-913.
90. Mastrangelo, I. A., Ahmed, M., Sato, T., Liu, W., Wang, C., Hough, P., and Smith, S. O. (2006) High-resolution atomic force microscopy of soluble Abeta42 oligomers, *J Mol Biol 358*, 106-119.
91. Hsiao, K., Chapman, P., Nilsen, S., Eckman, C., Harigaya, Y., Younkin, S., Yang, F., and Cole, G. (1996) Correlative memory deficits, Abeta elevation, and amyloid plaques in transgenic mice, *Science 274*, 99-102.
92. Maat-Schieman, M. L., van Duinen, S. G., Haan, J., and Roos, R. A. (1992) Morphology of cerebral plaque-like lesions in hereditary cerebral hemorrhage with amyloidosis (Dutch), *Acta Neuropathol 84*, 674-679.
93. Chou, F. C., Chou, C. H., Shapira, R., and Kibler, R. F. (1976) Basis of microheterogeneity of myelin basic protein, *J Biol Chem 251*, 2671-2679.
94. Richter-Landsberg, C. (2000) The oligodendroglia cytoskeleton in health and disease, *J Neurosci Res 59*, 11-18.
95. Beems, T., Simons, K. S., Van Geel, W. J., De Reus, H. P., Vos, P. E., and Verbeek, M. M. (2003) Serum- and CSF-concentrations of brain specific proteins in hydrocephalus, *Acta Neurochir (Wien) 145*, 37-43.
96. Abdo, W. F., van de Warrenburg, B. P., Munneke, M., van Geel, W. J., Bloem, B. R., Kremer, H. P., and Verbeek, M. M. (2006) CSF analysis differentiates multiple-system atrophy from idiopathic late-onset cerebellar ataxia, *Neurology 67*, 474-479.
97. Roher, A. E., Lowenson, J. D., Clarke, S., Woods, A. S., Cotter, R. J., Gowing, E., and Ball, M. J. (1993) beta-Amyloid-(1-42) is a major component of cerebrovascular amyloid deposits: implications for the pathology of Alzheimer disease, *Proc Natl Acad Sci U S A 90*, 10836-10840.

98. Dolev, I., and Michaelson, D. M. (2006) The nucleation growth and reversibility of Amyloid-beta deposition in vivo, *J Alzheimers Dis 10*, 291-301.
99. McGowan, E., Pickford, F., Kim, J., Onstead, L., Eriksen, J., Yu, C., Skipper, L., Murphy, M. P., Beard, J., Das, P., Jansen, K., Delucia, M., Lin, W. L., Dolios, G., Wang, R., Eckman, C. B., Dickson, D. W., Hutton, M., Hardy, J., and Golde, T. (2005) Abeta42 is essential for parenchymal and vascular amyloid deposition in mice, *Neuron 47*, 191-199.
100. Findeis, M. A. (2007) The role of amyloid beta peptide 42 in Alzheimer's disease, *Pharmacol Ther 116*, 266-286.
101. Hoos, M. D., Ahmed, M., Smith, S. O., and Van Nostrand, W. E. (2007) Inhibition of familial cerebral amyloid angiopathy mutant amyloid beta-protein fibril assembly by myelin basic protein, *J Biol Chem 282*, 9952-9961.
102. Nelson, R., and Eisenberg, D. (2006) Recent atomic models of amyloid fibril structure, *Curr Opin Struct Biol 16*, 260-265.
103. Harauz, G., Ishiyama, N., Hill, C. M., Bates, I. R., Libich, D. S., and Fares, C. (2004) Myelin basic protein-diverse conformational states of an intrinsically unstructured protein and its roles in myelin assembly and multiple sclerosis, *Micron 35*, 503-542.
104. Bartolini, M., Bertucci, C., Bolognesi, M. L., Cavalli, A., Melchiorre, C., and Andrisano, V. (2007) Insight into the kinetic of amyloid beta (1-42) peptide self-aggregation: elucidation of inhibitors' mechanism of action, *Chembiochem 8*, 2152-2161.
105. Susi, H., and Byler, D. M. (1983) Protein structure by Fourier transform infrared spectroscopy: second derivative spectra, *Biochem Biophys Res Commun 115*, 391-397.
106. Haris, P. I., and Chapman, D. (1994) Analysis of polypeptide and protein structures using Fourier transform infrared spectroscopy, *Methods Mol Biol 22*, 183-202.
107. Jackson, M., and Mantsch, H. H. (1995) The use and misuse of FTIR spectroscopy in the determination of protein structure, *Crit Rev Biochem Mol Biol 30*, 95-120.
108. Bitan, G., Kirkitadze, M. D., Lomakin, A., Vollers, S. S., Benedek, G. B., and Teplow, D. B. (2003) Amyloid beta -protein (Abeta) assembly: Abeta 40 and Abeta 42 oligomerize through distinct pathways, *Proc Natl Acad Sci U S A 100*, 330-335.
109. Hoshi, M., Sato, M., Matsumoto, S., Noguchi, A., Yasutake, K., Yoshida, N., and Sato, K. (2003) Spherical aggregates of beta-amyloid (amylospheroid) show high neurotoxicity and activate tau protein kinase I/glycogen synthase kinase-3beta, *Proc Natl Acad Sci U S A 100*, 6370-6375.
110. DeKosky, S. T., Abrahamson, E. E., Ciallella, J. R., Paljug, W. R., Wisniewski, S. R., Clark, R. S., and Ikonomovic, M. D. (2007) Association of increased cortical soluble abeta42 levels with diffuse plaques after severe brain injury in humans, *Arch Neurol 64*, 541-544.

111. Borchelt, D. R., Thinakaran, G., Eckman, C. B., Lee, M. K., Davenport, F., Ratovitsky, T., Prada, C. M., Kim, G., Seekins, S., Yager, D., Slunt, H. H., Wang, R., Seeger, M., Levey, A. I., Gandy, S. E., Copeland, N. G., Jenkins, N. A., Price, D. L., Younkin, S. G., and Sisodia, S. S. (1996) Familial Alzheimer's disease-linked presenilin 1 variants elevate Abeta1-42/1-40 ratio in vitro and in vivo, *Neuron 17*, 1005-1013.
112. Behrouz, N., Defossez, A., Delacourte, A., and Mazzuca, M. (1991) The immunohistochemical evidence of amyloid diffuse deposits as a pathological hallmark in Alzheimer's disease, *J Gerontol 46*, B209-212.
113. Wisniewski, H. M., Bancher, C., Barcikowska, M., Wen, G. Y., and Currie, J. (1989) Spectrum of morphological appearance of amyloid deposits in Alzheimer's disease, *Acta Neuropathol 78*, 337-347.
114. Whitaker, J. N. (1998) Myelin basic protein in cerebrospinal fluid and other body fluids, *Mult Scler 4*, 16-21.
115. Van Nostrand, W. E., Melchor, J. P., Keane, D. M., Saporito-Irwin, S. M., Romanov, G., Davis, J., and Xu, F. (2002) Localization of a fibrillar amyloid beta-protein binding domain on its precursor, *J Biol Chem 277*, 36392-36398.
116. Libich, D. S., Robertson, V. J., Monette, M. M., and Harauz, G. (2004) Backbone resonance assignments of the 18.5 kDa isoform of murine myelin basic protein (MBP), *J Biomol NMR 29*, 545-546.
117. Libich, D. S., and Harauz, G. (2008) Solution NMR and CD spectroscopy of an intrinsically disordered, peripheral membrane protein: evaluation of aqueous and membrane-mimetic solvent conditions for studying the conformational adaptability of the 18.5 kDa isoform of myelin basic protein (MBP), *Eur Biophys J 37*, 1015-1029.
118. Ide, T., and Kamijo, Y. (2008) Myelin basic protein in cerebrospinal fluid: a predictive marker of delayed encephalopathy from carbon monoxide poisoning, *Am J Emerg Med 26*, 908-912.
119. Ottens, A. K., Golden, E. C., Bustamante, L., Hayes, R. L., Denslow, N. D., and Wang, K. K. (2008) Proteolysis of multiple myelin basic protein isoforms after neurotrauma: characterization by mass spectrometry, *J Neurochem 104*, 1404-1414.
120. Liu, M. C., Akle, V., Zheng, W., Kitlen, J., O'Steen, B., Larner, S. F., Dave, J. R., Tortella, F. C., Hayes, R. L., and Wang, K. K. (2006) Extensive degradation of myelin basic protein isoforms by calpain following traumatic brain injury, *J Neurochem 98*, 700-712.
121. Abdo, W. F., De Jong, D., Hendriks, J. C., Horstink, M. W., Kremer, B. P., Bloem, B. R., and Verbeek, M. M. (2004) Cerebrospinal fluid analysis differentiates multiple system atrophy from Parkinson's disease, *Mov Disord 19*, 571-579.
122. Chalmers, K., Wilcock, G., and Love, S. (2005) Contributors to white matter damage in the frontal lobe in Alzheimer's disease, *Neuropathol Appl Neurobiol 31*, 623-631.

123. Duan, J. H., Wang, H. Q., Xu, J., Lin, X., Chen, S. Q., Kang, Z., and Yao, Z. B. (2006) White matter damage of patients with Alzheimer's disease correlated with the decreased cognitive function, *Surg Radiol Anat 28*, 150-156.
124. Kimura, M., Inoko, H., Katsuki, M., Ando, A., Sato, T., Hirose, T., Takashima, H., Inayama, S., Okano, H., Takamatsu, K., and et al. (1985) Molecular genetic analysis of myelin-deficient mice: shiverer mutant mice show deletion in gene(s) coding for myelin basic protein, *J Neurochem 44*, 692-696.
125. Papenfuss, T. L., Thrash, J. C., Danielson, P. E., Foye, P. E., Hllbrush, B. S., Sutcliffe, J. G., Whitacre, C. C., and Carson, M. J. (2007) Induction of Golli-MBP expression in CNS macrophages during acute LPS-induced CNS inflammation and experimental autoimmune encephalomyelitis (EAE), *ScientificWorldJournal 7*, 112-120.
126. Yamamoto, N., Van Nostrand, W. E., and Yanagisawa, K. (2006) Further evidence of local ganglioside-dependent amyloid beta-protein assembly in brain, *Neuroreport 17*, 1735-1737.
127. Hayashi, H., Kimura, N., Yamaguchi, H., Hasegawa, K., Yokoseki, T., Shibata, M., Yamamoto, N., Michikawa, M., Yoshikawa, Y., Terao, K., Matsuzaki, K., Lemere, C. A., Selkoe, D. J., Naiki, H., and Yanagisawa, K. (2004) A seed for Alzheimer amyloid in the brain, *J Neurosci 24*, 4894-4902.
128. Chan, K. F., Robb, N. D., and Chen, W. H. (1990) Myelin basic protein: interaction with calmodulin and gangliosides, *J Neurosci Res 25*, 535-544.
129. South, S. A., Deibler, G. E., Tzeng, S. F., Badache, A., Kirchner, M. G., Muja, N., and De Vries, G. H. (2000) Myelin basic protein (MBP) and MBP peptides are mitogens for cultured astrocytes, *Glia 29*, 81-90.
130. Tzeng, S. F., Deibler, G. E., and DeVries, G. H. (1999) Myelin basic protein and myelin basic protein peptides induce the proliferation of Schwann cells via ganglioside GM1 and the FGF receptor, *Neurochem Res 24*, 255-260.
131. Tzeng, S. F., Deibler, G. E., and DeVries, G. H. (1995) Exogenous myelin basic protein promotes oligodendrocyte death via increased calcium influx, *J Neurosci Res 42*, 768-774.
132. Deshpande, A., Mina, E., Glabe, C., and Busciglio, J. (2006) Different conformations of amyloid beta induce neurotoxicity by distinct mechanisms in human cortical neurons, *J Neurosci 26*, 6011-6018.
133. Watson, D., Castano, E., Kokjohn, T. A., Kuo, Y. M., Lyubchenko, Y., Pinsky, D., Connolly, E. S., Jr., Esh, C., Luehrs, D. C., Stine, W. B., Rowse, L. M., Emmerling, M. R., and Roher, A. E. (2005) Physicochemical characteristics of soluble oligomeric Abeta and their pathologic role in Alzheimer's disease, *Neurol Res 27*, 869-881.